

# Enamel ridge alignments in ungulates: a cut above

Daniela E. Winkler, Jordi Marcé-Nogué, and Thomas M. Kaiser

## Introduction

Efficient mastication in ungulate herbivores is related to enamel ridge morphology as well as tooth crown height, both of which are found to be adapted to more browse or grass-dominated diets. During ontogeny, the dentition undergoes a change in morphology, as teeth are subsequently worn down. Consequently, a loss in functionality is expected to occur in later life stages, while the dentition should maintain a functional optimum during an individual's growth and reproductive periods.

Comminution of herbivorous diets requires post-canine morphology characterized by shear-cutting ridges combined with compression basins. During mastication, opposing enamel ridges act against each other to disintegrate larger food components into smaller pieces, which are subsequently compressed in dentin basins to extract cell components. All extant ungulate herbivores with either selenodont or selenolophodont cheek teeth show this distinct morphology. The number, complexity and width of ridges as well as tooth crown height are regarded as adaptations to the special demands of grazing and browsing diets (Archer & Sanson 2002, Heywood 2009, Kaiser et al. 2010, Famoso et al. 2013).

Despite the diversity in molar morphologies and mechanical demands of diets, adaptive trends exist in dental form, function, and biomechanical constraints in ungulates. Firstly, newly erupted post-canine teeth are not immediately fully functional, they need a certain degree of wear in order to expose enamel ridges and initiate occlusion with their antagonists. Kurtén (1983) suggested more rapid wear of the tip of the tooth crown in antelopes. For *Equus quagga*, Winkler and Kaiser (2015a) have shown that the tip of premolar and molar tooth crowns is composed of proportionally more dentin and cementum as compared to the rest of the crown. This might be useful to facilitate rapid wear of the crown apex and thus faster occlusion, while the base of the tooth is adapted to resist wear and high stress loads due to a larger enamel content. Secondly, the post-canine dentition should maintain high chewing efficiency for a prolonged time, but at least until the end of reproductive age. Rapid wear of the dentition is suggested to lead to earlier senescence, as seen in captive browsing ungulates that received more abrasive diets than they would have found in the wild, resulting in more abrasion-dominated mesowear patterns (Kaiser et al. 2009). In adult individuals of several cetartiodactyl and perissodactyl species, the upper third molar (M3) shows significantly higher relative proportions of enamel compared to the first upper molar (M1) (Winkler & Kaiser 2015b). This is in accordance with observations in museum collections, where ruminant jaws are usually found with the third molar only just fully erupted, and yet the first molar severely worn (Damuth & Janis 2011). Winkler

& Kaiser (2015b) postulated the "functional compensation hypothesis", proposing that for both terrestrial Cetartiodactyla and Perissodactyla, the M3 maintains high functionality and is morphologically "enhanced" to compensate for the functional loss associated with advanced wear in the M1. For hypsodont taxa only, this had been already suggested by Solounias et al. (1994), who noted that the second and third molars are more hypsodont than the first molar and can hence retain high functionality after the first molar has been worn down. Further support for the functional compensation hypothesis comes from Kaiser (2002), who showed for the extinct three-toed horse *Cormohipparion* sp., that in all cheek tooth positions with the exception of the M3, the occlusal planes successively exposed by wear tend to lose some functional "optimization" in terms of shearing blade orientation in advanced individual age.

It can be expected that a functional compensation of M3 for loss of masticatory efficiency in more anterior tooth positions is a general trait in the evolution of herbivorous ungulates, because it is not only evident in a larger enamel proportion in M3s, but also in the orientation of enamel ridges. Rensberger (1973) suggested that enamel ridges should be aligned almost perpendicular towards the chewing direction to reach the highest shearing efficiency. If such a condition were favourable, a notion that is challenged here, one would expect enamel ridges of the M3 to be aligned at angles close to 90° with the main direction of occlusal movements. To test for functional compensation, the following hypotheses are posed:

1. The M3 compensates for functional losses in more anterior tooth positions and has hence a larger proportion of enamel ridges aligned to higher angles than M1 and M2.
2. Enamel ridge alignments of younger ontogenetic stages have significantly higher enamel ridge alignments compared to senile stages of the same individual. A "prime age" should be identifiable as representing most functionally favourable traits along the tooth row.
3. M3 is built more resistant to withstand higher forces. Enamel ridges are more strictly oriented at high angles to optimize shearing contacts during the displacement-limited power-stroke. M1 has less strictly oriented enamel ridges, which ensure shearing contacts under a higher degree of freedom in lateral displacement.

By comparing enamel ridge alignments of ruminant cetartiodactyls in the upper second molar (M2), Kaiser et al. (2010) found that species with more grass in their natural diet showed a higher proportion of enamel ridges aligned at low angles to the direction of the chewing stroke. They

used functional residual (FR) images of enamel ridges on the occlusal surface employing the FR algorithm (first described in Kaiser 2002). The current study employs the FR algorithm, but with a smaller Gaussian blur setting (8 pixel instead of 35 pixel in Kaiser et al. 2010). It is anticipated that this will better preserve the original morphology in order to identify subtle differences between tooth positions and ontogenetic stages. It is important to note, that the results of this chapter will thus not immediately be comparable to those of Kaiser et al. (2010).

With the exception of equids, the molar tooth row spans approximately over 50 % of the postcanine dentitions' antero-posterior dimension (Janis 1990a,b, Mendoza et al. 2002). Hence, M1 and P4 constitute the masticatory centre of the tooth row (except for camelids, where the centre is expected to shift towards M1 and M2 as premolars are reduced (Janis 1990b)). The M3 is always closest to the temporomandibular joint. Based on their position in the jaw, teeth are always under the influence of distinct constraints imposed on them. While the M3 is expected to experience the highest bite forces (Greaves 2012), the orthal displacement (opening gape) as well as the lateral displacement (chewing stroke) at this position are smallest/shortest (Greaves 2012). The contrary applies for M1. Lower bite forces (due to the longer lever of the lower jaw corpus) and more extensive lateral displacement will immediately translate into less precise guidance of the occlusal movements as compared to more posterior tooth positions (Taylor et al. 2013). It therefore can be assumed that enamel ridge alignments, if an evolutionary response to local functional thresholds in the M1 occurs, are signified by traits indicative of a force-limited but displacement-

optimized system, while the M3 is displacement-limited (due to its position in the jaw), but force-optimized.

A dataset comprised of 22 cetartiodactyl and perissodactyl taxa with diverse dental morphologies, ranging from brachydont browsing species to hypsodont grazers, was employed to investigate common dental morphological adaptations towards maintaining high efficiency of the masticatory apparatus. Hereby specifically the functional traits of enamel ridge morphology towards specific demands of life stage and tooth position in the jaw are examined.

CT scanning techniques are applied to virtually wear down upper and lower molars of one side, in order to create hypothetical future occlusal surfaces of an individual. Those hypothetical surfaces are then treated as ontogenetic wear stages. While extant Perissodactyla possess an enlarged and elongated premolar tooth row (P2–P4), ruminants often have shortened premolar tooth rows (Mendoza et al. 2002). These specific dental traits are most pronounced between specialized perissodactyl grazers like extant equids, in which the premolar tooth row exceeds the molar tooth row (M1–M3) in length, and grazing ruminant Cetartiodactyla and camelids which have elongated the third molar and reduced the premolar tooth row (Janis 1988, 1990a,b, Solounias & Dawson-Saunders 1988). The role of premolars and molars in the masticatory process is hence less comparable between Perissodactyla and Cetartiodactyla and likely such morphologies are also a result of dietary trait evolution. The molar tooth row, however, is never reduced in size and hence can be expected to be a substantial component in efficient food comminution in ruminants, camelids and perissodactyls.

## Material and Methods

The material used in this chapter is curated at the Zoological Museum Hamburg (ZMH) or Museum für Naturkunde Berlin (ZMB) (compare Tab. 8.1) and consists of one individual per species. Specimens were selected according to individual age and dental wear stage: All permanent teeth should be fully mineralized and the M3 unworn or in early wear to cover the longest functional time span of the permanent dentition. If undamaged, preferably right dentitions were selected in order to create a consistent sample.

CT data of upper and lower occluding dentitions were obtained on the vltomelx s (GE phoenix|x-ray) at Section Paleontology, Institute of Geosciences (Rheinische Friedrich-Wilhelms-Universität Bonn, Germany) and for the larger specimens (Rhinocerotidae) on a medical CT at the Universitätsklinikum Hamburg Eppendorf (UKE). Exact voxel sizes of each specimen are given in the supplementary content of Winkler and Kaiser (2015a,b). CT data were reconstructed and segmented in VGStudio MAX 2.2 (Volume Graphics Heidelberg) following the procedure described in Winkler and Kaiser (2015b) to obtain volume models composed of enamel only. These models were cut with clipping-planes to create hypothetical future ontogenetic stages (Fig. 8.1).

The four subsequent stages represent the occlusal surfaces with close to 100 % (subadult = stage 1), 75 % (adult young = stage 2), 50 % (adult old = stage 3) and

25 % (senile = stage 4) of the observed crown height without clipping. It is important to note that the hypothetical wear stages therefore take the different eruption times of the molars into account. During stage 3, for example, the M3 is worn down to 50 % of the *unworn* crown-height, because individuals were selected with unworn M3 or very early wear. For M1, on the contrary, stage 3 represents 50 % of the *initial* crown height in the specimen, which has already experienced a substantial amount of wear and hence crown height loss.

2D images in occlusal view were obtained for each stage and exported to Adobe Photoshop CS5 (Adobe, Dublin). All images were equally scaled to 4400×3400 pixels. Fissures in the enamel which resulted in gaps within an otherwise continuous ridge were manually filled. Then an FR algorithm with 8 pixel Gaussian blur was applied and the resulting grey-scaled matrix converted into a one-bit BMP using the 50 % dichotomisation algorithm in Adobe Photoshop CS5 to smooth enamel ridges, which often appear noisy and pixelated after extraction from VGStudio MAX. Kaiser et al. (2010) applied an FR algorithm with a 35 pixel Gaussian blur, resulting in fusion or elimination of thin enamel ridges, which do not function as shearing edges (Fig. 8.1E). Only a slight smoothing was applied in order to preserve also smaller morphological features, as these should be compared between ontogenetic stages of

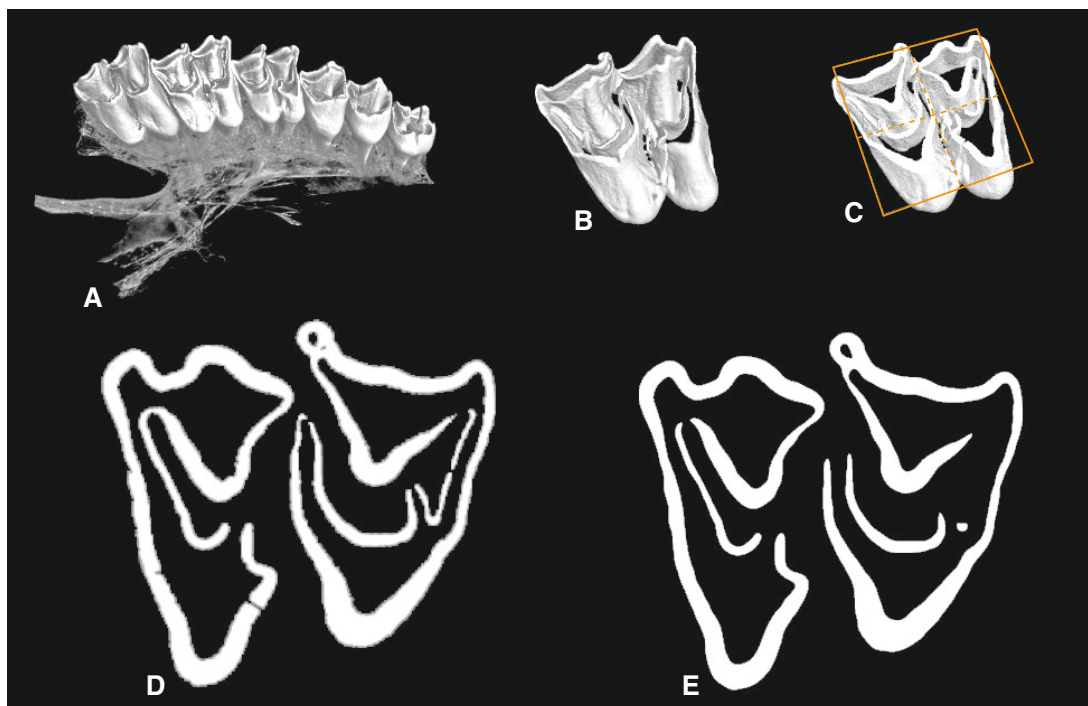


**Fig. 8.1.** Extraction of enamel ridge images from CT data. **A**, Original volume data of *Ozotoceros bezoarticus* (upper right dentition); **B**, extracted enamel volume of the second molar; **C**, same as in B with clipping plane at stage 2 (approx. 75 % of the initial crown height); **D**, extracted 2D image of enamel ridges at stage 2; **E**, resulting final image after FR calculation.

an individual, which a stronger Gaussian blur might have obliterated. A complete FR example image sequence is given in the Appendix (Fig. 8.A1) for *Elaphurus davidianus*.

Each image was oriented in anatomical position towards the chewing direction, which was set vertically (Fig. 8.2A). The computation of enamel ridge alignments was conducted in ArcView GIS 3.2 (esri, New York) following a script written by Andreas Musolff (Helmholtz-Zentrum für Umweltforschung, Leipzig, Germany). First,

each image was vectorized and converted to polylines on which a mark was placed every 100 pixels (Fig. 8.2B). Measurement of angles was achieved by fitting a tangent through two adjacent marks (Fig. 8.2C). Only the buccal (leading) edges were considered, as trailing edges do not significantly contribute to food disintegration in the initial chewing stroke (Fig. 8.2D).

Angle counts were collapsed to  $0^\circ$ – $90^\circ$ , with  $91^\circ$  equaling  $89^\circ$  etc. This is applicable under the assumption that

**Table 8.1.** Sample composition. Each species is represented by one specimen. Diet classification after Mendoza et al. (2002): HBR, high-level browser; GBR, general browser; FGR, fresh-grass grazer; GGR, general grazer; OMF, open-habitat mixed-feeder.

Species	Specimen ID	Order	Family	Diet	Side	Crown height (M3)
<i>Antilocapra americana</i>	ZMH-10162	Cetartiodactyla	Antilocapridae	GBR	left	hypodont
<i>Alcelaphus buselaphus</i>	ZMH-7487	Cetartiodactyla	Bovidae	GGR	left	hypodont
<i>Antelope cervicapra</i>	ZMH-9349	Cetartiodactyla	Bovidae	GGR	right	hypodont
<i>Antidorcas marsupialis</i>	ZMH-8268	Cetartiodactyla	Bovidae	OMF	left	hypodont
<i>Aepyceros melampus</i>	ZMH-5809	Cetartiodactyla	Bovidae	OMF	right	hypodont
<i>Camelus bactrianus</i>	ZMH-1870	Cetartiodactyla	Camelidae	OMF	right	hypodont
<i>Capra ibex</i>	ZMH-6983	Cetartiodactyla	Bovidae	OMF	right	hypodont
<i>Ceratotherium simum</i>	ZMH-2552	Perissodactyla	Rhinocerotidae	GGR	left	hypodont
<i>Connochaetes taurinus</i>	ZMH-6777	Cetartiodactyla	Bovidae	GGR	right	hypodont
<i>Diceros bicornis</i>	ZMH-9379Z	Perissodactyla	Rhinocerotidae	GBR	right	brachydont
<i>Damaliscus pygargus</i>	ZMB_Mam_55243	Cetartiodactyla	Bovidae	GGR	right	hypodont
<i>Elaphurus davidianus</i>	ZMB_Mam_75425	Cetartiodactyla	Cervidae	FGR	right	mesodont
<i>Equus quagga</i>	ZMB_Mam_70335	Perissodactyla	Equidae	GGR	right	hypodont
<i>Hemitragus jemlahicus</i>	ZMH-7747	Cetartiodactyla	Bovidae	OMF	left	hypodont
<i>Kobus ellipsiprymnus</i>	ZMH-447	Cetartiodactyla	Bovidae	FGR	right	hypodont
<i>Lama glama</i>	ZMH-8254	Cetartiodactyla	Camelidae	OMF	left	hypodont
<i>Lama huanachus</i>	ZMH-286	Cetartiodactyla	Camelidae	OMF	left	hypodont
<i>Litocranius walleri</i>	ZMB_Mam_39663	Cetartiodactyla	Bovidae	HBR	right	brachydont
<i>Naemorhedus goral</i>	ZMH-478	Cetartiodactyla	Bovidae	OMF	left	hypodont
<i>Ozotoceros bezoarticus</i>	ZMH-7800	Cetartiodactyla	Cervidae	OMF	right	brachydont
<i>Redunca fulvorufa</i>	ZMH-7632	Cetartiodactyla	Bovidae	FGR	right	hypodont
<i>Rangifer tarandus</i>	ZMH-7104	Cetartiodactyla	Cervidae	GBR	right	brachydont

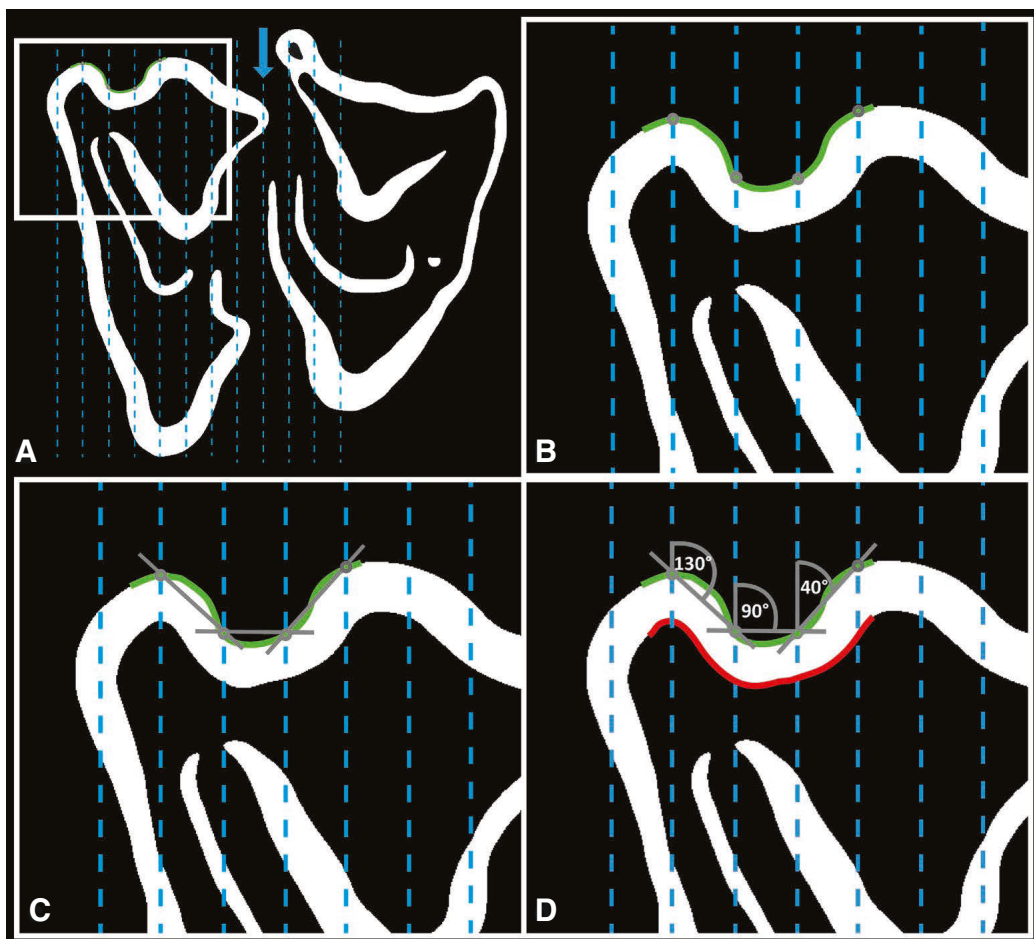


**Fig. 8.2.** Computation of enamel ridge alignments (ERA) for a sample part of an enamel ridge. ERAs are always computed for the leading edges of an occlusal surface. **A**, The blue arrow indicates the chewing direction; **B**, marks are placed along the leading edge (green); **C**, tangents are fitted through adjacent marks resulting in **D**, with the ERAs shown. The trailing edge (red) is not considered.

functional significance for tilts of the same angle clockwise and counter-clockwise to the chewing direction is equivalent (Kaiser et al. 2010).

Computational models for *A. buselaphus*, *A. cervicapra*, *A. melampus*, *C. simum*, *C. taurinus*, *D. bicornis*, *E. quagga*, *K. ellipsiprymnus*, and *L. walleri* were created and provided by Dr. Jordi Marcé-Nogué based on pictures sent by courtesy of Dr. Soledad de Esteban-Trivigno. Some of these models were CT-scanned and used later in Zhou et

al. (2019). Bite forces were calculated in ANSYS (version 16.1) for central positions on lower m1, m2 and m3 in each species according to the equilibrium laws of static mechanics where only force values and distances from the applied points are necessary. The combined input muscle force for masseter, temporal and pterygoid muscles was set to 1 N in all models. This way allometric scaling of muscle forces with body mass is avoided and only the relative magnitude of bite forces along the jaw and between tooth positions is displayed. This procedure is favourable as the enamel ridge alignments are shown to be phylogenetically independent and do not scale with body mass.

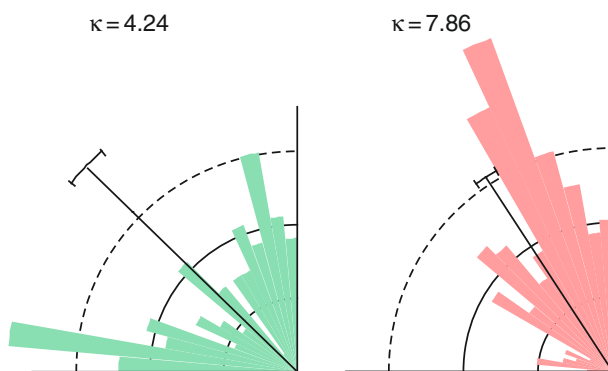


**Fig. 8.3.** Example ERA distributions with low (left) and high (right) concentrations.

## Statistics

Linear statistical analyses were conducted in R version 2.15.1 (R.D.C. Team 2009) and circular statistics in Oriana 4 (Kovach Computing), respectively. Enamel ridge alignments (ERA) were expressed as frequencies and the circular statistical parameters circular median ( $\theta$ ), concentration ( $\kappa$ ) and mean vector ( $\mu$ ) computed per ontogenetic stage and tooth position. Concentration is a dimensionless value that describes the dispersion of a circular dataset. The lower the  $\kappa$ -value (with  $\kappa = 0$  corresponding to uniformity), the higher the dispersion (Fig. 8.3). Data of all ontogenetic

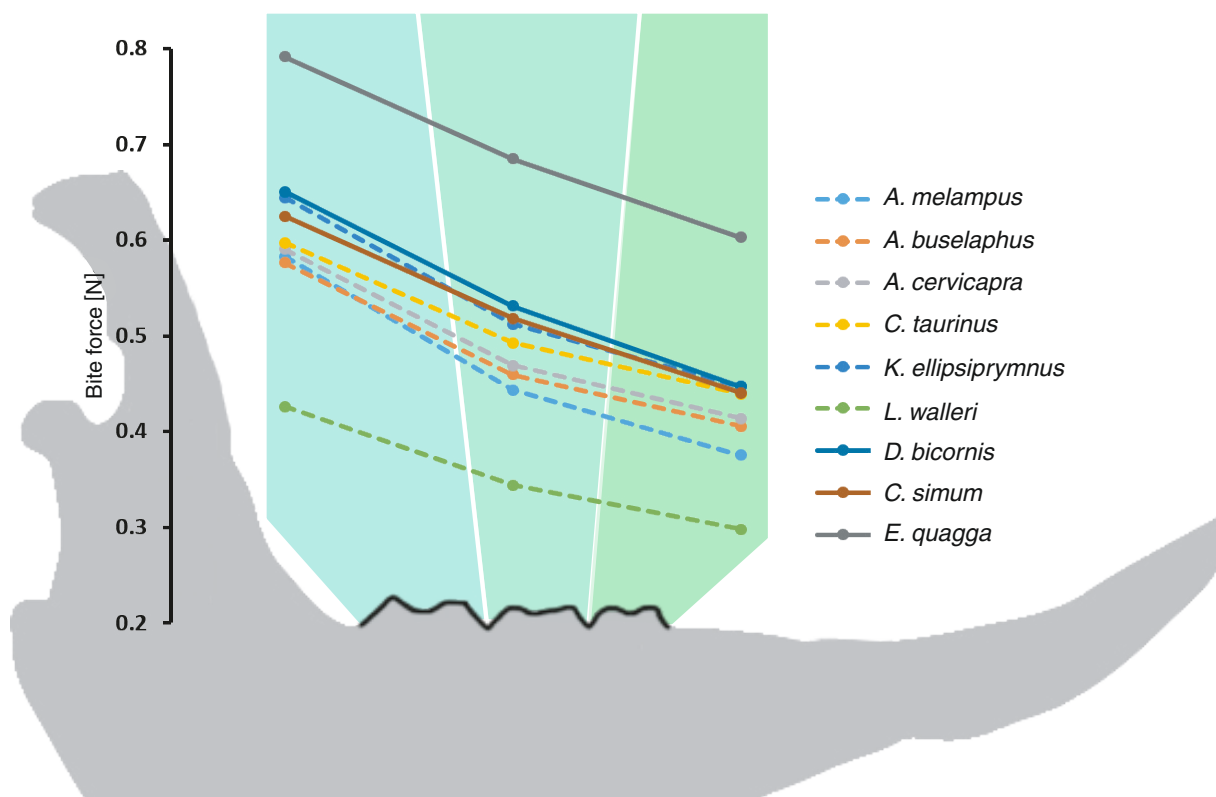


**Fig. 8.4.** Relative bite force per tooth position under an input muscle force of 1N. Continuous lines represent Perissodactyla, dashed lines Artiodactyla.

stages per tooth were pooled to compute an overall value for the tooth (total  $\theta$ ,  $\kappa$  and  $\mu$ ). In Oriana, the Watson U2 and Mardia-Whatson-Wheeler test were employed to detect significant differences between ontogenetic stages and tooth positions. Both tests are sensitive to differences in mean and variance. Results were only treated as significant if they were below a critical p-value of 0.05 in both tests.

Enamel ridge alignments were clustered in two ( $0^\circ$ – $44^\circ$ ,  $45^\circ$ – $90^\circ$ ) and three clusters ( $0^\circ$ – $29^\circ$ ,  $30^\circ$ – $59^\circ$ ,  $60^\circ$ – $90^\circ$ ) and expressed as frequencies. Percentage data were then arcsine transformed in order to normalise them. To test for normality and heteroscedasticity of the data, the Shapiro-Wilk normality test and a robust Brown-Forsythe Levene-type test were applied. If data violated the assumption of normality, a log-transformation was applied and the tests on the transformed data were repeated. This had to be done with the circular parameter concentration ( $\kappa$ ). If the data then met the requirements of normality and homoscedasticity, a one-way ANOVAs with post-hoc Tukey

test to detect significant differences between means was performed. The packages used were ‘stats’ version 3.3.0 (R.D.C. Team 2009) and ‘car’ version 2.0.25 (Fox and Weisberg 2011). For non-normally distributed, heteroscedastic data, a robust Welch-Yuen test with 15 % trimming and a heteroscedastic pair-wise comparison test (analogous to Dunnett’s T3 test; Lincon test) following the procedure of Calandra et al. (2012) and Schulz et al. (2013) were applied.

Phylogenetically informed MANOVAs using the package “geiger” version 2.0.3 (Harmon et al. 2015) were conducted, which simulates new sets of dependent variables on the phylogenetic tree under a Brownian-motion model to ensure phylogenetic independence of variables. The phylogeny is based on the supertree of Bininda-Emonds et al. (2007). Species were used as the independent variable to test the circular statistical parameters circular median ( $\theta$ ), concentration ( $\kappa$ ) and mean vector ( $\mu$ ) as well as ERA for upper and lower molars as dependent variables.

## Results

### Phylogenetic independence

Phylogenetic MANOVAs were conducted for the mean circular statistical variables for each tooth position and ERA frequencies clustered in three clusters, independently for upper and lower teeth. No dependant variable showed a significant relation with phylogeny (Tab. 8.2). Hence the results can be treated independent of phylogeny and thus are not discussed further in a phylogenetic context.

### Relative bite forces along the jaw

Relative bite forces are found to decrease with increasing distance from the temporomandibular joint. The resulting bite force curves are displayed for each species in Figure 8.4.

**Table 8.2.** Test statistics for phylogenetic MANOVAs. Species was used as the independent variable. No significant influence of phylogeny was detected. *df*, degree of freedom; *F*, test value; *p*, significance level.

Parameter	Wilks' lambda	Approx. <i>F</i>	Numerator <i>df</i>	Denominator <i>df</i>	<i>p</i> (> <i>F</i> )	<i>p</i> (phy)
Circular median ( $\theta$ )	0.609	1.6023	6	15	0.214	0.811
Concentration ( $\kappa$ )	0.701	1.0677	6	15	0.424	0.580
Mean vector ( $\mu$ )	0.627	1.4902	6	15	0.247	0.751
ERA for upper jaw	0.507	1.294	9	12	0.332	0.168
ERA for lower jaw	0.519	1.235	9	12	0.359	0.155

**Table 8.3.** Total number of significant variability between enamel ridge alignments between wear stages of individual tooth position. The source of significant differences is given in the Appendix Table A1.

Species	Family	Diet	n Significant differences						
			Upper jaw			Lower jaw			Total
			M1	M2	M3	m1	m2	m3	
<i>A. americana</i>	Antilocapridae	GBR	3	3	2	0	0	1	9
<i>A. buselaphus</i>	Bovidae	GGR	1	3	3	0	0	0	7
<i>A. cervicapra</i>	Bovidae	GGR	0	2	0	3	1	0	6
<i>A. marsupialis</i>	Bovidae	OMF	0	2	4	0	1	0	7
<i>A. melampus</i>	Bovidae	OMF	0	1	3	0	1	0	5
<i>C. bactrianus</i>	Camelidae	OMF	0	0	3	0	0	0	3
<i>C. ibex</i>	Bovidae	OMF	3	0	1	0	0	3	7
<i>C. simum</i>	Rhinocerotidae	GGR	1	2	2	0	1	1	7
<i>C. taurinus</i>	Bovidae	GGR	0	0	0	0	0	0	0
<i>D. bicornis</i>	Rhinocerotidae	GBR	2	0	0	0	2	3	7
<i>D. pygargus</i>	Bovidae	GGR	1	1	3	0	0	0	5
<i>E. davidianus</i>	Cervidae	FGR	3	3	2	0	0	0	8
<i>E. quagga</i>	Equidae	GGR	0	0	0	0	0	0	0
<i>H. jemlahicus</i>	Bovidae	OMF	0	3	0	2	0	0	5
<i>K. ellipsiprymnus</i>	Bovidae	FGR	0	0	2	0	0	0	2
<i>L. glama</i>	Camelidae	OMF	3	0	0	0	0	0	3
<i>L. huanachus</i>	Camelidae	OMF	0	0	0	0	0	2	2
<i>L. walleri</i>	Bovidae	HBR	2	3	3	0	0	0	8
<i>N. goral</i>	Bovidae	OMF	0	2	1	0	0	0	3
<i>O. bezoarticus</i>	Cervidae	OMF	4	1	5	4	0	1	15
<i>R. fulvorufula</i>	Bovidae	FGR	0	3	3	0	2	3	11
<i>R. tarandus</i>	Cervidae	GBR	3	4	5	0	0	0	12
total			26	33	42	9	8	14	

**Table 8.4.** Total number of significant differences per ontogenetic stage position between tooth positions. Note that the total number of differences is lowest for stage 2 in the upper jaw. When Cervidae are excluded, this relation is even stronger.

Species	Family	Diet	n Significant differences								
			Upper jaw				Lower jaw				
			Stage 1	Stage 2	Stage 3	Stage 4	Stage 1	Stage 2	Stage 3	Stage 4	Total
<i>A. americana</i>	Antilocapridae	GBR	2	1	0	0	2	1	2	1	9
<i>A. buselaphus</i>	Bovidae	GGR	0	0	1	1	0	0	0	1	3
<i>A. cervicapra</i>	Bovidae	GGR	0	0	1	0	1	0	1	0	3
<i>A. marsupialis</i>	Bovidae	OMF	0	0	0	1	0	0	0	0	1
<i>A. melampus</i>	Bovidae	OMF	2	1	2	0	1	1	1	2	10
<i>C. bactrianus</i>	Camelidae	OMF	0	0	0	0	0	0	1	0	1
<i>C. ibex</i>	Bovidae	OMF	0	0	1	2	2	1	1	1	8
<i>C. simum</i>	Rhinocerotidae	GGR	0	0	3	2	1	0	0	1	7
<i>C. taurinus</i>	Bovidae	GGR	0	0	0	0	0	0	0	0	0
<i>D. bicornis</i>	Rhinocerotidae	GBR	0	1	0	2	0	2	2	0	7
<i>D. pygargus</i>	Bovidae	GGR	2	0	1	1	0	0	0	0	4
<i>E. davidianus</i>	Cervidae	FGR	0	1	1	2	2	0	1	2	9
<i>E. quagga</i>	Equidae	GGR	0	0	0	0	0	0	0	0	0
<i>H. jemlahicus</i>	Bovidae	OMF	3	0	0	0	0	0	0	2	5
<i>K. ellipsiprymnus</i>	Bovidae	FGR	2	0	0	0	0	0	0	0	2
<i>L. glama</i>	Camelidae	OMF	1	0	1	2	0	0	0	0	4
<i>L. huanachus</i>	Camelidae	OMF	0	0	1	0	1	1	0	0	3
<i>L. walleri</i>	Bovidae	GBR	1	0	1	1	0	0	0	0	3
<i>N. goral</i>	Bovidae	OMF	1	0	1	2	1	0	0	0	5
<i>O. bezoarticus</i>	Cervidae	OMF	2	2	0	2	2	3	3	3	17
<i>R. fulvorufula</i>	Bovidae	FGR	2	1	0	1	1	0	0	0	5
<i>R. tarandus</i>	Cervidae	GBR	3	2	2	2	0	0	0	0	9
Total			21	9	16	21	14	9	12	13	
Without Cervidae			16	4	13	15	10	8	9	10	

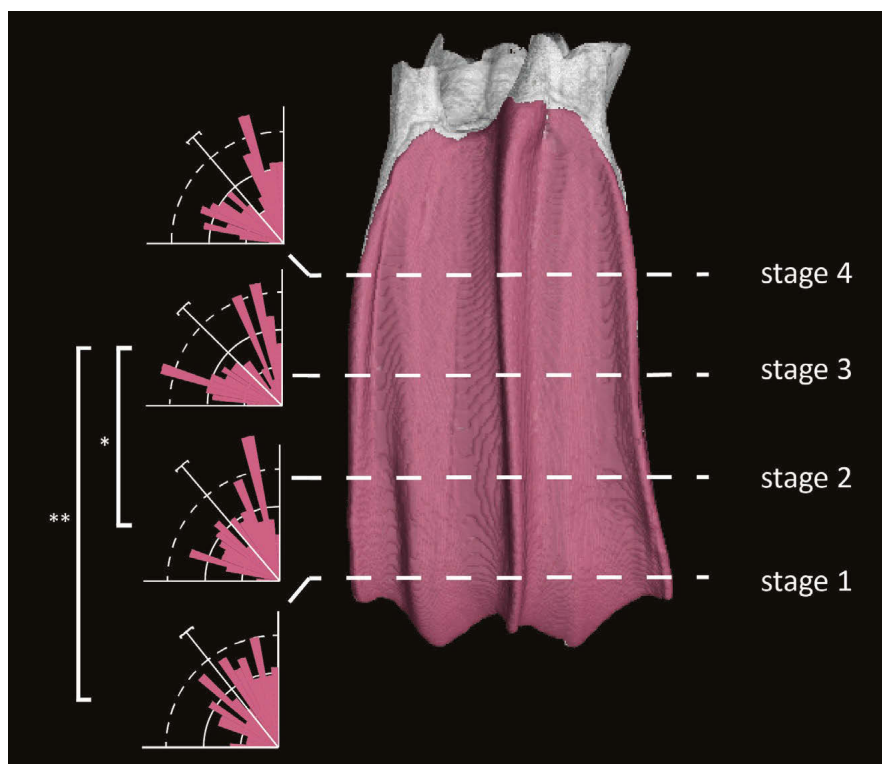


**Fig. 8.5.** Rose diagrams of enamel ridge alignments per ontogenetic stage in an upper M2 of *Antidorcas marsupialis*. The angle distribution pattern of stage 3 is significantly different from stage 1 and stage 2. Rose diagrams show the mean vector with 95 % confidence intervals and angle frequencies from 0°–90°. Inner circle = 3 %, middle circle = 6 %, outer dashed circle = 9 %.

### ERA between wear stages of individual tooth positions

Enamel ridge alignments of successive ontogenetic stages of individual tooth positions are very variable between taxa and feeding types. The source of the observed difference can be both mean angle distribution and/or variance. However, generally two trends can be observed: 1) ERAs of upper teeth are more variable between stages of individual tooth positions than ERAs of lower teeth. 2) For both, upper and lower teeth, either the first and/or the last stage are significantly different from the wear stages in between (see Appendix Tab. 8.1).

Enamel ridge alignments of successive ontogenetic stages for upper third molars are most variable, followed by upper second molars and upper first molars. An example for significantly different enamel ridge alignments is given in Figure 8.5. When analysed according to diet, the number of differences between stages is not normally distributed and cannot be normalized by transformation. Therefore, the procedure for non-normally distributed, heteroscedastic data was followed to further analyse them.

The highest total variability was found for *O. bezoarticus* (Tab. 8.3), the lowest for *C. taurinus* and *E. quagga*. All cervids in the sample have a high variability between ontogenetic stages, while camelids, on the contrary, show few significant differences. Due to the uneven representation of families in the sample, no statistical analyses were performed regarding number of differences per family.

### ERA at corresponding wear stages between teeth

When comparing ERA at corresponding stages between molar teeth, the three cervids exhibit the highest variability besides *Aepyceros melampus*. In all species, ERAs of molars are most variable during wear stages 1 and 4, though this trend is more pronounced in the upper jaw. Moreover, for the upper and lower jaw, stage 2 has the most similar ERA patterns between molars. Cervids have lower crowned teeth than the other taxa in the sample, which might be the source for the observed high variability of ERA between wear stages. If cervids are excluded from the dataset, variability is only found between tooth positions in *A. americana*, *A. melampus*, *D. bicornis* and *R. fulvorufa* for stage 2 in the upper jaw (Tab. 8.4).

### Total ERA per tooth

For each tooth position, angle distributions from stages 1–4 were summed up to produce an estimate of the overall ERA count for the respective tooth. This estimate is referred to as total ERA. Total ERAs are found to be significantly different between molars in most taxa (Tab. 8.5). Upper and lower M3s are distinctly different in their ERAs from M1s and M2s, while in both, upper and lower jaw, M1s and M2 are more similar in ERAs. To detect the source of the differences, total ERAs per tooth were pooled for all species (Tab. 8.6) and described with the circular parameters  $\theta$ ,  $\kappa$  and  $\mu$ .

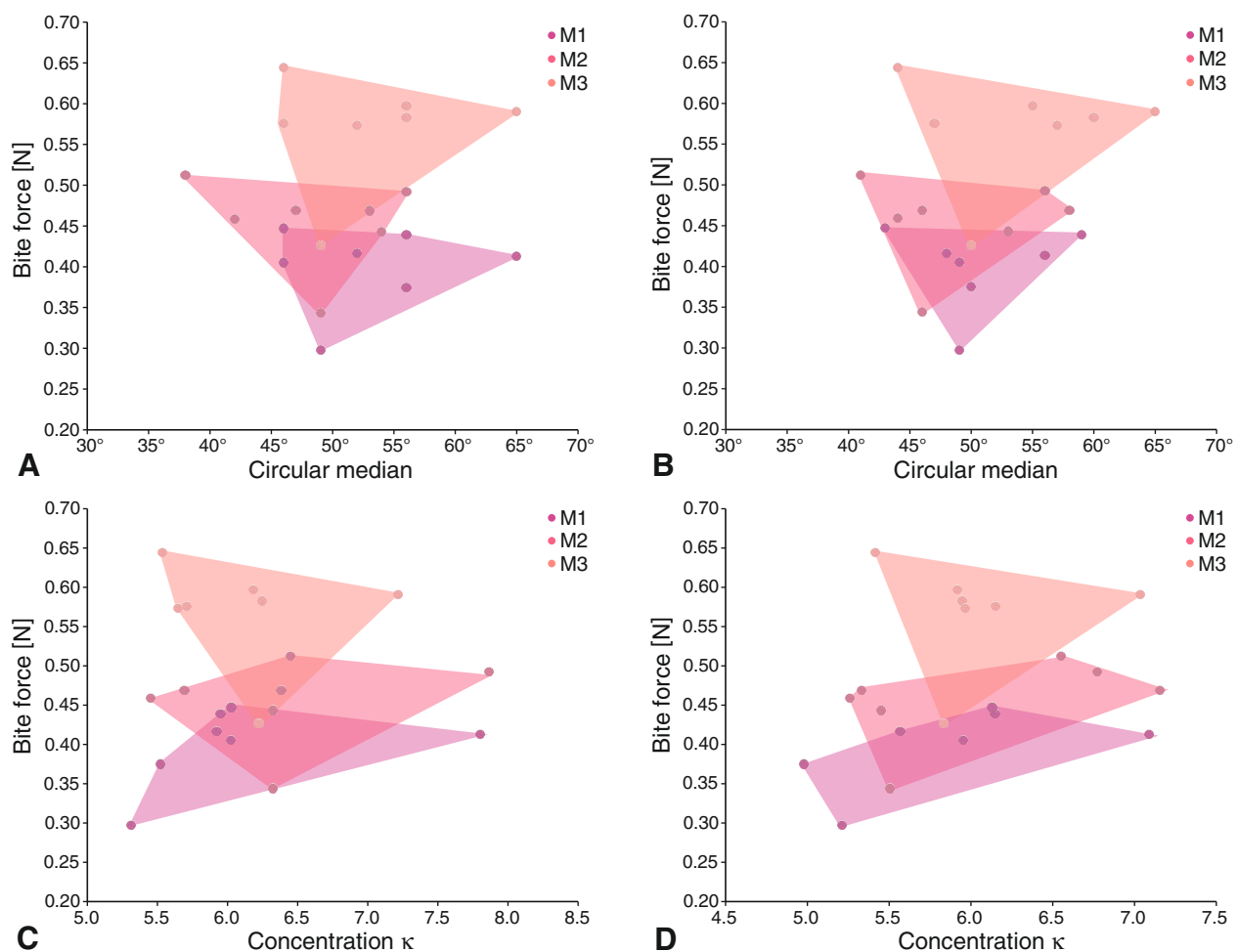


**Fig. 8.6.** Relative bite forces per tooth position related to the circular statistical parameters circular median ( $\theta$ ) and concentration ( $\kappa$ ). **A**, circular median for stage 2; **B**, total circular median; **C**, concentration for stage 2; **D**, total concentration.

**Table 8.5.** Comparisons between total ERA per tooth position. Significances are only accepted if they were produced by both Watsons  $U^2$  and Mardia-Whatson-Wheeler test. \*\*\*,  $p=0.001$ ; \*\*,  $p=0.01$ ; \*,  $p=0.05$ .

Species	Group					
	m1 vs m2	m1 vs m3	m2 vs m3	M1 vs M2	M1 vs M3	M2 vs M3
<i>A. americana</i>		***	***		***	
<i>A. buselaphus</i>	*		*	**		***
<i>A. cervicapra</i>	**	**			**	*
<i>A. marsupialis</i>	***	***		***	***	
<i>A. melampus</i>				***		*
<i>C. bactrianus</i>	*	***		*		
<i>C. ibex</i>	**	***	***		***	
<i>C. simum</i>	***	**		**		*
<i>C. taurinus</i>	**					*
<i>D. bicornis</i>			*	*	***	**
<i>D. pygargus</i>			**		***	***
<i>E. davidianus</i>	***	***	**	**	**	*
<i>E. quagga</i>				*	**	
<i>H. jemlahicus</i>	***	**		***	***	
<i>K. ellipsiprymnus</i>				*	**	
<i>L. glama</i>	**				**	
<i>L. huanachus</i>		**			**	
<i>L. walleri</i>				*	*	
<i>N. goral</i>	*	**	*	*	***	***
<i>O. bezoarticus</i>	***	***	***	***	***	*
<i>R. fulvorufula</i>					**	***
<i>R. tarandus</i>		*	**	***	***	

### Circular median ( $\theta$ )

In both upper and lower jaws,  $\theta$  shows the same pattern with  $M3 > M1 > M2$  (Tab. 8.6). This pattern is not significant for lower or upper molars. In the bovid subset, bite forces do not correlate with  $\theta$  (Fig. 8.6A,B). A post-hoc Tukey test (not displayed here) showed that lower molars have significantly higher  $\theta$  only than upper molars.

**Table 8.6.** Descriptive statistics of circular statistical parameters per tooth position pooled for all species. SD, standard deviation.

Tooth	Circular median ( $\theta$ )		Concentration ( $\kappa$ )		Mean vector ( $\mu$ )	
	Mean	SD	Mean	SD	Mean	SD
m1	55.136°	4.622°	5.634	0.612	51.750°	2.813°
m2	53.227°	5.944°	5.773	0.624	50.357°	4.026°
m3	55.955°	6.622°	6.771	1.265	53.993°	5.120°
M1	49.000°	5.782°	5.537	0.559	47.902°	4.011°
M2	47.818°	6.162°	5.896	0.542	47.135°	4.423°
M3	52.545°	6.906°	6.167	0.523	50.522°	4.918°

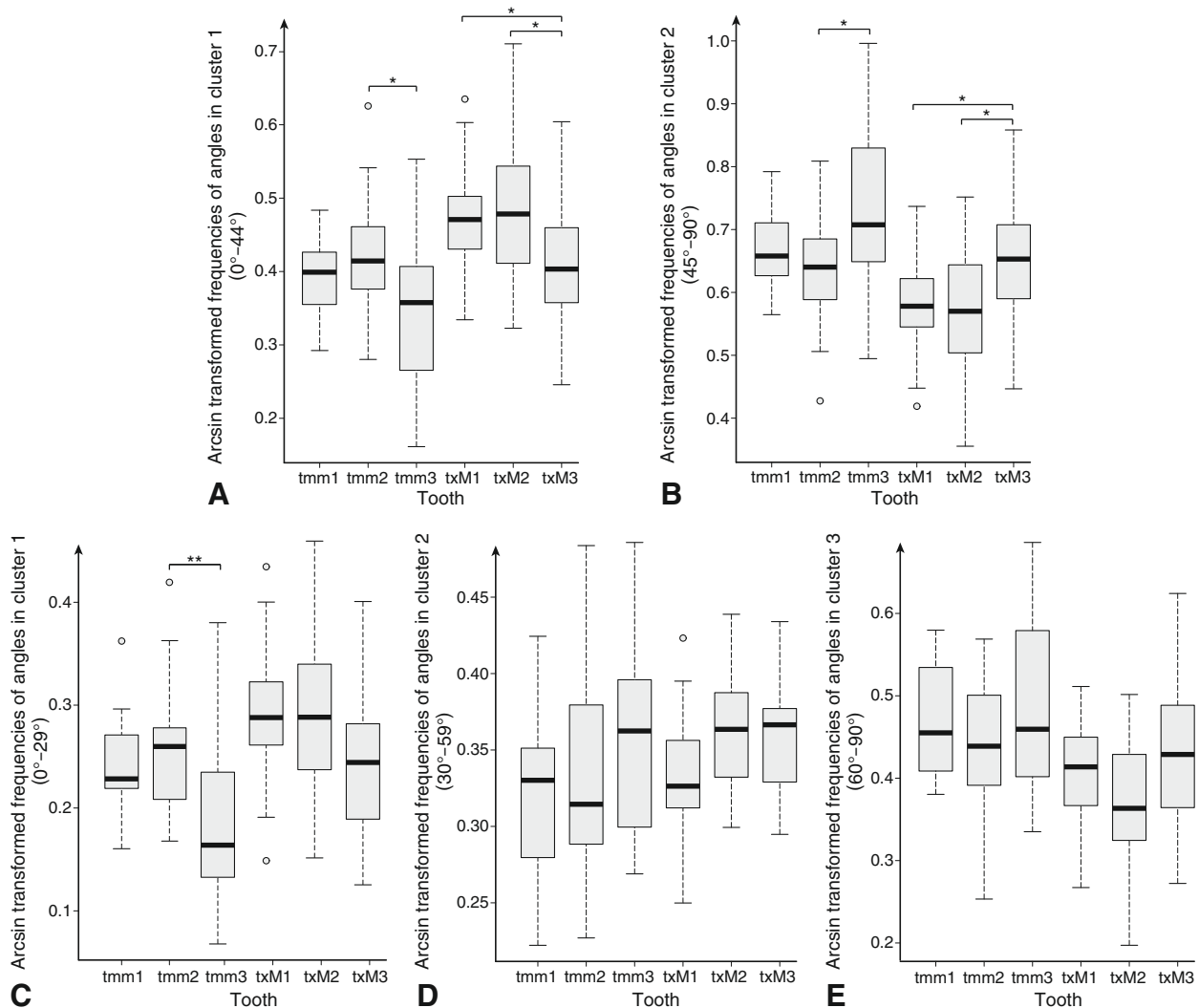


**Fig. 8.7.** Boxplots of significant differences between tooth positions for total ERA per cluster. **A, B**, ERA distributed in two clusters, test statistic from Lincon. **C-E**, ERA in three clusters, test statistic from Tukey. \*\*\* $p=0.001$ ; \*\* $p=0.01$ ; \* $p=0.05$ .

### Concentration ( $\kappa$ )

$\kappa$  is increasing from M1 to M2 to M3 in upper and lower molars, with values for lower m1s and m2s being very similar. Lower m3s have significantly higher  $\kappa$  than m2s (Tukey:  $p=0.001$ ) and m1s (Tukey:  $p=0.000$ ). For upper molars, significant differences are found between M1s and M3s (Tukey:  $P=0.028$ ). Test statistics are given in Table 8.7. The bite force calculations for the bovid subset illustrate that both bite forces and concentration  $\kappa$  follow the same gradient (M3>M2>M1, Fig. 8.7C,D).

### Mean vector ( $\mu$ )

As expected,  $\mu$  is found to exhibit the same pattern as  $\theta$  with M3>M1>M2. The significances are also very similar to those for mean  $\theta$  (compare Tab. 8.7).

### Clustered total ERAs per tooth

The frequency of observed ERAs is normally distributed in all clusters. When assigned to two clusters (0-44°, 45-90°), ERAs show unequal variances (Levene:  $p=0.000$ ).

**Table 8.7.** Results of post-hoc Tukey test for circular median, concentration and mean vector per tooth position. Significances are printed in bold. lwr, lower end point of the interval; upr, upper end point of the interval;  $p$ , significance level.

Circular median ( $\theta$ )				Concentration ( $\kappa$ )				Mean vector ( $\mu$ )							
	diff. means	lwr	upr	$p$		diff. means	lwr	upr	$p$		diff. means	lwr	upr	$p$	
m1 m2	-0.033	-0.125	0.059	0.901	0.011	-0.034	0.055	0.982	0.982	-0.024	-0.090	0.041	0.889		
m1 m3	0.014	-0.078	0.106	0.998	0.075	0.031	0.120	<b>0.000</b>	0.000	0.039	-0.026	0.104	0.510		
m2 m3	0.048	-0.045	0.140	0.668	0.065	0.020	0.109	<b>0.001</b>	0.001	0.063	-0.002	0.129	0.062		
M1 M2	-0.021	-0.113	0.072	0.987	0.028	-0.017	0.072	0.466	0.466	-0.013	-0.079	0.052	0.991		
M1 M3	0.062	-0.030	0.154	0.381	0.047	0.003	0.092	<b>0.028</b>	0.028	0.046	-0.020	0.111	0.333		
M2 M3	0.083	-0.010	0.175	0.107	0.020	-0.024	0.064	0.787	0.787	0.059	-0.006	0.124	0.100		

Therefore, the distribution into two clusters is analysed using the procedure for non-normally distributed, heteroscedastic data.

In all tooth positions, the majority of angles fall into the 50°–90° and 45°–90° clusters (Fig. 8.7A–E). The most pronounced frequency differences between clusters are observed in upper and lower M3s for distribution in two clusters. Lower m3s have significantly more ERAs in the

45–90° cluster than lower m2s (Lincon:  $p=0.021$ ), while upper M3s have significantly more ERAs in this cluster than upper M1s (Lincon:  $p=0.040$ ) and M2s (Lincon:  $p=0.028$ ).

When assigned to three clusters, the only significant difference is detected in the 0–29° cluster, where lower m3s have significantly lower ERA frequencies than lower m2s (Tukey:  $p=0.005$ ).

## Discussion

No influence of phylogeny on enamel ridge alignments (ERAs) was found, thus all results obtained for ungulates here are interpreted as following a general adaptive pattern. ERAs towards the chewing direction are tooth position specific and show a consistent pattern for all tested species.

### Hypothesis 1 (H1)

Total ERAs are not found to have significantly higher circular median ( $\theta$ ) or mean vector ( $\mu$ ) in M3s than in M1s and M2s. However, a trend for M3s to have higher ERAs than the anterior molars can be consistently observed in the sample. When clustered in lower (cluster 1: 0°–44°) and higher (cluster 2: 45°–90°) alignments, upper and lower M3s show significantly higher angle frequencies in the 45°–90° cluster. Moreover, upper and lower M3s show the highest concentration ( $\kappa$ ) values.  $\kappa$  is a measurement of angle dispersion. Low  $\kappa$ -values are characteristic of a dispersed angle pattern which is created by more complexly folded enamel ridges or differently aligned enamel ridges between ontogenetic stages. M3 having the highest  $\kappa$ -values over the whole tooth crown shows that its enamel ridges are either less complexly folded or very precisely aligned for each ontogenetic stage. The complexity of enamel ridges can be expected to be similar between teeth, as it is a strong indicator of diet (Archer and Sanson 2002; Heywood 2009), and therefore the second explanation is considered as more likely. M3 is morphologically conservative over the tooth crown and hence has more precisely aligned angles towards the chewing direction. This conserved morphology can also be considered as indicative for a maintained functionality once anterior tooth positions wear out and lose chewing efficiency. Hypothesis 1 (H1) can hence be partly accepted and is reformulated to:

The M3 compensates for functional loss in more anterior tooth positions by having a larger proportion of enamel ridges aligned to higher angles than M1 and M2 and by maintaining precise alignments over the whole tooth crown.

The results of this chapter also show that enamel ridge alignments close to 90° do not occur as frequently as hypothesized by Rensberger (1973), at least not when alignments are analysed in a 2D projection. One has to keep in mind that all data in this study are reducing the measured angle to two dimensions, thus the real, natural curvature of enamel ridges is lost. It is therefore suggested that either adequate chewing efficiency can also be achieved by lower aligned enamel ridges, or the natural curvature would actually result in higher aligned enamel ridges, which cannot be detected here. Nevertheless, it

seems that the degrees of freedom of the masticatory movement during the power stroke are higher than anticipated. Consequently, lateral chewing movements would not be as strictly aligned as expected in a rather simplistic model and a more antero-posterior (proal) component to the chewing stroke would also make higher ERAs efficient shearing blades as suggested in this study.

### Hypothesis 2 (H2)

Ontogenetic differences in ERAs are mostly related to the youngest and/or the oldest (senile) stage of a tooth position (see Appendix Tab. 8.1). This does not fully support the hypothesis that younger ontogenetic stages should be more optimized in enamel ridge alignments. Significant differences in ERAs of wear stage 2 and 3 compared to stage 4 would be expected if that was the case. However, the “prime age”, which is expected to be represented by stages 2 and 3, are only for *C. simum*, *E. davidianus*, *R. tarandus* and *O. bezoarticus* in more than one tooth position distinctly different from other stages. It is striking that three Cervidae are amongst these taxa. Cervidae are, with the Rhinocerotidae and *L. walleri*, the most brachydont taxa in the sample. In brachydont taxa and GBRs, the variability of ERAs between stages is significantly higher than in all other families and dietary categories. Such obvious variability in crown morphology during wear has also been noted by Fortelius (1985b) in a Pleistocene rhinoceros and interpreted as compensation and reciprocal change during wear in brachydont taxa. It can therefore be concluded that crown hypsodonty does not only represent a proportional increase in crown height, but is also accompanied by a harmonisation of ERAs.

Stage 2 seems to be the most homogenous stage in ERAs in the upper and lower jaw, which indicates that orientation of enamel ridges is most similar in all molar teeth during the prime age. Though enamel ridges are not found to be significantly higher aligned during stage 2, they seem to undergo an optimization in terms of functional similarity. Chewing efficiency is thus least different between molars during the prime age. This optimization might be necessary in order to fulfil high energetic demands during peak reproduction on basis of a highly abrasive diet. If indeed chewing efficiency is increased through functional similarity, it would enable these species to incorporate higher amounts of abrasive forage during the prime age and process it with fewer chewing strokes, hereby not significantly increasing tooth wear. Without such an optimization, teeth would be exposed to higher wear which could only be countered

by even greater crown height. As expected, a limitation to crown height exists in order to not distort ossification of the mandible and maxilla, thus an additional increase in crown height is unlikely.

With older age, differences between tooth positions become more pronounced, especially when M1 wears out (Damuth and Janis 2011). The M3 (in both upper and lower jaw) meanwhile maintains higher angulated and more precisely aligned enamel ridges than the M1 and M2, which supports functional compensation of the M3 as proposed in H1 and by Winkler et al. (2015b). In other words, during the prime age, the first and second molars are not distinguishable in ERAs from M3 and optimized chewing efficiency during this stage can be inferred, which is more pronounced in hypodont than in brachydont species.

Hypothesis 2 (H2) is only partly supported and should be rephrased to: Enamel ridge alignments are optimized during the prime age in terms of homogenous function, but not in terms of general higher alignments.

### Hypothesis 3 (H3)

The lower overall concentration values for M1s and M2s compared to M3s indicate that enamel ridges are less strictly oriented in the first two molars. Upper and lower M1s have the lowest concentration values. This is likely to be related to a higher number of thin ridges aligned at lower angles and to a changing enamel ridge orientation over the tooth crown in M1s and M2s and more consistent enamel ridge morphology in M3s.

The temporomandibular joint allows for both lateral and antero-posterior movements, though the chewing stroke for most ungulates is described as unilateral, transverse chewing characterized by pronounced medio-lateral jaw movements (Fortelius 1985a, Williams et al. 2007, Kaiser et al. 2010). During the opening of the mouth, the condylar head of the mandible rotates within the mandibular fossa up to a certain point, when the condylar head and articular disc translate to allow for further jaw opening. It is intuitively comprehensible that the opening is smaller in close proximity to the temporomandibular joint. Therefore, the lateral displacement is also smallest close to the joint. Mastication on the tooth positions closest to the jaw joint hence has to be adapted to disintegrating food particles efficiently under displacement-limited conditions. A precise guidance and orientation of enamel ridges is thus favourable in this setting. Moreover, the data showed that larg-

est bite forces can be generated closest to the jaw joint. The highest relative bite force was always computed for the third molar. The biomechanical constraints of the jaw morphology (shorter lateral displacement in combination with higher forces close to the temporomandibular joint) are combined with more precisely aligned enamel ridges at the third molar.

Disintegration of plant matter requires crack propagation through anisotropic, tough tissues. The dental shear-cutting system of extant herbivorous ungulates achieves this by tooth position-specific adaptations: On the third molar, cracks are driven through the tissue by shear-cutting with a higher force over enamel ridges which have predominant directions. On the first molar, cracks are propagated through a longer chewing stroke over dispersed enamel ridges, which ensure multiple contacts. The more anterior tooth positions might also display more degrees of freedom during translation. The presence of less precisely aligned enamel ridges at more anterior tooth positions could hence be an advantage, as it would maximize contacts during the longer, less strictly guided chewing stroke. Lower guidance and more antero-posterior components would bring lower aligned enamel ridges in more favourable positions for shearing.

The hypothesis of a more robust build in general for M3s could not be proven by this study; however, data on enamel volume by Winkler and Kaiser (2015b) show that M3s have higher enamel proportions which either indicates wider enamel ridges or smaller dentin basins. The assumption that enamel ridges of the M3s are wider is likely, because wider ridges would better withstand the higher bite forces. The lower variability in enamel ridge orientation seen in M3s could also be a consequence from the higher enamel content: as wider ridges take a larger space on the occlusal surface, there would be less space for changes in ridge orientation (e.g., plications). Higher concentration of ERAs in M3s needs to be accounted for and might not be solely adaptive to occlusal function, but result from space constraints in the occlusal surface and also related to the narrow space close to the jaw's angle, where bending forces are large and thus lateral alveolar bone sheets would have to be inflated in order to transmit forces. The latter could be a biomechanical constraint not yet considered in FEA models accordingly. Future FEA studies on stress distribution along the jaw using artificially low enamel thicknesses for third molars might contribute to the understanding of this phenomenon and decide whether it is adaptive or a morphological constraint.

## Conclusion

Virtual 3D reconstructions of enamel ridge morphologies based on computer tomographic data have great value in measuring chewing direction of subsequent ontogenetic stages using the GIS-based approach described in this chapter. Enamel ridge alignments of third molars are found to be higher angulated and significantly more concentrated than those of first and second molars. For subsequent ontogenetic stages, the second wear stage, which is considered to resemble the prime reproductive

age of an individual, shows the fewest differences between molar tooth positions on enamel ridge orientation. These findings might represent an adaptation towards more homogenous tooth function during peak reproduction. Tooth-position specific bite forces along the jaw decline along the molar tooth row with increasing distance from the temporomandibular joint. This indicates that enamel ridge alignments are an adaptation towards more load-optimized and displacement-limited conditions close to the

jaw joint, while more anterior tooth positions are adapted towards higher degrees of lateral displacement. The higher dispersion of enamel ridge angles in first molars hereby suggests a benefit under a less guided and less powerful chewing stroke, as it ensures maximum contacts between enamel ridges. The shorter displacement of the posterior lower jaw is compensated by higher bite forces at the M3.

Molar teeth of Perissodactyla and Cetartiodactyla do not form a homogenous functional unit during the whole

ontogeny. Their functionality is optimized during the prime age of an individual, but afterwards M1 and M2 functionality declines. The M3 compensates for functional loss of M1 and M2. This study has important implications for future studies on tooth function and dietary reconstruction: Wear stage and tooth position need to be carefully considered in order to accommodate morphological variability within the tooth crown, but also general biomechanical constraints that universally apply, independent of diet and taxonomy.

## Acknowledgments

We thank the Museum für Naturkunde Berlin for specimen loan, Jan-Hendrik Buhk at Universitätsklinikum Eppendorf for CT scanning of large specimens, and all members of the DFG research unit

771 for fruitful discussions during and after the project duration. We highly acknowledge the helpful comments and suggestions from Gina Semprebon and Indré Žliobaitė who reviewed this chapter.

## References

- \* indicates publications that originated from the DFG Research Unit 771.
- Archer, D. & Sanson, G. (2002): Form and function of the selenodont molar in southern African ruminants in relation to their feeding habits. *Journal of Zoology* 257: 13–26.
- Bininda-Emonds, O. R. P., Cardillo, M., Jones, K. E., MacPhee, R. D. E., Beck, R. M. D., Grenyer, R., Price, S. A., Vos, R. A., Gittleman, J. L. & Purvis, A. (2007): The delayed rise of present-day mammals. *Nature* 446: 507–512.
- \*Calandra, I., Schulz, E., Pinnow, M., Krohn, S. & Kaiser, T. M. (2012): Teasing apart the contributions of hard items on 3D dental microtextures in primates. *Journal of Human Evolution* 63: 85–98.
- Damuth, J. & Janis, C. M. (2011): On the relationship between hypsodonty and feeding ecology in ungulate mammals, and its utility in palaeoecology. *Biological Reviews* 86: 733–758.
- Famoso, N. A., Feranec, R. S. & Davis, E. B. (2013): Occlusal enamel complexity and its implications for lophodonty, hypsodonty, body mass and diet in extinct and extant ungulates. *Palaeogeography, Palaeoclimatology, Palaeoecology* 387: 211–216.
- Fortelius, M. (1985a): Ungulate cheek teeth: developmental, functional, and evolutionary interrelations. *Acta Zoologica Fennica* 180: 1–76.
- Fortelius, M. (1985b): The functional significance of wear-induced change in the occlusal morphology of herbivore cheek teeth, exemplified by *Dicerorhinus etruscus* upper molars. *Acta Zoologica Fennica* 170: 157–158.
- Fox, J. & Weisberg, S. (2011): An {R} Companion to Applied Regression, Second Edition. Sage Publishing, Thousand Oaks.
- Greaves, W. S. (2012): The Mammalian Jaw – A Mechanical Analysis. Cambridge University Press, Cambridge.
- Harmon, L., Weir, J., Brock, C., Glor, R., Challenger, W., Hunt, G. et al. (2015): Package ‘geiger’. In: R package version 2.0.3.
- Heywood, J. J. N. (2009): Functional anatomy of bovid upper molar occlusal surfaces with respect to diet. *Journal of Zoology* 281: 1–11.
- Janis, C. M. (1988): An estimation of tooth volume and hypsodonty indices in ungulate mammals, and the correlation of these factors with dietary preference. In: Russel, D. E., Santoro, J. P. & Signogneau-Russel, D. (eds.): Teeth Revisited: Proceedings of the VII International Symposium on Dental Morphology. Mémoires du Muséum national d’Histoire naturelle C 53: 367–387.
- Janis, C. M. (1990a): Correlation of cranial and dental variables with dietary preferences: a comparison of macropodoid and ungulate mammals. *Memoirs of the Queensland Museum* 28: 349–366.
- Janis, C. M. (1990b): Correlation of cranial and dental variables with body size in ungulates and macropodoids. In: Damuth, J. & MacFadden, B. J. (eds.): Body Size in Mammalian Paleobiology. Cambridge University Press, Cambridge: 255–299.
- Kaiser, T. M. (2002): Functional significance of ontogenetic gradients in the enamel ridge pattern of the upper cheek dentition of the Miocene hipparrisonine horse *Cormohipparrison occidentale* (Equidae, Perissodactyla): Senckenbergiana lethaea 82: 167–180.
- Kaiser, T. M., Brasch, J., Castell, J. C., Schulz, E. & Clauss, M. (2009): Tooth wear in captive wild ruminant species differs from that of free-ranging conspecifics. *Mammalian Biology* 74: 425–437.
- Kaiser, T. M., Fickel, J., Streich, W. J., Hummel, J. & Clauss, M. (2010): Enamel ridge alignment in upper molars of ruminants in relation to their natural diet. *Journal of Zoology* 281: 12–25.
- Kurten, B. (1983): Variation and dynamics of a fossil antelope population. *Paleobiology* 9: 62–69.
- Mendoza, M., Janis, C. M. & Palmqvist, P. (2002): Characterizing complex craniodental patterns related to feeding behaviour in ungulates: a multivariate approach. *Journal of Zoology* 258: 223–246.
- R.D.C. Team (2009): R: A language and environment for statistical computing. In: R Foundation for Statistical Computing, Vienna.
- Rensberger, J. M. (1973): An occlusion model for mastication and dental wear in herbivorous mammals. *Journal of Paleontology* 47: 515–528.
- \*Schulz, E., Calandra, I. & Kaiser, T. M. (2013): Feeding ecology and chewing mechanics in hooved mammals: 3D tribology of enamel wear. *Wear* 300: 169–179.
- Solounias, N. & Dawson-Saunders, B. (1988): Dietary adaptations and palaeoecology of the late Miocene ruminants from Pikermi and Samos in Greece. *Palaeogeography, Palaeoclimatology, Palaeoecology* 65: 149–172.
- Solounias, N., Fortelius, M. & Freeman, P. (1994): Molar wear rates in ruminants: A new approach. *Annales Zoologici Fennici* 31: 219–227.
- \*Taylor, L. A., Kaiser, T. M., Schwitzer, C., Müller, D. W. H., Codron, D., Clauss, M. & Schulz, E. (2013): Detecting inter-cusp and inter-tooth wear patterns in rhinocerotids. *PLoS One* 8: e80921.
- Williams, S. H., Vinyard, C. J., Wall, C. E. & Hylander, W. L. (2007): Masticatory motor patterns in ungulates: a quantitative assessment of jaw-muscle coordination in goats, alpacas and horses. *Journal of Experimental Zoology Part A: Comparative Experimental Biology* 307A: 226–240.
- \*Winkler, D. E. & Kaiser, T. M. (2015a): Uneven distribution of enamel in the tooth crown of a Plains Zebra (*Equus quagga*). *PeerJ* 3: e1002.
- \*Winkler, D. E. & Kaiser, T. M. (2015b): Structural morphology of molars in large mammalian herbivores: Enamel content varies between tooth positions. *PLoS One* 10(8): e0135716.
- \*Zhou, Z., Winkler, D. E., Fortuny, J., Kaiser, T. M. & Marcé-Nogue, J. (2019): Why ruminants chew sloppily: Biomechanics discern a phylogenetic pattern. *PLoS ONE* 14(4): e0214510.

## Appendix

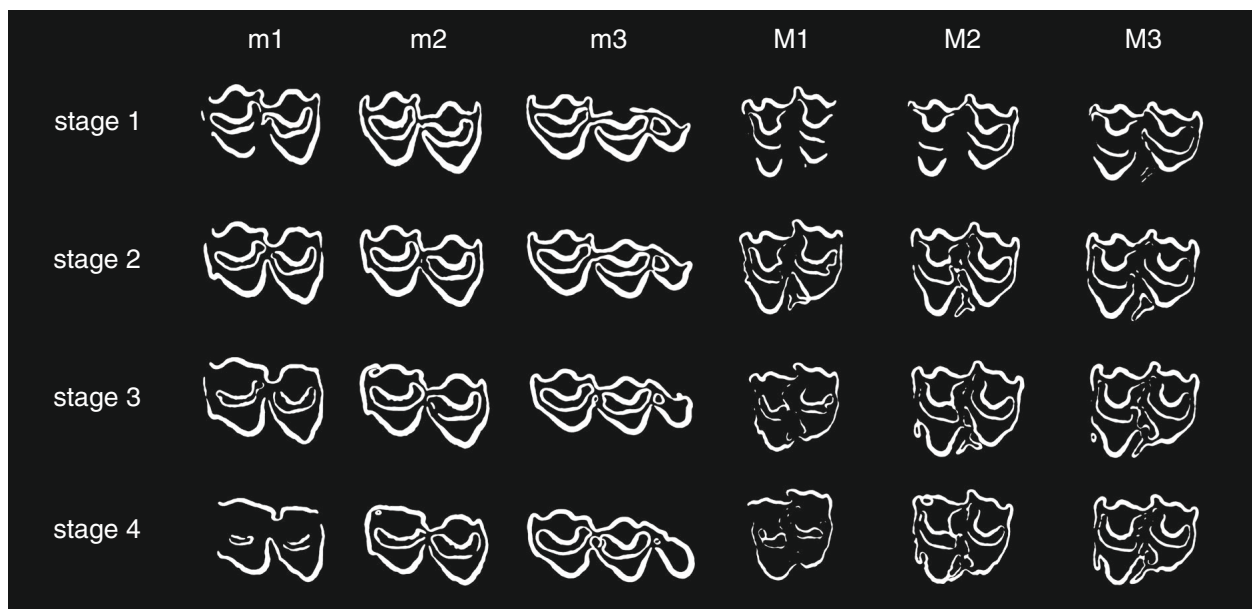


**Fig. 8.A1.** FR image sequence of the lower and upper molar tooth row of *Elaphurus davidianus*. The individual images are not true to scale.

**Table 8.A1.** Source of detected significant differences between ontogenetic stages. ns, no significant difference found.

Species	Difference between stages					
	M1	M2	M3	m1	m2	m3
<i>A. americana</i>	1 vs. 2/3/4	1 vs. 2/3/4	1 vs. 3/4	ns	ns	1 vs. 4
<i>A. buselaphus</i>	1 vs. 4	1 vs. 2/3/4	1 vs. 2/3/4	ns	ns	ns
<i>A. cervicapra</i>	ns	1 vs. 2/3	ns	4 vs. 1/2/3	2 vs. 4	ns
<i>A. marsupialis</i>	ns	3 vs. 1/2	1 vs. 2/3/4 2 vs. 4	ns	1 vs. 4	ns
<i>A. melampus</i>	ns	1 vs. 4	1 vs. 2/3/4	ns	1 vs. 4	ns
<i>C. bactrianus</i>	ns	ns	1 vs. 2/3/4	ns	ns	ns
<i>C. ibex</i>	1 vs. 3/4 2 vs. 4	ns	1 vs. 3	ns	ns	1 vs. 2/3/4
<i>C. simum</i>	2 vs. 3	5 vs. 1/2	1 vs. 2/3	ns	2 vs. 4	3 vs. 4
<i>C. taurinus</i>	ns	ns	ns	ns	ns	ns
<i>D. bicornis</i>	1 vs. 2/3	ns	ns	ns	3 vs. 1/2	4 vs. 1/2/3
<i>D. pygargus</i>	1 vs. 3	1 vs. 4	1 vs. 2/3/4	ns	ns	ns
<i>E. davidianus</i>	1 vs. 2/4 2 vs. 4	1 vs. 3/4 2 vs. 4	1 vs. 3 2 vs. 4	ns	ns	ns
<i>E. quagga</i>	ns	ns	ns	ns	ns	ns
<i>H. jemlahicus</i>	ns	1 vs. 2/3/4	ns	1 vs. 3/4	ns	ns
<i>K. ellipsiprymnus</i>	ns	ns	1 vs. 3/4	ns	ns	ns
<i>L. glama</i>	1 vs. 3/4 2 vs. 4	ns	ns	ns	ns	ns
<i>L. huanachus</i>	ns	ns	ns	ns	ns	4 vs. 1/2
<i>L. walleri</i>	1 vs. 3/4	4 vs. 1/2/3	1 vs. 2/3/4	ns	ns	ns
<i>N. goral</i>	ns	1 vs. 2/3	1 vs. 4	ns	ns	ns
<i>O. bezoarticus</i>	1 vs. 3/4 4 vs. 2/3	1 vs. 4	1 vs. 2/3/4 2 vs. 3/4 1 vs. 2/3/4 2 vs. 4	ns	ns	3 vs. 4
<i>R. fulvorufula</i>	ns	1 vs. 2/3/4	1 vs. 2/3/4	ns	1 vs. 3/4	1 vs. 2/3/4
<i>R. tarandus</i>	1 vs. 3/4 2 vs. 4	1 vs. 2/3/4 2 vs. 4	1 vs. 2/3/4 2 vs. 3/4	ns	ns	ns

**Table 8.A2.** Descriptive circular statistics for *A. americana*. n, number of observed angles; SD, circular standard deviation; SE, standard error of mean.

	Stage	n	$\mu$ Mean vector	$\theta$ Circular median	$\kappa$ Concentration	Circular variance	SD	SE	95 % Confidence interval ( $\pm$ ) for $\mu$
m1	1	170	52.145°	58°	5.785	0.091	25.020°	1.916°	48.388° 55.901°
	2	154	52.847°	55°	5.594	0.094	25.493°	2.051°	48.826° 56.868°
	3	133	50.016°	51°	5.096	0.104	26.865°	2.325°	45.458° 54.575°
	4	118	51.358°	55°	4.722	0.113	28.059°	2.577°	46.305° 56.411°
m2	1	153	53.609°	58°	6.880	0.076	22.743°	1.837°	50.008° 57.210°
	2	132	53.501°	58°	6.087	0.086	24.324°	2.114°	49.356° 57.646°
	3	129	47.268°	50°	5.608	0.094	25.458°	2.238°	42.880° 51.655°
	4	130	47.836°	50°	5.310	0.100	26.248°	2.298°	43.330° 52.341°
m3	1	95	65.604°	67°	13.238	0.039	16.064°	1.648°	62.374° 68.835°
	2	130	59.369°	64°	6.083	0.086	24.333°	2.131°	55.191° 63.548°
	3	135	57.613°	62°	6.986	0.075	22.555°	1.939°	53.811° 61.415°
	4	139	57.718°	61°	7.043	0.074	22.455°	1.903°	53.987° 61.448°
M1	1	180	44.084°	41°	6.596	0.079	23.274°	1.733°	40.687° 47.481°
	2	179	41.917°	40°	5.250	0.101	26.416°	1.971°	38.053° 45.781°
	3	175	38.028°	38°	5.505	0.096	25.721°	1.941°	34.223° 41.834°
	4	159	38.555°	38°	5.205	0.102	26.546°	2.102°	34.435° 42.675°
M2	1	169	48.093°	49°	6.689	0.078	23.095°	1.775°	44.614° 51.572°
	2	180	43.626°	42°	5.592	0.094	25.499°	1.898°	39.906° 47.346°
	3	183	42.388°	41°	4.987	0.107	27.197°	2.007°	38.454° 46.322°
	4	170	44.424°	43.5°	5.159	0.103	26.679°	2.042°	40.419° 48.428°
M3	1	99	58.052°	63°	6.732	0.078	23.015°	2.311°	53.522° 62.582°
	2	127	51.533°	50°	7.001	0.074	22.530°	1.997°	47.617° 55.448°
	3	151	45.826°	47°	5.922	0.089	24.697°	2.007°	41.891° 49.761°
	4	191	42.614°	42°	5.811	0.091	24.957°	1.803°	39.079° 46.149°
Total	m1	575	51.685°	55°	5.314	0.100	26.238°	1.092°	49.544° 53.827°
	m2	544	50.962°	56°	5.879	0.089	24.797°	1.062°	48.881° 53.043°
	m3	499	59.664°	64°	7.236	0.072	22.128°	0.990°	57.724° 61.604°
	M1	693	40.744°	39°	5.550	0.095	25.605°	0.971°	38.840° 42.648°
	M2	702	44.595°	44°	5.485	0.096	25.775°	0.971°	42.691° 46.499°
	M3	568	48.183°	49°	5.933	0.089	24.672°	1.034°	46.157° 50.210°

**Table 8.A3.** Descriptive circular statistics for *A. buselaphus*. n, number of observed angles; SD, circular standard deviation; SE, standard error of mean.

	Stage	n	$\mu$ Mean vector	$\theta$ Circular median	$\kappa$ Concentration	Circular variance	SD	SE	95 % Confidence interval ( $\pm$ ) for $\mu$
m1	1	216	47.856°	49°	5.936	0.088	24.665°	1.676°	44.570° 51.142°
	2	184	50.429°	52°	6.121	0.086	24.250°	1.785°	46.928° 53.929°
	3	121	51.413°	51°	6.104	0.086	24.287°	2.205°	47.090° 55.736°
	4	84	54.381°	58°	6.400	0.082	23.662°	2.579°	49.326° 59.437°
m2	1	223	50.302°	50°	5.598	0.094	25.481°	1.704°	46.962° 53.642°
	2	226	49.661°	50°	5.076	0.105	26.925°	1.788°	46.156° 53.165°
	3	214	47.162°	47°	5.579	0.095	25.531°	1.743°	43.745° 50.578°
	4	168	47.828°	49°	5.305	0.100	26.261°	2.023°	43.863° 51.793°
m3	1	162	52.562°	54°	6.164	0.085	24.156°	1.896°	48.846° 56.278°
	2	170	53.704°	52°	6.242	0.084	23.989°	1.838°	50.102° 57.307°
	3	178	50.137°	51°	5.950	0.088	24.631°	1.844°	46.522° 53.751°
	4	178	54.240°	58°	6.247	0.084	23.978°	1.795°	50.721° 57.759°
M1	1	159	50.956°	51°	6.784	0.077	22.919°	1.816°	47.396° 54.516°
	2	188	47.004°	48°	6.024	0.087	24.465°	1.782°	43.510° 50.497°
	3	157	46.274°	46°	5.704	0.092	25.218°	2.010°	42.334° 50.214°
	4	143	47.229°	48°	5.513	0.096	25.701°	2.146°	43.022° 51.436°
M2	1	191	52.025°	52°	6.249	0.084	23.975°	1.733°	48.628° 55.421°
	2	239	43.445°	42°	5.451	0.097	25.864°	1.670°	40.170° 46.719°
	3	235	42.063°	41°	5.156	0.103	26.687°	1.738°	38.656° 45.47°
	4	210	40.781°	38.5°	4.940	0.108	27.344°	1.883°	37.089° 44.473°
M3	1	216	51.185°	53°	6.676	0.078	23.120°	1.571°	48.105° 54.266°
	2	266	44.582°	46°	5.711	0.092	25.200°	1.543°	41.558° 47.607°
	3	257	44.020°	44°	6.537	0.080	23.387°	1.457°	41.163° 46.877°
	4	261	42.715°	41°	6.242	0.084	23.989°	1.483°	39.808° 45.623°
Total	m1	605	50.261°	51°	6.043	0.087	24.422°	0.992°	48.317° 52.205°
	m2	831	48.817°	49°	5.370	0.098	26.083°	0.903°	47.047° 50.588°
	m3	688	52.654°	53°	6.123	0.086	24.246°	0.923°	50.844° 54.464°
	M1	647	47.859°	49°	5.953	0.088	24.626°	0.967°	45.964° 49.755°
	M2	875	44.341°	44°	5.260	0.101	26.388°	0.891°	42.595° 46.087°
	M3	1000	45.383°	47°	6.151	0.085	24.184°	0.764°	43.886° 46.881°

**Table 8.A4.** Descriptive circular statistics for *A. cervicapra*. n, number of observed angles; SD, circular standard deviation; SE, standard error of mean.

	Stage	n	$\mu$ Mean vector	$\theta$ Circular median	$\kappa$ Concentration	Circular variance	SD	SE	95 % Confidence interval ( $\pm$ ) for $\mu$
m1	1	79	56.334°	55°	8.496	0.061	20.297°	2.282°	51.860° 60.808°
	2	81	55.325°	59°	6.294	0.083	23.881°	2.600°	50.130° 60.521°
	3	71	54.378°	55°	6.161	0.085	24.162°	2.864°	48.764° 59.993°
	4	57	63.265°	70°	5.617	0.094	25.434°	3.364°	56.671° 69.859°
m2	1	117	61.090°	67°	8.061	0.064	20.875°	1.929°	57.309° 64.871°
	2	111	55.376°	59°	7.225	0.072	22.147°	2.100°	51.259° 59.494°
	3	95	56.549°	59°	7.038	0.074	22.465°	2.303°	52.035° 61.063°
	4	132	54.027°	62°	5.114	0.104	26.812°	2.329°	49.460° 58.593°
m3	1	75	65.002°	68°	10.059	0.051	18.553°	2.141°	60.804° 69.200°
	2	86	63.715°	67°	10.413	0.049	18.218°	1.964°	59.866° 67.565°
	3	98	59.913°	59.5°	9.038	0.057	19.637°	1.983°	56.026° 63.799°
	4	95	60.862°	64°	8.114	0.064	20.803°	2.133°	56.681° 65.043°
M1	1	61	58.014°	61°	8.760	0.059	19.967°	2.555°	53.005° 63.023°
	2	97	55.618°	55°	7.804	0.066	21.243°	2.155°	51.392° 59.843°
	3	98	53.889°	54°	6.634	0.079	23.201°	2.341°	49.300° 58.479°
	4	61	56.022°	55°	5.892	0.089	24.766°	3.167°	49.814° 62.229°
M2	1	71	63.327°	67°	12.819	0.040	16.336°	1.938°	59.527° 67.126°
	2	153	50.439°	53°	6.383	0.082	23.697°	1.914°	46.688° 54.190°
	3	94	54.981°	56°	7.691	0.067	21.410°	2.207°	50.655° 59.307°
	4	73	59.380°	62°	7.063	0.074	22.421°	2.622°	54.240° 64.520°
M3	1	36	61.333°	66°	7.612	0.068	21.531°	3.586°	54.303° 68.362°
	2	85	62.377°	65°	7.217	0.072	22.160°	2.401°	57.669° 67.085°
	3	82	57.702°	65°	6.127	0.086	24.235°	2.673°	52.462° 62.942°
	4	93	59.777°	64°	7.800	0.066	21.248°	2.202°	55.461° 64.094°
Total	m1	288	56.920°	61°	6.451	0.081	23.559°	1.387°	54.202° 59.639°
	m2	455	56.734°	61°	6.481	0.081	23.498°	1.100°	54.577° 58.892°
	m3	354	62.179°	64°	9.153	0.056	19.506°	1.036°	60.147° 64.210°
	M1	317	55.631°	56°	7.087	0.073	22.380°	1.256°	53.169° 58.093°
	M2	391	55.607°	58°	7.156	0.073	22.263°	1.125°	53.402° 57.812°
	M3	296	60.148°	65°	7.033	0.074	22.472°	1.305°	57.590° 62.706°

**Table 8.A5.** Descriptive circular statistics for *A. marsupialis*. n, number of observed angles; SD, circular standard deviation; SE, standard error of mean.

	Stage	n	$\mu$ Mean vector	$\theta$ Circular median	$\kappa$ Concentration	Circular variance	SD	SE	95 % Confidence interval ( $\pm$ ) for $\mu$
m1	1	160	52.125°	58°	5.315	0.100	26.236°	2.071°	48.066° 56.184°
	2	132	53.451°	62°	4.946	0.107	27.325°	2.374°	48.798° 58.104°
	3	109	50.162°	60°	4.215	0.128	29.968°	2.862°	44.551° 55.774°
	4	80	55.114°	64°	4.549	0.118	28.668°	3.198°	48.846° 61.383°
m2	1	154	55.136°	61°	6.564	0.080	23.336°	1.878°	51.454° 58.819°
	2	156	51.915°	59°	5.103	0.104	26.844°	2.145°	47.709° 56.120°
	3	160	51.613°	61°	5.136	0.103	26.746°	2.111°	47.476° 55.751°
	4	132	49.200°	50°	4.994	0.106	27.175°	2.361°	44.572° 53.828°
m3	1	94	64.460°	65.5°	11.618	0.044	17.198°	1.773°	60.984° 67.936°
	2	113	60.292°	62°	8.724	0.059	20.010°	1.881°	56.604° 63.980°
	3	112	57.007°	60°	7.878	0.066	21.135°	1.996°	53.095° 60.919°
	4	128	53.450°	57°	7.255	0.072	22.098°	1.951°	49.625° 57.276°
M1	1	134	52.443°	55°	6.077	0.086	24.347°	2.101°	48.326° 56.561°
	2	125	51.362°	57°	5.201	0.102	26.556°	2.371°	46.714° 56.010°
	3	112	48.765°	49.5°	5.081	0.104	26.910°	2.538°	43.789° 53.740°
	4	124	45.716°	49°	4.990	0.106	27.187°	2.437°	40.939° 50.493°
M2	1	155	51.399°	55°	6.084	0.086	24.331°	1.952°	47.573° 55.226°
	2	160	49.576°	50°	6.224	0.084	24.027°	1.897°	45.856° 53.295°
	3	178	44.936°	42°	5.039	0.105	27.037°	2.023°	40.971° 48.901°
	4	168	49.617°	50°	5.289	0.100	26.308°	2.026°	45.644° 53.589°
M3	1	108	61.817°	64°	9.542	0.054	19.079°	1.835°	58.219° 65.414°
	2	159	53.065°	54°	7.147	0.073	22.277°	1.765°	49.605° 56.526°
	3	166	52.501°	52°	6.966	0.075	22.591°	1.752°	49.067° 55.935°
	4	168	51.313°	57°	6.145	0.085	24.197°	1.864°	47.658° 54.968°
Total	m1	495	49.672°	53°	5.275	0.100	26.347°	1.182°	47.354° 51.990°
	m2	661	48.784°	50°	5.541	0.095	25.630°	0.995°	46.832° 50.735°
	m3	601	54.028°	56°	6.908	0.075	22.693°	0.925°	52.215° 55.841°
	M1	481	52.547°	60°	4.780	0.112	27.860°	1.268°	50.062° 55.032°
	M2	602	52.086°	58°	5.359	0.099	26.114°	1.063°	50.003° 54.169°
	M3	447	58.427°	61°	8.145	0.064	20.761°	0.981°	56.504° 60.351°

**Table 8.A6.** Descriptive circular statistics for *A. melampus*. n, number of observed angles; SD, circular standard deviation; SE, standard error of mean.

	Stage	n	$\mu$ Mean vector	$\theta$ Circular median	$\kappa$ Concentration	Circular variance	SD	SE	95 % Confidence interval ( $\pm$ ) for $\mu$
m1	1	86	57.980°	65.5°	6.366	0.082	23.731°	2.556°	52.969° 62.991°
	2	92	55.605°	60°	6.439	0.081	23.583°	2.456°	50.790° 60.420°
	3	68	48.175°	50°	5.155	0.103	26.689°	3.231°	41.842° 54.509°
	4	62	53.247°	61°	5.775	0.091	25.044°	3.176°	47.020° 59.473°
m2	1	80	62.355°	69°	6.970	0.075	22.584°	2.523°	57.410° 67.300°
	2	96	52.614°	58°	5.712	0.092	25.199°	2.568°	47.580° 57.649°
	3	81	51.681°	57°	5.846	0.090	24.875°	2.760°	46.270° 57.092°
	4	76	45.570°	51.5°	5.316	0.099	26.231°	3.004°	39.681° 51.458°
m3	1	73	55.959°	63°	5.402	0.098	25.996°	3.038°	50.004° 61.914°
	2	93	61.858°	67°	7.002	0.074	22.527°	2.334°	57.283° 66.433°
	3	93	61.143°	66°	9.256	0.056	19.390°	2.010°	57.203° 65.082°
	4	107	55.689°	61°	6.671	0.078	23.130°	2.234°	51.310° 60.068°
M1	1	109	49.312°	56°	5.013	0.106	27.115°	2.592°	44.230° 54.393°
	2	105	49.240°	49°	5.522	0.096	25.678°	2.502°	44.335° 54.145°
	3	92	46.107°	44.5°	4.714	0.113	28.086°	2.922°	40.379° 51.834°
	4	59	44.447°	42°	4.662	0.115	28.266°	3.672°	37.250° 51.645°
M2	1	110	53.795°	55°	5.962	0.088	24.604°	2.343°	49.202° 58.388°
	2	111	52.136°	54°	6.324	0.083	23.818°	2.258°	47.710° 56.563°
	3	120	47.886°	49°	5.065	0.105	26.957°	2.456°	43.071° 52.701°
	4	122	48.503°	48°	4.986	0.107	27.199°	2.458°	43.685° 53.321°
M3	1	68	68.417°	69°	16.478	0.031	14.340°	1.739°	65.008° 71.825°
	2	113	52.265°	56°	6.244	0.084	23.986°	2.254°	47.847° 56.683°
	3	127	51.795°	54°	5.224	0.101	26.491°	2.347°	47.195° 56.395°
	4	122	53.009°	58°	5.654	0.093	25.342°	2.291°	48.518° 57.500°
Total	m1	308	54.187°	60°	5.841	0.090	24.885°	1.416°	51.411° 56.963°
	m2	333	53.170°	58°	5.615	0.094	25.438°	1.392°	50.442° 55.899°
	m3	366	58.727°	64°	6.810	0.077	22.871°	1.194°	56.385° 61.068°
	M1	365	47.711°	50°	4.980	0.107	27.217°	1.422°	44.923° 50.498°
	M2	463	50.497°	53°	5.453	0.097	25.860°	1.200°	48.144° 52.849°
	M3	430	55.019°	60°	5.947	0.088	24.640°	1.187°	52.692° 57.345°

**Table 8.A7.** Descriptive circular statistics for *C. bactrianus*. n, number of observed angles; SD, circular standard deviation; SE, standard error of mean.

	Stage	n	$\mu$ Mean vector	$\theta$ Circular median	$\kappa$ Concentration	Circular variance	SD	SE	95 % Confidence interval ( $\pm$ ) for $\mu$
m1	1	142	56.169°	60°	6.390	0.082	23.682°	1.985°	52.277° 60.060°
	2	148	50.291°	55°	5.765	0.091	25.069°	2.058°	46.257° 54.325°
	3	102	48.311°	50°	5.366	0.099	26.093°	2.579°	43.254° 53.367°
	4	76	52.125°	52.5°	6.815	0.077	22.862°	2.620°	46.989° 57.261°
m2	1	155	60.994°	64°	7.331	0.071	21.972°	1.763°	57.537° 64.451°
	2	166	54.534°	58.5°	5.876	0.089	24.804°	1.923°	50.766° 58.303°
	3	178	54.894°	62°	5.352	0.099	26.131°	1.955°	51.060° 58.727°
	4	160	51.578°	57°	5.749	0.092	25.106°	1.982°	47.692° 55.463°
m3	1	112	67.813°	71.5°	10.425	0.049	18.207°	1.720°	64.442° 71.184°
	2	140	60.146°	64°	6.717	0.078	23.043°	1.945°	56.332° 63.960°
	3	143	57.764°	62°	6.067	0.086	24.369°	2.035°	53.775° 61.754°
	4	162	52.064°	56.5°	5.566	0.095	25.564°	2.005°	48.132° 55.995°
M1	1	130	52.069°	55°	5.895	0.089	24.760°	2.169°	47.818° 56.321°
	2	144	48.736°	50°	4.834	0.110	27.683°	2.302°	44.223° 53.249°
	3	138	47.695°	49°	4.815	0.111	27.745°	2.357°	43.074° 52.315°
	4	107	48.737°	55°	4.487	0.119	28.896°	2.787°	43.274° 54.200°
M2	1	170	54.414°	56°	6.534	0.080	23.394°	1.792°	50.900° 57.927°
	2	173	52.225°	54°	6.058	0.087	24.390°	1.852°	48.595° 55.856°
	3	191	50.593°	52°	5.364	0.099	26.098°	1.885°	46.897° 54.289°
	4	185	50.209°	53°	5.185	0.102	26.604°	1.952°	46.382° 54.037°
M3	1	117	57.323°	60°	8.450	0.061	20.355°	1.881°	53.636° 61.009°
	2	136	53.369°	55.5°	5.770	0.091	25.055°	2.145°	49.164° 57.575°
	3	146	52.296°	55°	5.741	0.092	25.127°	2.077°	48.225° 56.367°
	4	170	50.182°	53°	5.311	0.100	26.244°	2.009°	46.243° 54.122°
Total	m1	468	51.960°	56°	5.912	0.089	24.720°	1.141°	49.723° 54.197°
	m2	659	55.462°	61°	5.862	0.090	24.837°	0.966°	53.568° 57.356°
	m3	557	58.817°	64°	6.274	0.083	23.921°	1.012°	56.832° 60.802°
	M1	519	49.312°	52°	4.954	0.107	27.300°	1.196°	46.967° 51.656°
	M2	719	51.806°	54°	5.687	0.093	25.258°	0.941°	49.962° 53.650°
	M3	569	52.992°	57°	5.933	0.089	24.673°	1.033°	50.967° 55.017°

**Table 8.A8.** Descriptive circular statistics for *C. ibex*. n, number of observed angles; SD, circular standard deviation; SE, standard error of mean.

	Stage	n	$\mu$ Mean vector	$\theta$ Circular median	$\kappa$ Concentration	Circular variance	SD	SE	95 % Confidence interval ( $\pm$ ) for $\mu$
m1	1	171	49.221°	51°	5.306	0.100	26.258°	2.005°	45.291° 53.150°
	2	146	50.626°	50°	5.359	0.099	26.112°	2.157°	46.396° 54.855°
	3	122	49.260°	47°	5.033	0.105	27.055°	2.445°	44.467° 54.052°
	4	90	55.572°	60°	6.244	0.084	23.985°	2.525°	50.621° 60.522°
m2	1	175	49.457°	55°	5.167	0.103	26.656°	2.011°	45.514° 53.400°
	2	166	48.909°	55°	5.663	0.093	25.319°	1.962°	45.062° 52.756°
	3	168	48.800°	55°	5.719	0.092	25.182°	1.940°	44.996° 52.603°
	4	151	49.349°	57°	5.337	0.099	26.173°	2.126°	45.181° 53.518°
m3	1	169	56.131°	59°	8.838	0.058	19.873°	1.528°	53.136° 59.126°
	2	191	50.434°	52°	6.936	0.075	22.644°	1.637°	47.225° 53.643°
	3	192	48.513°	49°	7.092	0.073	22.371°	1.613°	45.351° 51.675°
	4	201	47.359°	48°	6.722	0.078	23.034°	1.623°	44.177° 50.541°
M1	1	183	52.384°	54°	6.782	0.077	22.923°	1.693°	49.066° 55.703°
	2	190	48.532°	50°	5.138	0.103	26.740°	1.936°	44.736° 52.328°
	3	173	49.061°	50°	4.840	0.110	27.664°	2.099°	44.946° 53.175°
	4	115	53.715°	62°	4.619	0.116	28.415°	2.644°	48.532° 58.897°
M2	1	167	51.373°	55°	6.067	0.086	24.370°	1.883°	47.681° 55.065°
	2	173	48.234°	51°	5.647	0.093	25.358°	1.925°	44.460° 52.008°
	3	161	48.403°	51°	5.645	0.093	25.365°	1.996°	44.490° 52.316°
	4	167	46.858°	49°	5.492	0.096	25.757°	1.990°	42.957° 50.760°
M3	1	124	56.660°	62°	6.327	0.083	23.811°	2.136°	52.473° 60.847°
	2	164	53.130°	56°	6.426	0.081	23.609°	1.841°	49.520° 56.740°
	3	173	53.272°	52°	7.694	0.067	21.406°	1.626°	50.084° 56.460°
	4	138	55.317°	54.5°	7.384	0.070	21.887°	1.862°	51.668° 58.967°
Total	m1	529	50.714°	51°	5.352	0.099	26.131°	1.134°	48.490° 52.937°
	m2	660	49.126°	55°	5.460	0.097	25.841°	1.004°	47.157° 51.095°
	m3	753	50.425°	53°	7.117	0.073	22.329°	0.813°	48.831° 52.018°
	M1	661	50.648°	52°	5.267	0.100	26.368°	1.024°	48.641° 52.655°
	M2	668	48.722°	51°	5.683	0.093	25.270°	0.976°	46.808° 50.636°
	M3	599	54.402°	56°	6.913	0.075	22.684°	0.926°	52.587° 56.218°

**Table 8.A9.** Descriptive circular statistics for *C. simum*. n, number of observed angles; SD, circular standard deviation; SE, standard error of mean.

	Stage	n	$\mu$ Mean vector	$\theta$ Circular median	$\kappa$ Concentration	Circular variance	SD	SE	95 % Confidence interval ( $\pm$ ) for $\mu$
m1	1	99	52.119°	56°	5.210	0.102	26.532°	2.662°	46.901° 57.338°
	2	90	49.877°	52°	4.503	0.119	28.834°	3.032°	43.933° 55.821°
	3	60	53.334°	59°	4.488	0.119	28.893°	3.721°	46.040° 60.629°
	4	59	55.311°	61°	5.298	0.100	26.281°	3.416°	48.615° 62.007°
m2	1	106	54.399°	61°	5.471	0.097	25.813°	2.503°	49.492° 59.306°
	2	121	48.943°	52°	5.626	0.094	25.411°	2.307°	44.421° 53.465°
	3	125	48.708°	51°	4.956	0.107	27.292°	2.436°	43.932° 53.484°
	4	127	49.508°	57°	4.248	0.127	29.831°	2.640°	44.333° 54.683°
m3	1	67	46.758°	47°	6.662	0.078	23.147°	2.825°	41.220° 52.295°
	2	101	50.438°	51°	5.550	0.095	25.605°	2.544°	45.451° 55.425°
	3	115	47.615°	48°	5.036	0.105	27.046°	2.517°	42.680° 52.550°
	4	121	55.506°	58°	7.105	0.073	22.348°	2.030°	51.527° 59.485°
M1	1	188	51.648°	56°	5.640	0.093	25.377°	1.848°	48.025° 55.271°
	2	204	51.892°	58°	5.298	0.100	26.283°	1.837°	48.291° 55.494°
	3	187	48.228°	50°	4.867	0.109	27.578°	2.013°	44.283° 52.173°
	4	137	47.454°	53°	4.598	0.116	28.492°	2.429°	42.693° 52.215°
M2	1	102	57.899°	62°	6.730	0.078	23.018°	2.277°	53.435° 62.362°
	2	144	55.677°	58.5°	5.963	0.088	24.603°	2.048°	51.663° 59.691°
	3	172	51.374°	55°	5.825	0.090	24.923°	1.898°	47.653° 55.094°
	4	194	48.849°	54°	5.241	0.101	26.441°	1.895°	45.134° 52.565°
M3	1	151	40.594°	42°	4.762	0.112	27.923°	2.267°	36.149° 45.039°
	2	107	54.106°	55°	6.027	0.087	24.458°	2.361°	49.477° 58.736°
	3	126	56.933°	63°	6.163	0.085	24.159°	2.150°	52.719° 61.147°
	4	160	56.395°	63°	5.475	0.096	25.801°	2.036°	52.403° 60.388°
Total	m1	308	52.323°	58°	5.086	0.104	26.895°	1.003°	48.072° 52.006°
	m2	479	50.248°	54°	5.309	0.100	26.252°	0.949°	48.495° 52.215°
	m3	404	50.574°	51°	5.873	0.090	24.812°	0.994°	54.097° 57.995°
	M1	716	50.039°	55°	4.828	0.110	27.703°	1.575°	49.235° 55.411°
	M2	763	50.355°	55°	4.954	0.107	27.299°	1.245°	47.808° 52.689°
	M3	621	56.046°	62°	5.817	0.090	24.943°	1.239°	48.145° 53.004°

**Table 8.A10.** Descriptive circular statistics for *C. taurinus*. n, number of observed angles; SD, circular standard deviation; SE, standard error of mean.

	Stage	n	$\mu$ Mean vector	$\theta$ Circular median	$\kappa$ Concentration	Circular variance	SD	SE	95 % Confidence interval ( $\pm$ ) for $\mu$
m1	1	80	60.382°	58.5°	7.183	0.072	22.217°	2.482°	55.517° 65.247°
	2	104	51.477°	52.5°	6.116	0.086	24.262°	2.376°	46.819° 56.135°
	3	78	56.017°	61.5°	6.021	0.087	24.472°	2.767°	50.592° 61.442°
	4	63	51.518°	58°	5.158	0.103	26.682°	3.356°	44.940° 58.096°
m2	1	130	53.017°	54°	6.928	0.075	22.657°	1.985°	49.125° 56.909°
	2	127	50.422°	50°	6.733	0.077	23.014°	2.040°	46.423° 54.421°
	3	90	53.450°	56°	7.031	0.074	22.477°	2.367°	48.810° 58.091°
	4	141	49.149°	48°	5.525	0.095	25.671°	2.158°	44.917° 53.380°
m3	1	156	53.125°	52°	6.958	0.075	22.605°	1.808°	49.580° 56.670°
	2	156	54.132°	56°	7.887	0.066	21.122°	1.690°	50.819° 57.445°
	3	149	55.834°	54°	8.995	0.057	19.687°	1.612°	52.674° 58.994°
	4	145	53.965°	55°	6.887	0.076	22.731°	1.886°	50.268° 57.662°
M1	1	90	57.164°	61°	6.729	0.078	23.022°	2.424°	52.411° 61.916°
	2	108	54.612°	58.5°	5.951	0.088	24.631°	2.367°	49.971° 59.252°
	3	99	54.483°	59°	6.182	0.085	24.117°	2.421°	49.737° 59.229°
	4	77	51.746°	55°	5.930	0.089	24.680°	2.809°	46.239° 57.252°
M2	1	143	53.226°	57°	6.503	0.080	23.455°	1.959°	49.385° 57.067°
	2	122	54.455°	56°	7.862	0.066	21.158°	1.914°	50.703° 58.208°
	3	112	52.711°	54°	7.010	0.074	22.513°	2.125°	48.545° 56.878°
	4	93	54.906°	58°	5.895	0.089	24.759°	2.564°	49.880° 59.932°
M3	1	187	49.927°	49°	6.126	0.086	24.239°	1.770°	46.457° 53.398°
	2	163	53.151°	56°	6.187	0.085	24.107°	1.886°	49.454° 56.848°
	3	133	55.718°	58°	6.118	0.086	24.256°	2.101°	51.600° 59.836°
	4	170	53.084°	56°	5.473	0.096	25.807°	1.976°	49.210° 56.958°
Total	m1	325	54.797°	58°	5.966	0.088	24.595°	1.363°	52.126° 57.468°
	m2	488	51.319°	52°	6.388	0.082	23.686°	1.071°	49.219° 53.418°
	m3	606	54.258°	54°	7.574	0.069	21.589°	0.876°	52.540° 55.976°
	M1	374	54.609°	59°	6.147	0.085	24.193°	1.249°	52.160° 57.058°
	M2	470	53.754°	56°	6.774	0.077	22.937°	1.057°	51.682° 55.826°
	M3	653	52.732°	55°	5.916	0.089	24.710°	0.966°	50.839° 54.625°

**Table 8.A11.** Descriptive circular statistics for *D. bicornis*. n, number of observed angles; SD, circular standard deviation; SE, standard error of mean.

	Stage	n	$\mu$ Mean vector	$\theta$ Circular median	$\kappa$ Concentration	Circular variance	SD	SE	95 % Confidence interval ( $\pm$ ) for $\mu$
m1	1	92	50.476°	55°	4.903	0.108	27.459°	2.857°	44.876° 56.077°
	2	70	60.147°	68.5°	4.968	0.107	27.255°	3.251°	53.773° 66.520°
	3	48	54.269°	59°	5.438	0.097	25.900°	3.732°	46.952° 61.586°
	4	42	61.873°	69°	7.225	0.072	22.146°	3.414°	55.180° 68.566°
m2	1	71	43.934°	49°	4.429	0.121	29.114°	3.447°	37.178° 50.691°
	2	110	44.162°	44°	4.237	0.127	29.877°	2.841°	38.593° 49.730°
	3	78	59.826°	67°	5.737	0.092	25.137°	2.842°	54.254° 65.397°
	4	52	52.850°	61°	4.833	0.110	27.688°	3.832°	45.338° 60.361°
m3	1	74	39.551°	40°	4.623	0.116	28.403°	3.294°	33.094° 46.009°
	2	88	48.909°	49°	5.116	0.104	26.807°	2.852°	43.317° 54.501°
	3	95	46.010°	49°	5.021	0.106	27.092°	2.774°	40.571° 51.449°
	4	86	58.567°	65°	5.412	0.098	25.968°	2.796°	53.086° 64.047°
M1	1	78	57.057°	62°	5.998	0.088	24.522°	2.773°	51.621° 62.493°
	2	142	40.785°	38.5°	4.514	0.119	28.795°	2.411°	36.060° 45.511°
	3	130	42.434°	40°	4.951	0.107	27.309°	2.390°	37.748° 47.121°
	4	111	48.499°	54°	4.677	0.114	28.213°	2.672°	43.261° 53.737°
M2	1	126	50.718°	54.5°	5.703	0.092	25.221°	2.244°	46.320° 55.117°
	2	154	46.779°	45.5°	5.269	0.100	26.364°	2.121°	42.622° 50.937°
	3	187	48.908°	50°	5.700	0.092	25.226°	1.842°	45.297° 52.519°
	4	195	49.766°	55°	5.216	0.102	26.512°	1.895°	46.051° 53.481°
M3	1	78	54.041°	61°	6.859	0.076	22.781°	2.577°	48.990° 59.093°
	2	123	48.463°	51°	6.879	0.076	22.746°	2.049°	44.447° 52.480°
	3	139	46.673°	49°	6.132	0.086	24.225°	2.052°	42.649° 50.696°
	4	154	45.197°	48°	6.590	0.079	23.286°	1.874°	41.523° 48.872°
Total	m1	252	55.824°	62°	5.153	0.103	26.696°	1.679°	52.533° 59.115°
	m2	311	49.587°	54°	4.457	0.120	29.007°	1.641°	46.371° 52.804°
	m3	343	48.548°	50°	4.786	0.111	27.841°	1.500°	45.608° 51.489°
	M1	461	45.908°	47°	4.691	0.114	28.164°	1.309°	43.342° 48.474°
	M2	662	49.013°	51°	5.434	0.097	25.911°	1.005°	47.042° 50.984°
	M3	494	47.827°	50°	6.466	0.081	23.529°	1.057°	45.754° 49.900°

**Table 8.A12.** Descriptive circular statistics for *D. pygargus*. n, number of observed angles; SD, circular standard deviation; SE, standard error of mean.

	Stage	n	$\mu$ Mean vector	$\theta$ Circular median	$\kappa$ Concentration	Circular variance	SD	SE	95 % Confidence interval ( $\pm$ ) for $\mu$
m1	1	222	52.127°	56°	5.870	0.090	24.817°	1.663°	48.866° 55.387°
	2	207	50.110°	55°	5.335	0.099	26.179°	1.817°	46.549° 53.671°
	3	159	54.582°	59°	5.626	0.094	25.412°	2.012°	50.637° 58.527°
	4	155	52.236°	57°	5.484	0.096	25.779°	2.067°	48.183° 56.289°
m2	1	195	49.129°	51°	5.476	0.096	25.799°	1.845°	45.513° 52.745°
	2	177	51.423°	55°	5.591	0.094	25.501°	1.914°	47.671° 55.174°
	3	175	53.072°	59°	5.784	0.091	25.022°	1.889°	49.369° 56.775°
	4	213	48.708°	50°	5.216	0.102	26.515°	1.814°	45.153° 52.264°
m3	1	144	59.872°	63°	7.206	0.072	22.179°	1.847°	56.252° 63.492°
	2	157	55.125°	56°	6.980	0.075	22.566°	1.799°	51.598° 58.652°
	3	177	55.384°	57°	6.995	0.074	22.539°	1.693°	52.066° 58.702°
	4	183	54.002°	57°	6.460	0.081	23.541°	1.738°	50.594° 57.410°
M1	1	239	45.579°	43°	5.839	0.090	24.892°	1.608°	42.427° 48.732°
	2	235	47.857°	47°	5.923	0.089	24.696°	1.609°	44.703° 51.011°
	3	218	48.343°	53°	5.346	0.099	26.148°	1.768°	44.877° 51.809°
	4	185	50.434°	52°	5.213	0.102	26.522°	1.946°	46.618° 54.250°
M2	1	232	48.602°	49°	5.948	0.088	24.636°	1.615°	45.435° 51.768°
	2	293	45.872°	47°	5.692	0.093	25.247°	1.473°	42.985° 48.759°
	3	301	45.297°	44°	5.166	0.103	26.660°	1.534°	42.290° 48.304°
	4	314	42.441°	42°	4.928	0.108	27.382°	1.542°	39.417° 45.464°
M3	1	117	61.007°	63°	9.282	0.055	19.361°	1.789°	57.500° 64.514°
	2	187	52.206°	52°	5.644	0.093	25.365°	1.852°	48.575° 55.837°
	3	205	52.328°	56°	5.886	0.089	24.780°	1.728°	48.939° 55.716°
	4	192	52.722°	56°	5.497	0.096	25.744°	1.855°	49.085° 56.358°
Total	m1	743	52.116°	57°	5.561	0.095	25.576°	0.937°	50.280° 53.953°
	m2	760	50.460°	55°	5.469	0.097	25.816°	0.935°	48.627° 52.293°
	m3	661	55.923°	58°	6.821	0.076	22.851°	0.888°	54.182° 57.664°
	M1	877	47.893°	48°	5.567	0.095	25.561°	0.862°	46.203° 49.582°
	M2	1140	45.347°	46°	5.332	0.099	26.189°	0.774°	43.829° 46.865°
	M3	701	53.897°	57°	5.965	0.088	24.599°	0.928°	52.078° 55.716°

**Table 8.A13.** Descriptive circular statistics for *E. davidianus*. n, number of observed angles; SD, circular standard deviation; SE, standard error of mean.

	Stage	n	$\mu$ Mean vector	$\theta$ Circular median	$\kappa$ Concentration	Circular variance	SD	SE	95 % Confidence interval ( $\pm$ ) for $\mu$
m1	1	218	50.818°	54°	6.052	0.087	24.402°	1.651°	47.583° 54.054°
	2	235	48.285°	51°	5.794	0.091	24.999°	1.628°	45.093° 51.478°
	3	233	47.996°	51°	5.323	0.099	26.212°	1.714°	44.635° 51.356°
	4	162	52.857°	57°	5.338	0.099	26.170°	2.053°	48.833° 56.881°
m2	1	257	47.094°	46°	5.854	0.090	24.856°	1.548°	44.059° 50.130°
	2	238	47.356°	47°	6.026	0.087	24.460°	1.583°	44.252° 50.460°
	3	255	47.751°	48°	5.674	0.093	25.292°	1.582°	44.650° 50.851°
	4	242	47.837°	49°	5.808	0.091	24.964°	1.602°	44.696° 50.979°
m3	1	233	51.815°	54°	6.513	0.080	23.435°	1.534°	48.808° 54.821°
	2	236	50.845°	50°	6.910	0.075	22.690°	1.476°	47.952° 53.737°
	3	243	46.759°	49°	6.654	0.078	23.162°	1.484°	43.850° 49.669°
	4	253	47.260°	48°	6.792	0.077	22.905°	1.439°	44.440° 50.080°
M1	1	156	48.489°	49°	6.617	0.079	23.232°	1.858°	44.847° 52.132°
	2	239	42.571°	41°	5.537	0.095	25.639°	1.656°	39.325° 45.817°
	3	172	47.564°	47°	5.578	0.095	25.533°	1.944°	43.753° 51.375°
	4	159	47.935°	54°	4.723	0.113	28.054°	2.220°	43.583° 52.287°
M2	1	175	45.819°	44°	6.478	0.081	23.506°	1.775°	42.340° 49.299°
	2	247	41.996°	38°	6.711	0.078	23.054°	1.465°	39.124° 44.869°
	3	243	39.103°	36°	6.197	0.085	24.084°	1.543°	36.078° 42.128°
	4	248	39.913°	38°	5.367	0.098	26.092°	1.654°	36.670° 43.156°
M3	1	200	48.309°	49°	7.291	0.071	22.038°	1.557°	45.256° 51.361°
	2	230	43.134°	42°	6.537	0.080	23.388°	1.540°	40.114° 46.154°
	3	259	42.939°	42°	6.171	0.085	24.141°	1.498°	40.002° 45.876°
	4	267	38.686°	39°	5.634	0.094	25.390°	1.552°	35.644° 41.728°
Total	m1	848	49.730°	51°	5.598	0.094	25.482°	0.874°	48.017° 51.443°
	m2	992	47.507°	47°	5.834	0.090	24.903°	0.790°	45.959° 49.054°
	m3	965	49.110°	49°	6.660	0.078	23.150°	0.744°	47.650° 50.569°
	M1	726	46.203°	46°	5.478	0.096	25.793°	0.956°	44.329° 48.076°
	M2	913	41.403°	39°	6.060	0.087	24.384°	0.806°	39.823° 42.983°
	M3	956	42.949°	42°	6.178	0.085	24.125°	0.779°	41.421° 44.477°

**Table 8.A14.** Descriptive circular statistics for *E. quagga*. n, number of observed angles; SD, circular standard deviation; SE, standard error of mean.

	Stage	n	$\mu$ Mean vector	$\theta$ Circular median	$\kappa$ Concentration	Circular variance	SD	SE	95 % Confidence interval ( $\pm$ ) for $\mu$
m1	1	207	51.003°	56°	5.099	0.104	26.855°	1.863°	47.351° 54.655°
	2	196	51.104°	57°	5.230	0.101	26.474°	1.888°	47.404° 54.805°
	3	198	48.411°	50°	5.482	0.096	25.782°	1.829°	44.825° 51.997°
	4	155	46.518°	49°	5.040	0.105	27.035°	2.167°	42.269° 50.767°
m2	1	196	48.225°	51°	4.820	0.111	27.730°	1.977°	44.350° 52.100°
	2	209	48.636°	53°	5.020	0.106	27.093°	1.87°	44.970° 52.303°
	3	199	48.579°	49°	5.164	0.103	26.666°	1.887°	44.880° 52.278°
	4	167	47.640°	49°	5.369	0.098	26.084°	2.015°	43.690° 51.591°
m3	1	175	52.674°	58°	5.064	0.105	26.960°	2.034°	48.686° 56.662°
	2	195	51.926°	57°	5.403	0.098	25.992°	1.858°	48.283° 55.569°
	3	190	52.600°	57°	5.840	0.090	24.888°	1.803°	49.065° 56.134°
	4	167	53.647°	59°	5.435	0.097	25.908°	2.002°	49.723° 57.571°
M1	1	210	50.445°	55°	5.257	0.101	26.397°	1.818°	46.880° 54.009°
	2	210	48.731°	51°	5.541	0.095	25.629°	1.766°	45.269° 52.193°
	3	230	48.187°	51°	5.760	0.091	25.079°	1.651°	44.950° 51.425°
	4	198	48.624°	52°	5.461	0.097	25.838°	1.833°	45.030° 52.218°
M2	1	275	47.944°	49°	6.018	0.087	24.477°	1.474°	45.054° 50.834°
	2	253	46.037°	46°	5.731	0.092	25.151°	1.579°	42.941° 49.132°
	3	265	45.159°	46°	5.493	0.096	25.754°	1.58°	42.063° 48.256°
	4	217	47.307°	49°	5.569	0.095	25.556°	1.732°	43.912° 50.703°
M3	1	210	52.113°	54°	6.418	0.081	23.625°	1.628°	48.920° 55.305°
	2	241	51.924°	55°	5.676	0.093	25.286°	1.626°	48.735° 55.112°
	3	223	52.198°	57°	5.612	0.094	25.448°	1.702°	48.863° 55.534°
	4	225	51.319°	57°	5.308	0.100	26.254°	1.747°	47.894° 54.745°
Total	m1	756	49.431°	53°	5.193	0.102	26.580°	0.965°	47.539° 51.323°
	m2	771	48.300°	51°	5.073	0.105	26.934°	0.968°	46.402° 50.198°
	m3	727	52.677°	57°	5.425	0.097	25.933°	0.96°	50.795° 54.560°
	M1	848	48.980°	52°	5.499	0.096	25.737°	0.882°	47.250° 50.710°
	M2	1010	46.602°	48°	5.694	0.092	25.241°	0.793°	45.047° 48.157°
	M3	899	51.886°	56°	5.712	0.092	25.197°	0.839°	50.241° 53.531°

**Table 8.A15.** Descriptive circular statistics for *H. jemlahicus*. n, number of observed angles; SD, circular standard deviation; SE, standard error of mean.

	Stage	n	$\mu$ Mean vector	$\theta$ Circular median	$\kappa$ Concentration	Circular variance	SD	SE	95 % Confidence interval ( $\pm$ ) for $\mu$
m1	1	106	57.856°	63°	7.345	0.071	21.950°	2.130°	53.680° 62.032°
	2	105	57.225°	64°	6.515	0.080	23.431°	2.284°	52.747° 61.703°
	3	113	50.936°	55°	4.953	0.107	27.303°	2.563°	45.911° 55.961°
	4	81	50.892°	54°	5.124	0.103	26.780°	2.970°	45.069° 56.715°
m2	1	182	58.087°	64°	6.922	0.075	22.669°	1.679°	54.796° 61.378°
	2	195	57.433°	61°	6.714	0.078	23.050°	1.649°	54.201° 60.666°
	3	210	57.056°	61°	6.633	0.079	23.202°	1.599°	53.921° 60.192°
	4	176	56.486°	62°	5.690	0.093	25.252°	1.901°	52.760° 60.212°
m3	1	155	61.108°	64°	7.906	0.066	21.095°	1.693°	57.789° 64.427°
	2	150	62.660°	65°	10.276	0.050	18.345°	1.497°	59.725° 65.595°
	3	108	65.149°	68°	11.736	0.044	17.107°	1.646°	61.923° 68.375°
	4	141	64.422°	68°	10.850	0.047	17.827°	1.501°	61.480° 67.364°
M1	1	154	50.134°	51°	5.564	0.095	25.570°	2.057°	46.100° 54.167°
	2	145	51.208°	54°	5.653	0.093	25.344°	2.102°	47.088° 55.328°
	3	158	50.486°	51.5°	5.410	0.098	25.975°	2.063°	46.442° 54.531°
	4	130	53.182°	58°	5.463	0.097	25.833°	2.262°	48.748° 57.617°
M2	1	149	53.997°	55°	9.296	0.055	19.345°	1.584°	50.892° 57.102°
	2	168	49.635°	51°	6.494	0.080	23.473°	1.809°	46.088° 53.181°
	3	190	47.302°	49°	5.768	0.091	25.062°	1.816°	43.743° 50.861°
	4	192	49.098°	52°	5.811	0.091	24.959°	1.799°	45.572° 52.625°
M3	1	93	60.452°	65°	8.868	0.058	19.837°	2.056°	56.422° 64.482°
	2	126	53.787°	54°	7.036	0.074	22.467°	2.000°	49.867° 57.708°
	3	136	52.221°	55°	6.730	0.078	23.019°	1.972°	48.356° 56.087°
	4	145	53.580°	56°	6.511	0.080	23.440°	1.944°	49.768° 57.392°
Total	m1	405	54.425°	61°	5.753	0.091	25.098°	1.245°	51.984° 56.866°
	m2	763	57.270°	62°	6.464	0.081	23.532°	0.851°	55.602° 58.939°
	m3	554	63.172°	66°	9.752	0.053	18.860°	0.801°	61.602° 64.743°
	M1	587	51.169°	53°	5.511	0.096	25.708°	1.059°	49.092° 53.246°
	M2	699	49.817°	52°	6.409	0.082	23.642°	0.893°	48.066° 51.568°
	M3	500	54.562°	58°	6.944	0.075	22.630°	1.011°	52.580° 56.544°

**Table 8.A16.** Descriptive circular statistics for *K. ellipsiprymnus*. n, number of observed angles; SD, circular standard deviation; SE, standard error of mean.

	Stage	n	$\mu$ Mean vector	$\theta$ Circular median	$\kappa$ Concentration	Circular variance	SD	SE	95 % Confidence interval ( $\pm$ ) for $\mu$
m1	1	152	47.020°	49°	5.721	0.092	25.175°	2.039°	43.023° 51.017°
	2	141	47.546°	48°	5.692	0.093	25.247°	2.123°	43.384° 51.708°
	3	155	46.964°	49°	5.776	0.091	25.041°	2.009°	43.026° 50.901°
	4	123	48.845°	51°	6.169	0.085	24.145°	2.174°	44.582° 53.108°
m2	1	153	46.977°	50°	6.377	0.082	23.708°	1.915°	43.223° 50.730°
	2	143	48.388°	49°	6.460	0.081	23.542°	1.966°	44.533° 52.243°
	3	175	46.094°	45°	6.367	0.082	23.728°	1.792°	42.582° 49.606°
	4	177	47.834°	48°	5.957	0.088	24.616°	1.848°	44.212° 51.456°
m3	1	174	47.196°	48°	5.628	0.094	25.406°	1.923°	43.426° 50.966°
	2	195	45.430°	47°	5.560	0.095	25.578°	1.829°	41.845° 49.015°
	3	197	44.629°	43°	5.748	0.092	25.110°	1.786°	41.126° 48.131°
	4	170	44.451°	43°	5.806	0.091	24.969°	1.912°	40.702° 48.200°
M1	1	138	44.241°	43°	6.289	0.083	23.891°	2.031°	40.259° 48.223°
	2	162	40.877°	41°	6.026	0.087	24.461°	1.919°	37.114° 44.640°
	3	170	45.236°	44°	6.164	0.085	24.156°	1.850°	41.609° 48.864°
	4	146	44.633°	48°	6.179	0.085	24.124°	1.994°	40.724° 48.542°
M2	1	151	39.988°	39°	7.101	0.073	22.355°	1.818°	36.425° 43.551°
	2	152	40.313°	38°	6.449	0.081	23.563°	1.909°	36.570° 44.055°
	3	172	43.211°	42°	6.292	0.083	23.883°	1.819°	39.646° 46.777°
	4	177	45.538°	47°	6.684	0.078	23.106°	1.735°	42.136° 48.939°
M3	1	112	48.191°	54°	4.790	0.111	27.827°	2.624°	43.047° 53.334°
	2	129	46.851°	46°	5.535	0.095	25.644°	2.254°	42.431° 51.270°
	3	133	43.308°	39°	6.044	0.087	24.420°	2.115°	39.162° 47.454°
	4	151	43.844°	41°	5.450	0.097	25.866°	2.102°	39.724° 47.964°
Total	m1	571	47.530°	49°	5.815	0.090	24.948°	1.043°	45.486° 49.574°
	m2	648	47.283°	48°	6.264	0.084	23.944°	0.939°	45.442° 49.125°
	m3	736	45.406°	45°	5.673	0.093	25.295°	0.931°	43.581° 47.231°
	M1	616	43.726°	43°	6.129	0.086	24.232°	0.975°	41.814° 45.638°
	M2	652	42.418°	41°	6.551	0.080	23.361°	0.914°	40.626° 44.210°
	M3	525	45.360°	44°	5.415	0.098	25.961°	1.131°	43.142° 47.577°

**Table 8.A17.** Descriptive circular statistics for *L. glama*. n, number of observed angles; SD, circular standard deviation; SE, standard error of mean.

	Stage	n	$\mu$ Mean vector	$\theta$ Circular median	$\kappa$ Concentration	Circular variance	SD	SE	95 % Confidence interval ( $\pm$ ) for $\mu$
m1	1	56	44.716°	44°	4.176	0.129	30.131°	4.015°	36.845° 52.587°
	2	81	48.432°	47°	5.146	0.103	26.717°	2.963°	42.624° 54.241°
	3	96	47.878°	48°	4.887	0.109	27.512°	2.802°	42.385° 53.372°
	4	65	49.880°	51°	5.094	0.104	26.870°	3.327°	43.359° 56.402°
m2	1	72	40.458°	37°	5.387	0.098	26.036°	3.063°	34.453° 46.463°
	2	96	38.497°	37°	5.432	0.097	25.915°	2.641°	33.321° 43.674°
	3	106	40.109°	41°	5.654	0.093	25.341°	2.458°	35.291° 44.927°
	4	141	38.604°	36°	4.808	0.111	27.769°	2.334°	34.029° 43.178°
m3	1	63	43.195°	34°	4.212	0.128	29.979°	3.766°	35.812° 50.579°
	2	107	45.472°	44°	4.909	0.108	27.440°	2.647°	40.282° 50.662°
	3	110	46.802°	48°	5.125	0.103	26.777°	2.548°	41.806° 51.798°
	4	135	39.141°	37°	5.645	0.093	25.364°	2.180°	34.868° 43.414°
M1	1	91	43.499°	40°	6.665	0.078	23.141°	2.423°	38.748° 48.250°
	2	157	44.910°	45°	5.611	0.094	25.449°	2.028°	40.934° 48.886°
	3	127	44.707°	45°	4.690	0.114	28.167°	2.494°	39.818° 49.596°
	4	78	34.355°	27°	5.174	0.102	26.634°	3.010°	28.454° 40.257°
M2	1	66	40.646°	35°	6.108	0.086	24.277°	2.985°	34.795° 46.496°
	2	155	46.926°	46°	6.247	0.084	23.978°	1.924°	43.155° 50.697°
	3	136	46.116°	47°	6.666	0.078	23.139°	1.982°	42.231° 50.002°
	4	126	45.336°	44.5°	5.390	0.098	26.028°	2.315°	40.798° 49.874°
M3	1	55	38.302°	27°	4.656	0.115	28.286°	3.805°	30.842° 45.762°
	2	73	42.904°	39°	5.073	0.105	26.934°	3.147°	36.736° 49.073°
	3	119	43.883°	43°	5.003	0.106	27.148°	2.484°	39.014° 48.752°
	4	117	42.217°	42°	5.534	0.095	25.646°	2.367°	37.576° 46.858°
Total	m1	298	47.888°	48°	4.823	0.110	27.719°	1.602°	44.747° 51.030°
	m2	415	39.290°	38°	5.239	0.101	26.448°	1.296°	36.749° 41.830°
	m3	415	43.402°	41°	4.988	0.107	27.195°	1.332°	40.790° 46.014°
	M1	453	42.761°	41°	5.297	0.100	26.284°	1.233°	40.344° 45.178°
	M2	483	45.429°	45°	6.044	0.087	24.419°	1.110°	43.253° 47.604°
	M3	364	42.314°	40°	5.095	0.104	26.867°	1.406°	39.558° 45.069°

**Table 8.A18.** Descriptive circular statistics for *L. huanachus*. n, number of observed angles; SD, circular standard deviation; SE, standard error of mean.

	Stage	n	$\mu$ Mean vector	$\theta$ Circular median	$\kappa$ Concentration	Circular variance	SD	SE	95 % Confidence interval ( $\pm$ ) for $\mu$
m1	1	168	51.717°	53.5°	7.422	0.070	21.826°	1.683°	48.418° 55.015°
	2	172	48.579°	49°	6.266	0.084	23.939°	1.823°	45.004° 52.153°
	3	145	51.425°	52°	5.872	0.090	24.814°	2.058°	47.391° 55.460°
	4	91	50.414°	51°	6.266	0.084	23.938°	2.506°	45.500° 55.328°
m2	1	182	55.767°	58°	7.752	0.067	21.319°	1.579°	52.672° 58.863°
	2	188	50.690°	53°	6.354	0.082	23.756°	1.731°	47.297° 54.083°
	3	158	50.236°	52°	5.693	0.092	25.243°	2.005°	46.305° 54.168°
	4	139	50.597°	52°	6.315	0.083	23.837°	2.019°	46.639° 54.556°
m3	1	163	62.544°	65°	8.132	0.064	20.777°	1.626°	59.356° 65.732°
	2	210	55.190°	59°	6.281	0.083	23.907°	1.648°	51.959° 58.420°
	3	209	53.475°	54°	6.251	0.084	23.970°	1.656°	50.229° 56.722°
	4	201	53.127°	54°	7.545	0.069	21.633°	1.525°	50.138° 56.116°
M1	1	127	51.741°	52°	6.335	0.083	23.795°	2.109°	47.607° 55.876°
	2	135	49.592°	53°	6.514	0.080	23.434°	2.015°	45.643° 53.542°
	3	102	55.205°	59°	7.405	0.070	21.853°	2.162°	50.967° 59.444°
	4	73	57.641°	59°	7.045	0.074	22.453°	2.625°	52.494° 62.788°
M2	1	141	51.818°	53°	6.722	0.078	23.033°	1.938°	48.019° 55.617°
	2	149	47.612°	47°	6.092	0.086	24.312°	1.989°	43.712° 51.512°
	3	183	48.304°	48°	6.525	0.080	23.412°	1.729°	44.915° 51.693°
	4	178	48.942°	50°	6.418	0.082	23.626°	1.769°	45.475° 52.410°
M3	1	143	49.252°	50°	5.993	0.088	24.533°	2.049°	45.235° 53.269°
	2	152	50.239°	53.5°	5.511	0.096	25.706°	2.082°	46.157° 54.320°
	3	178	49.880°	52°	5.848	0.090	24.870°	1.862°	46.231° 53.529°
	4	183	49.571°	48°	6.245	0.084	23.982°	1.771°	46.099° 53.042°
Total	m1	576	50.504°	52°	6.429	0.081	23.604°	0.982°	48.578° 52.430°
	m2	667	51.970°	54°	6.423	0.081	23.615°	0.913°	50.180° 53.761°
	m3	783	55.751°	57°	6.736	0.077	23.007°	0.821°	54.140° 57.361°
	M1	437	52.883°	55°	6.631	0.079	23.207°	1.109°	50.709° 55.057°
	M2	651	49.085°	49°	6.408	0.082	23.646°	0.926°	47.270° 50.900°
	M3	656	49.739°	51°	5.899	0.089	24.752°	0.965°	47.847° 51.631°

**Table 8.A19.** Descriptive circular statistics for *L. walleri*. n, number of observed angles; SD, circular standard deviation; SE, standard error of mean.

	Stage	n	$\mu$ Mean vector	$\theta$ Circular median	$\kappa$ Concentration	Circular variance	SD	SE	95 % Confidence interval ( $\pm$ ) for $\mu$
m1	1	140	52.558°	58°	5.927	0.089	24.685°	2.083°	48.473° 56.642°
	2	143	51.525°	55°	5.882	0.089	24.789°	2.070°	47.466° 55.583°
	3	131	46.455°	50°	5.349	0.099	26.140°	2.280°	41.986° 50.925°
	4	90	54.717°	62°	5.536	0.095	25.642°	2.699°	49.426° 60.007°
m2	1	104	55.335°	62.5°	6.495	0.080	23.472°	2.299°	50.828° 59.843°
	2	154	49.647°	55°	5.729	0.092	25.155°	2.024°	45.679° 53.615°
	3	161	49.988°	56°	5.468	0.097	25.819°	2.032°	46.005° 53.971°
	4	139	47.504°	50°	5.159	0.103	26.680°	2.259°	43.076° 51.932°
m3	1	85	56.841°	62°	7.984	0.065	20.984°	2.274°	52.382° 61.300°
	2	157	51.484°	57°	5.598	0.094	25.484°	2.031°	47.503° 55.465°
	3	171	50.075°	53°	5.455	0.097	25.853°	1.974°	46.205° 53.944°
	4	169	46.998°	49°	5.276	0.100	26.344°	2.023°	43.033° 50.964°
M1	1	117	52.933°	57°	6.904	0.075	22.701°	2.097°	48.823° 57.043°
	2	186	45.605°	49°	5.313	0.100	26.241°	1.921°	41.839° 49.370°
	3	199	43.081°	47°	4.763	0.112	27.920°	1.975°	39.210° 46.953°
	4	169	42.947°	46°	5.156	0.103	26.688°	2.049°	38.930° 46.965°
M2	1	141	51.257°	51°	7.214	0.072	22.164°	1.865°	47.601° 54.913°
	2	203	47.737°	49°	6.323	0.083	23.820°	1.670°	44.463° 51.011°
	3	204	44.088°	42°	5.669	0.093	25.303°	1.769°	40.620° 47.555°
	4	222	40.672°	40°	4.520	0.118	28.774°	1.926°	36.895° 44.449°
M3	1	118	58.77°	60°	8.254	0.063	20.613°	1.896°	55.052° 62.487°
	2	182	48.766°	49°	6.222	0.084	24.031°	1.779°	45.278° 52.254°
	3	192	45.548°	47°	5.775	0.091	25.044°	1.805°	42.010° 49.086°
	4	197	45.538°	46°	5.305	0.100	26.263°	1.868°	41.876° 49.200°
Total	m1	504	51.073°	56°	5.615	0.094	25.438°	1.131°	48.855° 53.291°
	m2	558	50.291°	55°	5.565	0.095	25.566°	1.081°	48.173° 52.410°
	m3	582	50.586°	54°	5.618	0.094	25.431°	1.053°	48.522° 52.649°
	M1	671	45.508°	49°	5.210	0.102	26.532°	1.022°	43.504° 47.513°
	M2	770	45.447°	46°	5.507	0.096	25.716°	0.925°	43.633° 47.261°
	M3	689	48.714°	50°	5.835	0.090	24.902°	0.947°	46.857° 50.571°

**Table 8.A20.** Descriptive circular statistics for *N. goral*. n, number of observed angles; SD, circular standard deviation; SE, standard error of mean.

	Stage	n	$\mu$ Mean vector	$\theta$ Circular median	$\kappa$ Concentration	Circular variance	SD	SE	95 % Confidence interval ( $\pm$ ) for $\mu$
m1	1	127	52.072°	55°	6.609	0.079	23.248°	2.061°	48.033° 56.112°
	2	125	47.669°	46°	6.891	0.076	22.725°	2.031°	43.688° 51.650°
	3	108	48.553°	52°	6.377	0.082	23.708°	2.279°	44.086° 53.021°
	4	98	53.342°	57°	6.091	0.086	24.315°	2.453°	48.533° 58.151°
m2	1	235	48.145°	49°	7.258	0.072	22.092°	1.440°	45.323° 50.968°
	2	233	47.976°	49°	7.403	0.070	21.857°	1.431°	45.171° 50.780°
	3	219	47.978°	49°	7.254	0.072	22.099°	1.492°	45.053° 50.903°
	4	201	49.845°	50°	6.933	0.075	22.648°	1.596°	46.716° 52.973°
m3	1	202	54.808°	54°	8.877	0.058	19.826°	1.394°	52.075° 57.541°
	2	214	53.352°	53°	8.628	0.060	20.130°	1.375°	50.656° 56.048°
	3	210	52.695°	53°	8.571	0.060	20.201°	1.393°	49.964° 55.426°
	4	220	49.564°	49°	8.088	0.064	20.839°	1.404°	46.811° 52.316°
M1	1	154	47.813°	52°	5.458	0.097	25.846°	2.079°	43.736° 51.889°
	2	169	45.723°	46°	5.296	0.100	26.286°	2.019°	41.766° 49.680°
	3	131	48.317°	52°	5.361	0.099	26.107°	2.277°	43.853° 52.781°
	4	120	43.274°	46°	4.562	0.117	28.621°	2.607°	38.164° 48.384°
M2	1	188	48.367°	50.5°	6.442	0.081	23.576°	1.718°	45.000° 51.734°
	2	231	41.924°	42°	5.576	0.095	25.540°	1.678°	38.635° 45.213°
	3	226	40.995°	41°	5.302	0.100	26.270°	1.745°	37.575° 44.415°
	4	225	40.850°	42°	5.493	0.096	25.753°	1.714°	37.489° 44.210°
M3	1	169	54.711°	56°	8.427	0.061	20.385°	1.567°	51.639° 57.784°
	2	189	49.038°	51°	6.183	0.085	24.114°	1.752°	45.603° 52.472°
	3	201	49.769°	50°	6.835	0.076	22.826°	1.608°	46.616° 52.922°
	4	237	45.536°	48°	5.764	0.091	25.070°	1.626°	42.348° 48.724°
Total	m1	458	50.306°	52°	6.448	0.081	23.564°	1.100°	48.150° 52.462°
	m2	888	48.443°	49°	7.209	0.072	22.172°	0.743°	46.985° 49.900°
	m3	846	52.556°	52°	8.451	0.061	20.353°	0.699°	51.185° 53.927°
	M1	574	46.379°	48°	5.153	0.103	26.697°	1.112°	44.198° 48.559°
	M2	870	42.817°	44°	5.572	0.095	25.549°	0.865°	41.121° 44.512°
	M3	796	49.422°	51°	6.450	0.081	23.560°	0.834°	47.786° 51.057°

**Table 8.A21.** Descriptive circular statistics for *O. bezoarticus*. n, number of observed angles; SD, circular standard deviation; SE, standard error of mean.

	Stage	n	$\mu$ Mean vector	$\theta$ Circular median	$\kappa$ Concentration	Circular variance	SD	SE	95 % Confidence interval ( $\pm$ ) for $\mu$
m1	1	203	49.096°	51°	5.254	0.101	26.404°	1.850°	45.470° 52.723°
	2	151	40.631°	34°	4.604	0.116	28.468°	2.311°	36.100° 45.162°
	3	121	46.406°	48°	4.002	0.135	30.901°	2.800°	40.916° 51.895°
	4	95	55.936°	61°	4.045	0.134	30.705°	3.141°	49.780° 62.093°
m2	1	247	46.184°	46°	5.248	0.101	26.422°	1.678°	42.894° 49.474°
	2	266	45.156°	46°	5.700	0.092	25.228°	1.545°	42.129° 48.184°
	3	260	45.531°	43.5°	5.705	0.092	25.214°	1.561°	42.470° 48.592°
	4	174	40.302°	35.5°	5.365	0.099	26.097°	1.975°	36.430° 44.174°
m3	1	146	57.769°	61°	8.669	0.060	20.078°	1.661°	54.514° 61.025°
	2	216	52.289°	53°	6.814	0.077	22.864°	1.554°	49.243° 55.336°
	3	228	51.867°	56°	6.047	0.087	24.412°	1.615°	48.702° 55.032°
	4	216	50.773°	57°	5.364	0.099	26.098°	1.773°	47.298° 54.249°
M1	1	168	46.538°	46°	6.036	0.087	24.438°	1.883°	42.846° 50.229°
	2	223	38.761°	34°	6.182	0.085	24.116°	1.613°	35.599° 41.923°
	3	238	36.900°	32°	5.613	0.094	25.444°	1.647°	33.671° 40.128°
	4	219	38.317°	34°	4.450	0.120	29.035°	1.957°	34.480° 42.154°
M2	1	233	41.618°	40°	6.860	0.076	22.780°	1.491°	38.695° 44.541°
	2	258	36.084°	33°	6.872	0.076	22.758°	1.415°	33.309° 38.859°
	3	257	34.738°	31°	6.935	0.075	22.645°	1.411°	31.971° 37.504°
	4	278	35.098°	33°	6.217	0.084	24.041°	1.440°	32.274° 37.921°
M3	1	207	51.437°	55°	7.339	0.071	21.959°	1.525°	48.448° 54.427°
	2	224	43.147°	43°	6.620	0.079	23.228°	1.550°	40.108° 46.187°
	3	243	38.340°	34°	6.529	0.080	23.403°	1.500°	35.400° 41.280°
	4	252	35.854°	31°	6.287	0.083	23.895°	1.503°	32.907° 38.801°
Total	m1	570	47.408°	50°	4.431	0.121	29.108°	1.216°	45.024° 49.792°
	m2	947	44.638°	43°	5.481	0.096	25.784°	0.837°	42.998° 46.278°
	m3	806	52.788°	56°	6.301	0.083	23.865°	0.840°	51.142° 54.433°
	M1	848	39.680°	35°	5.357	0.099	26.118°	0.895°	37.925° 41.435°
	M2	1026	36.739°	33°	6.611	0.079	23.245°	0.725°	35.317° 38.160°
	M3	926	41.775°	40°	6.282	0.083	23.905°	0.785°	40.237° 43.313°

**Table 8.A22.** Descriptive circular statistics for *R. fulvorufula*. n, number of observed angles; SD, circular standard deviation; SE, standard error of mean.

	Stage	n	$\mu$ Mean vector	$\theta$ Circular median	$\kappa$ Concentration	Circular variance	SD	SE	95 % Confidence interval ( $\pm$ ) for $\mu$
m1	1	111	52.878°	52°	8.694	0.059	20.047°	1.902°	49.150° 56.606°
	2	168	45.871°	48°	5.733	0.092	25.146°	1.937°	42.073° 49.668°
	3	145	51.269°	52°	7.497	0.069	21.708°	1.801°	47.738° 54.801°
	4	120	50.873°	50.5°	6.750	0.077	22.982°	2.096°	46.764° 54.982°
m2	1	129	57.248°	61°	8.027	0.065	20.923°	1.841°	53.640° 60.857°
	2	180	48.247°	52°	6.519	0.080	23.424°	1.744°	44.828° 51.666°
	3	176	48.074°	49°	5.710	0.092	25.202°	1.897°	44.356° 51.793°
	4	171	46.364°	48°	5.869	0.090	24.820°	1.895°	42.648° 50.080°
m3	1	107	62.100°	64°	11.174	0.046	17.554°	1.696°	58.774° 65.425°
	2	159	53.838°	55°	6.777	0.077	22.932°	1.817°	50.276° 57.399°
	3	159	51.421°	51°	6.187	0.085	24.106°	1.909°	47.678° 55.164°
	4	160	54.058°	55°	6.878	0.076	22.747°	1.797°	50.536° 57.580°
M1	1	81	51.199°	48°	6.083	0.086	24.334°	2.700°	45.905° 56.493°
	2	126	46.329°	45°	5.185	0.102	26.605°	2.366°	41.691° 50.967°
	3	119	45.871°	44°	5.526	0.095	25.667°	2.349°	41.266° 50.476°
	4	82	47.803°	48°	5.499	0.096	25.739°	2.838°	42.239° 53.366°
M2	1	85	59.460°	60°	10.811	0.047	17.861°	1.937°	55.663° 63.256°
	2	159	40.515°	36°	5.866	0.090	24.827°	1.966°	36.661° 44.370°
	3	157	41.117°	37°	5.453	0.097	25.859°	2.060°	37.077° 45.156°
	4	186	40.652°	38°	5.433	0.097	25.913°	1.897°	36.934° 44.371°
M3	1	57	65.461°	67°	13.703	0.037	15.778°	2.089°	61.365° 69.557°
	2	128	47.991°	49°	6.282	0.083	23.906°	2.110°	43.854° 52.128°
	3	124	45.201°	49°	5.676	0.093	25.287°	2.268°	40.756° 49.646°
	4	176	46.564°	50°	5.714	0.092	25.193°	1.896°	42.847° 50.281°
Total	m1	544	49.878°	50°	6.772	0.077	22.941°	0.983°	47.952° 51.804°
	m2	656	49.515°	52°	6.171	0.085	24.141°	0.941°	47.670° 51.361°
	m3	585	54.801°	56°	6.950	0.075	22.618°	0.934°	52.970° 56.633°
	M1	408	47.468°	46°	5.478	0.096	25.793°	1.275°	44.969° 49.968°
	M2	587	43.553°	41°	5.604	0.094	25.467°	1.050°	41.495° 45.610°
	M3	485	48.901°	52°	5.903	0.089	24.741°	1.122°	46.702° 51.101°

**Table 8.A23.** Descriptive circular statistics for *R. tarandus*. n, number of observed angles; SD, circular standard deviation; SE, standard error of mean.

	Stage	n	$\mu$ Mean vector	$\theta$ Circular median	$\kappa$ Concentration	Circular variance	SD	SE	95 % Confidence interval ( $\pm$ ) for $\mu$
m1	1	136	60.706°	66°	7.267	0.072	22.077°	1.891°	56.999° 64.414°
	2	179	56.943°	62°	6.015	0.087	24.486°	1.828°	53.359° 60.526°
	3	170	53.884°	61°	5.067	0.105	26.953°	2.063°	49.839° 57.929°
	4	112	57.067°	61°	5.992	0.088	24.536°	2.315°	52.528° 61.606°
m2	1	215	57.787°	60°	6.208	0.084	24.061°	1.639°	54.574° 61.000°
	2	242	53.998°	57°	6.000	0.087	24.518°	1.574°	50.912° 57.084°
	3	227	54.272°	59°	5.866	0.090	24.828°	1.646°	51.046° 57.498°
	4	217	55.698°	63°	5.994	0.088	24.532°	1.663°	52.437° 58.958°
m3	1	163	60.318°	65°	6.463	0.081	23.534°	1.841°	56.709° 63.928°
	2	179	58.338°	64°	6.735	0.077	23.009°	1.718°	54.970° 61.706°
	3	199	55.101°	58°	6.208	0.084	24.062°	1.704°	51.762° 58.441°
	4	188	56.438°	62°	7.006	0.074	22.521°	1.641°	53.221° 59.655°
M1	1	165	50.019°	50°	6.293	0.083	23.883°	1.857°	46.378° 53.659°
	2	240	46.720°	46°	5.969	0.088	24.588°	1.585°	43.613° 49.828°
	3	229	49.379°	49°	5.398	0.098	26.008°	1.716°	46.015° 52.742°
	4	170	51.104°	56°	4.667	0.114	28.248°	2.162°	46.866° 55.341°
M2	1	192	56.344°	57°	9.267	0.056	19.377°	1.398°	53.604° 59.084°
	2	250	48.957°	49°	6.545	0.080	23.373°	1.477°	46.063° 51.852°
	3	254	48.383°	47°	5.566	0.095	25.565°	1.602°	45.243° 51.523°
	4	221	50.875°	52°	5.189	0.102	26.591°	1.785°	47.375° 54.376°
M3	1	103	65.053°	70°	8.450	0.061	20.356°	2.004°	61.123° 68.982°
	2	196	56.962°	61°	7.863	0.066	21.157°	1.510°	54.002° 59.922°
	3	224	53.164°	56°	7.181	0.072	22.220°	1.483°	50.256° 56.072°
	4	237	51.304°	54°	6.350	0.082	23.764°	1.542°	48.282° 54.327°
Total	m1	597	56.984°	62°	5.870	0.090	24.818°	1.014°	54.995° 58.972°
	m2	901	55.383°	59°	5.992	0.088	24.537°	0.816°	53.783° 56.984°
	m3	729	57.409°	62°	6.544	0.080	23.375°	0.865°	55.713° 59.104°
	M1	804	49.069°	50°	5.509	0.096	25.713°	0.905°	47.294° 50.844°
	M2	917	50.847°	52°	6.130	0.086	24.229°	0.799°	49.280° 52.413°
	M3	760	55.202°	58°	6.932	0.075	22.650°	0.821°	53.592° 56.811°

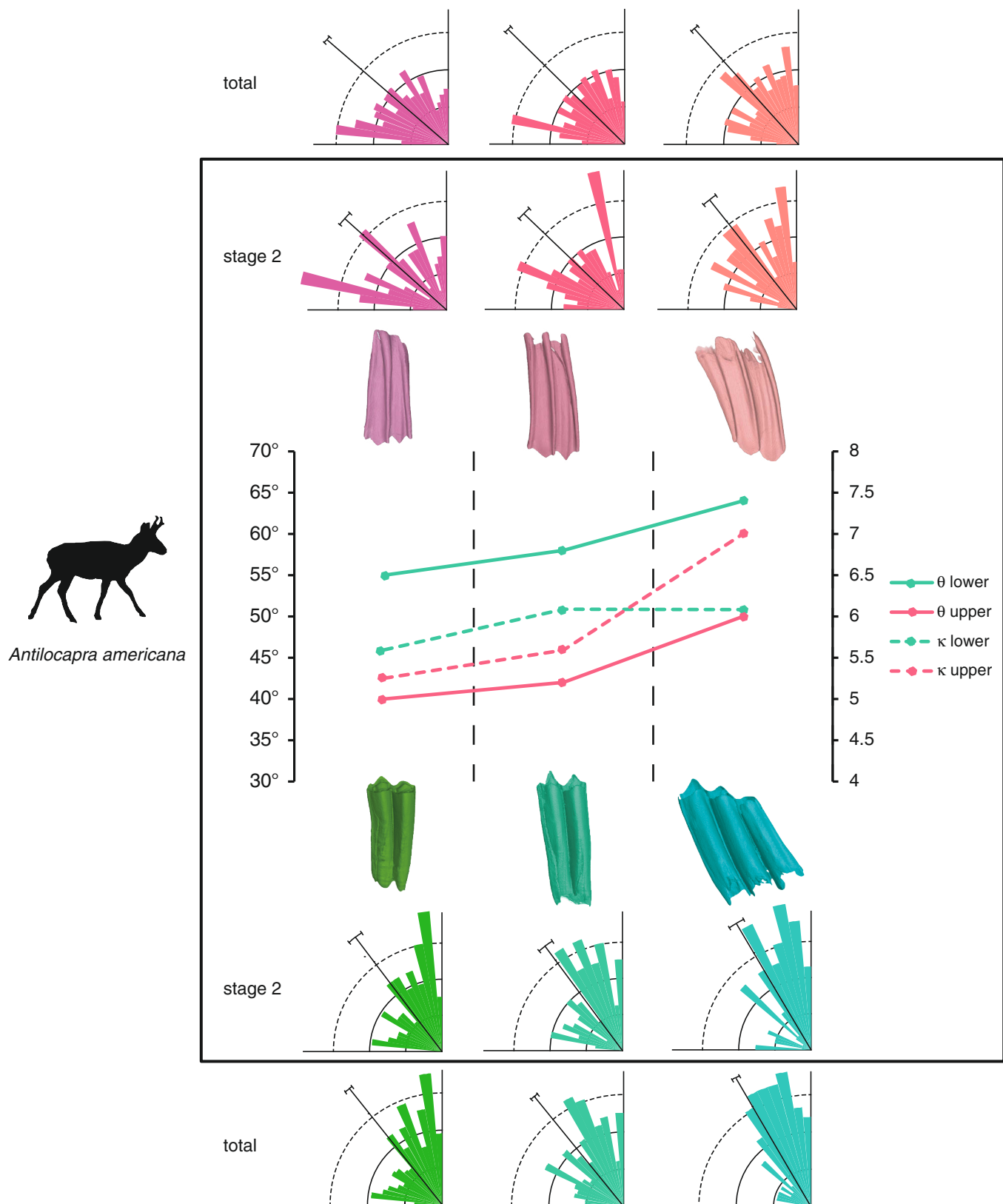


**Fig. 8.A2.** Summary of the most important statistical parameters for *Antilocapra americana*. ERAs are displayed as rose diagrams per tooth position for wear stage 2 and in total. The upper row shows upper M1–M3 (from left to right); the antagonistic lower teeth are in the lower row. The graphs show circular median ( $\theta$ ) and concentration ( $\kappa$ ) values per tooth position for stage 2.

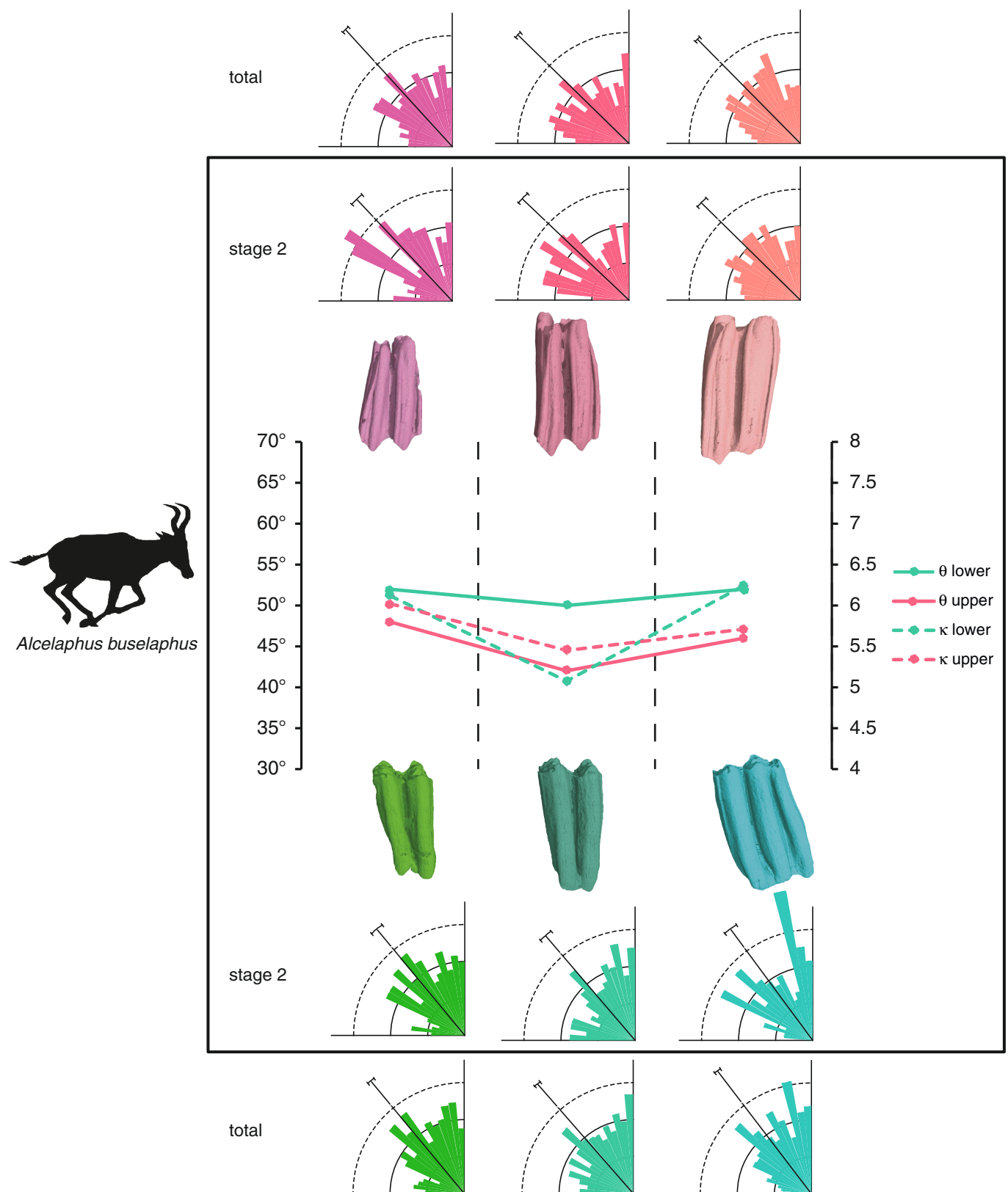


**Fig. 8.A3.** Summary of the most important statistical parameters for *Alcelaphus buselaphus*. ERAs are displayed as rose diagrams per tooth position for wear stage 2 and in total. The upper row shows upper M1-M3 (from left to right); the antagonistic lower teeth are in the lower row. The graphs show circular median ( $\theta$ ) and concentration ( $\kappa$ ) values per tooth position for stage 2.

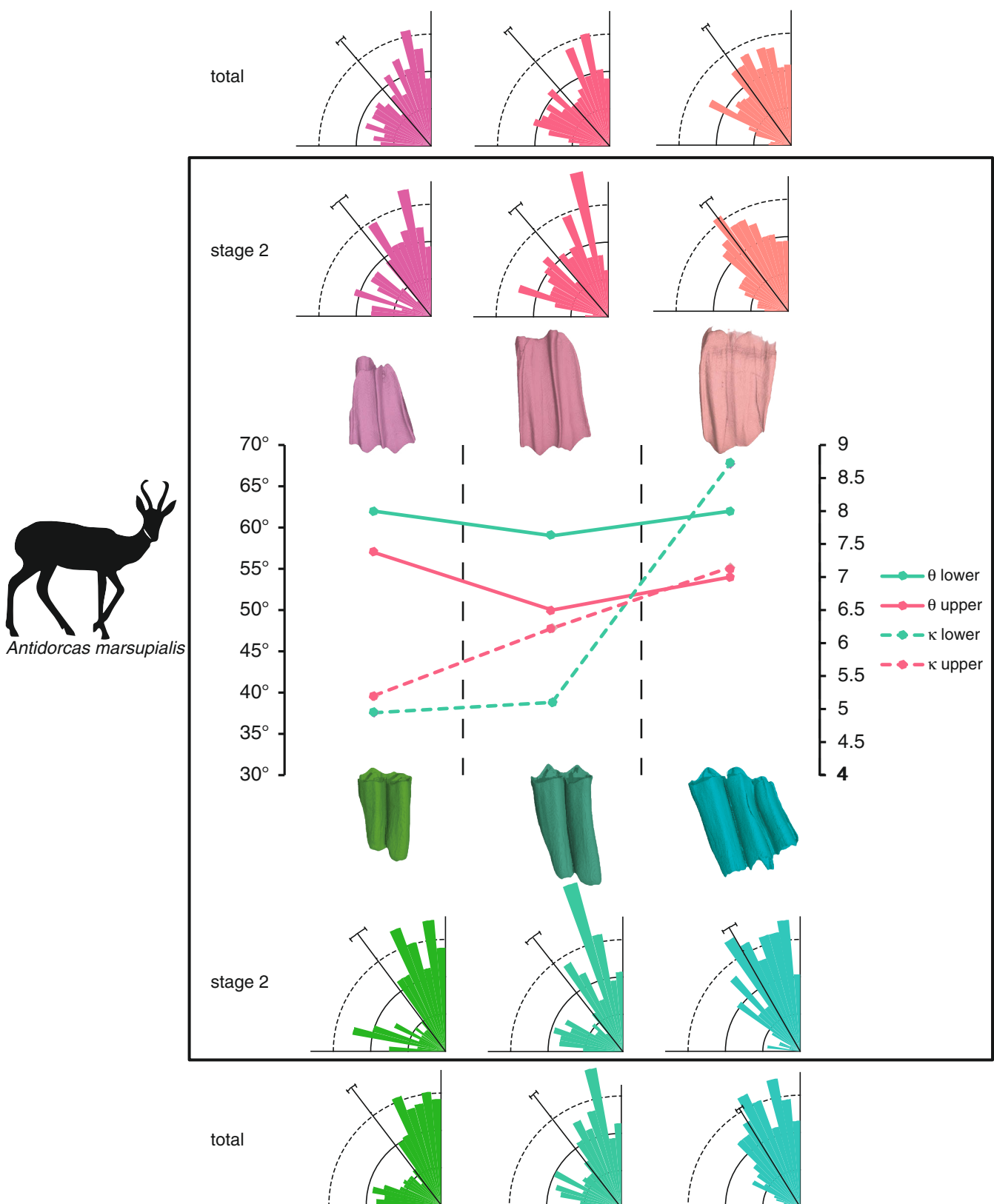


**Fig. 8.A4.** Summary of the most important statistical parameters for *Antidorcas marsupialis*. ERAs are displayed as rose diagrams per tooth position for wear stage 2 and in total. The upper row shows upper M1–M3 (from left to right); the antagonistic lower teeth are in the lower row. The graphs show circular median ( $\theta$ ) and concentration ( $\kappa$ ) values per tooth position for stage 2.

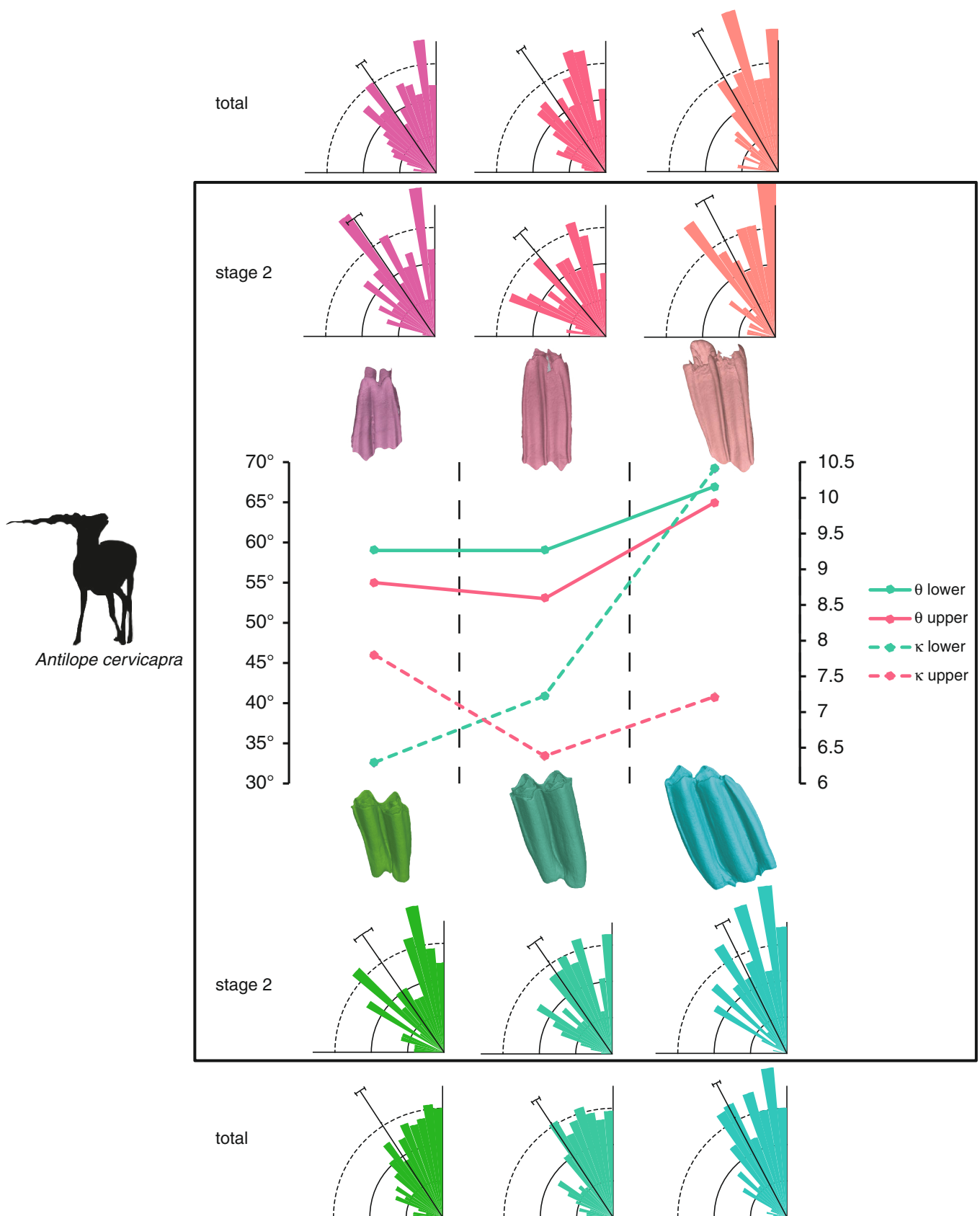


**Fig. 8.A5.** Summary of the most important statistical parameters for *Antilope cervicapra*. ERAs are displayed as rose diagrams per tooth position for wear stage 2 and in total. The upper row shows upper M1–M3 (from left to right); the antagonistic lower teeth are in the lower row. The graphs show circular median ( $\theta$ ) and concentration ( $\kappa$ ) values per tooth position for stage 2.

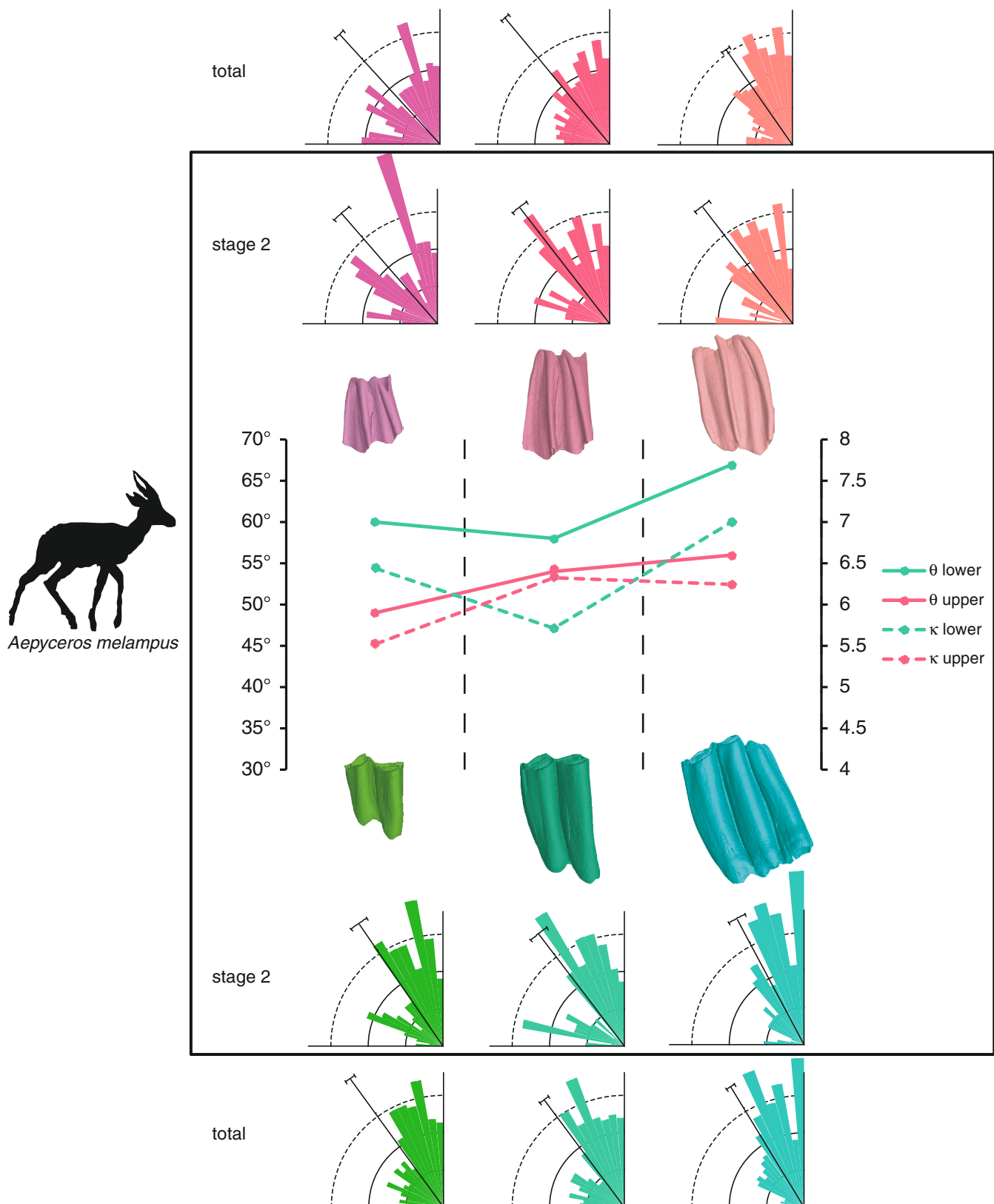


**Fig. 8.A6.** Summary of the most important statistical parameters for *Aepyceros melampus*. ERAs are displayed as rose diagrams per tooth position for wear stage 2 and in total. The upper row shows upper M1–M3 (from left to right); the antagonistic lower teeth are in the lower row. The graphs show circular median ( $\theta$ ) and concentration ( $\kappa$ ) values per tooth position for stage 2.

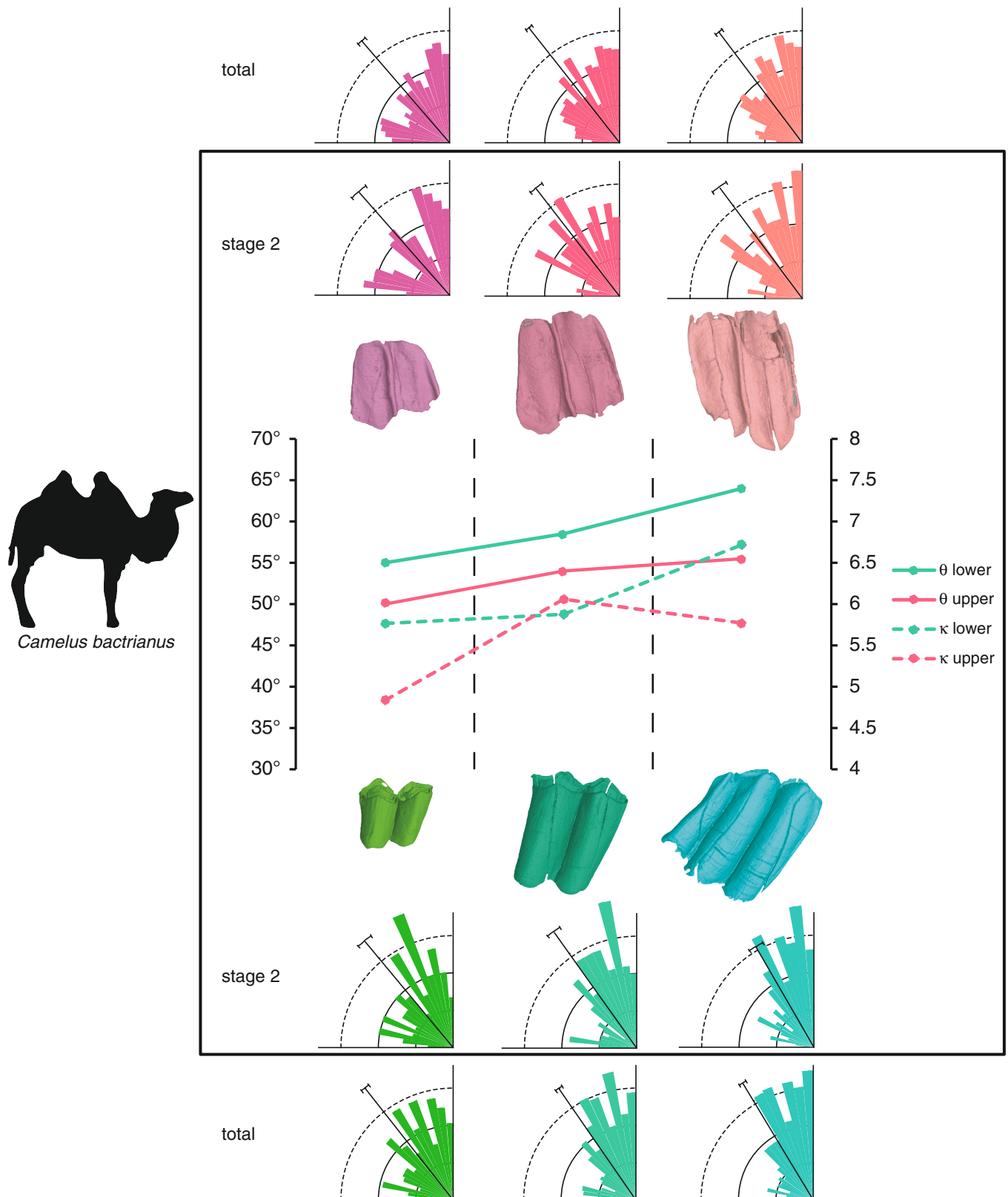


**Fig. 8.A7.** Summary of the most important statistical parameters for *Camelus bactrianus*. ERAs are displayed as rose diagrams per tooth position for wear stage 2 and in total. The upper row shows upper M1–M3 (from left to right); the antagonistic lower teeth are in the lower row. The graphs show circular median ( $\theta$ ) and concentration ( $\kappa$ ) values per tooth position for stage 2.

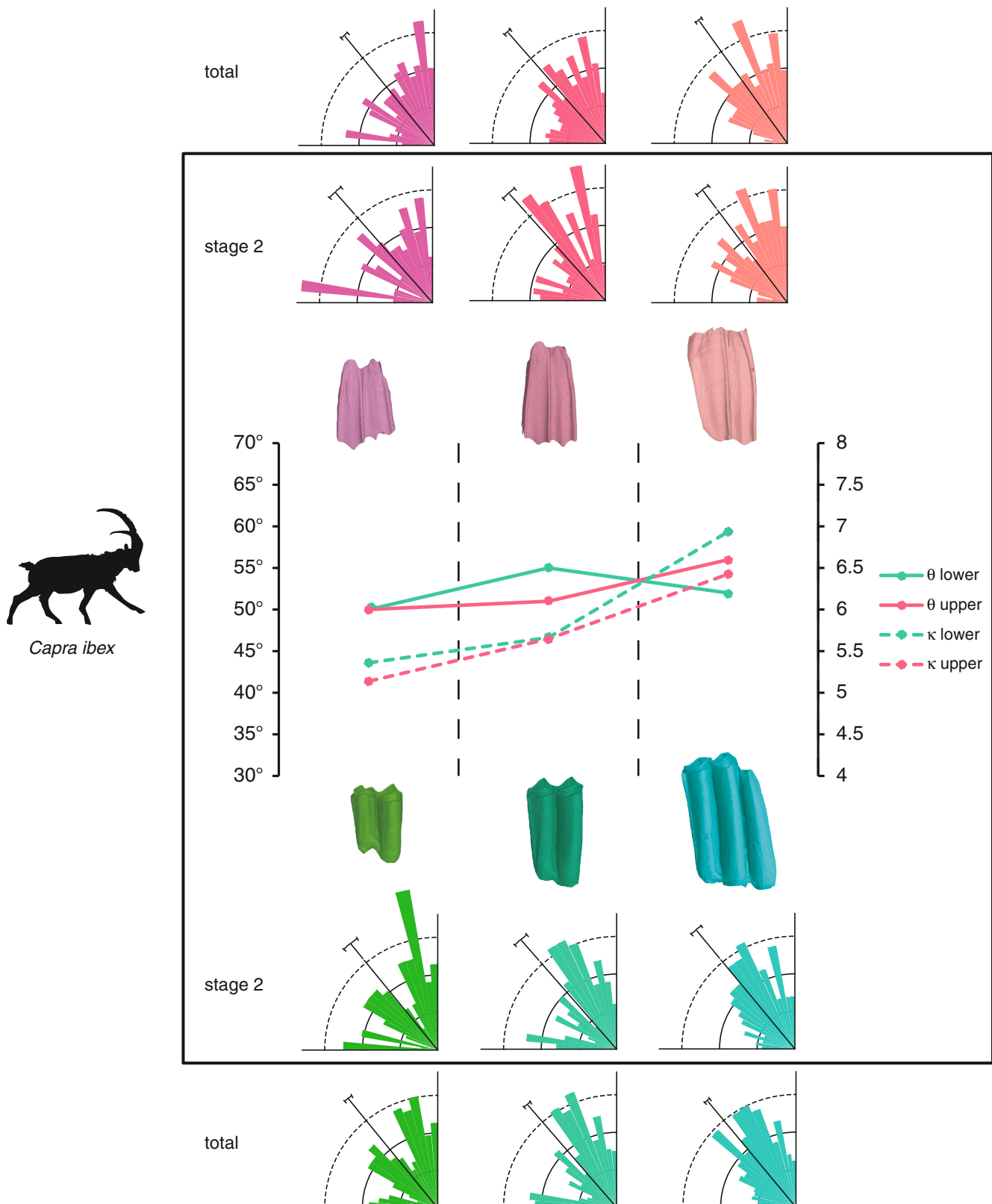


**Fig. 8.A8.** Summary of the most important statistical parameters for *Capra ibex*. ERAs are displayed as rose diagrams per tooth position for wear stage 2 and in total. The upper row shows upper M1–M3 (from left to right); the antagonistic lower teeth are in the lower row. The graphs show circular median ( $\theta$ ) and concentration ( $\kappa$ ) values per tooth position for stage 2.

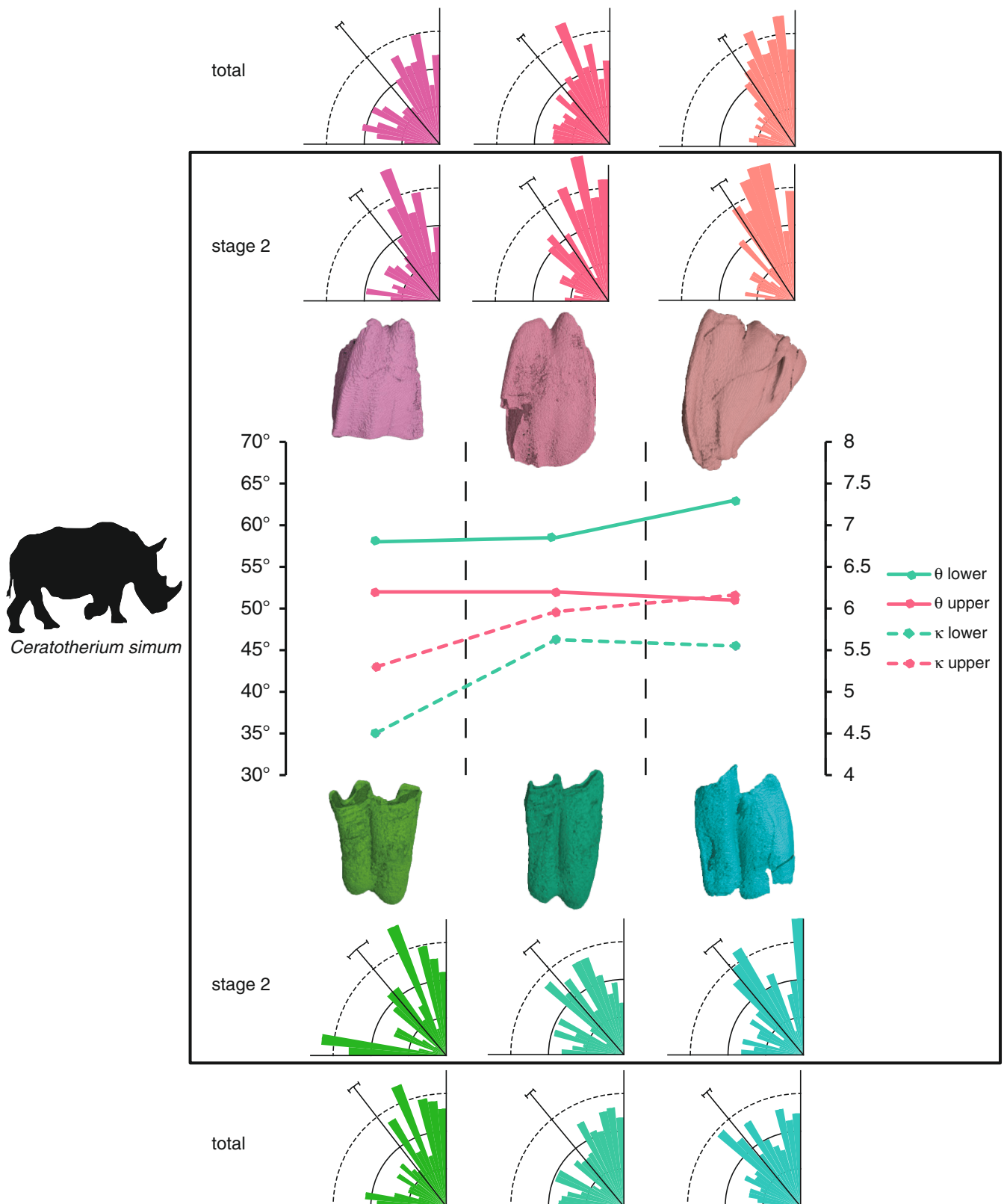


**Fig. 8.A9.** Summary of the most important statistical parameters for *Ceratotherium simum*. ERAs are displayed as rose diagrams per tooth position for wear stage 2 and in total. The upper row shows upper M1–M3 (from left to right); the antagonistic lower teeth are in the lower row. The graphs show circular median ( $\theta$ ) and concentration ( $\kappa$ ) values per tooth position for stage 2.

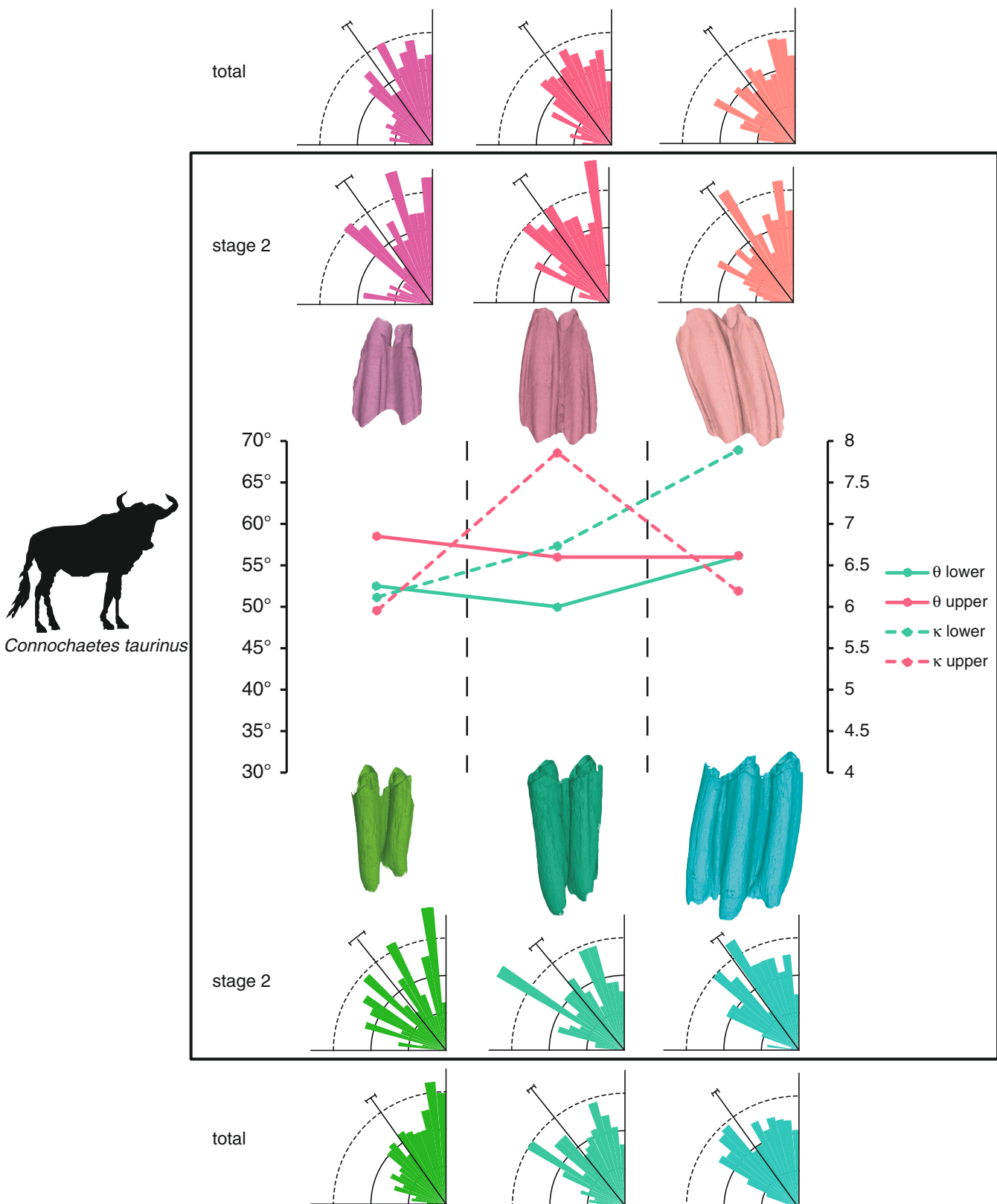


**Fig. 8.A10.** Summary of the most important statistical parameters for *Connochaetes taurinus*. ERAs are displayed as rose diagrams per tooth position for wear stage 2 and in total. The upper row shows upper M1–M3 (from left to right); the antagonistic lower teeth are in the lower row. The graphs show circular median ( $\theta$ ) and concentration ( $\kappa$ ) values per tooth position for stage 2.

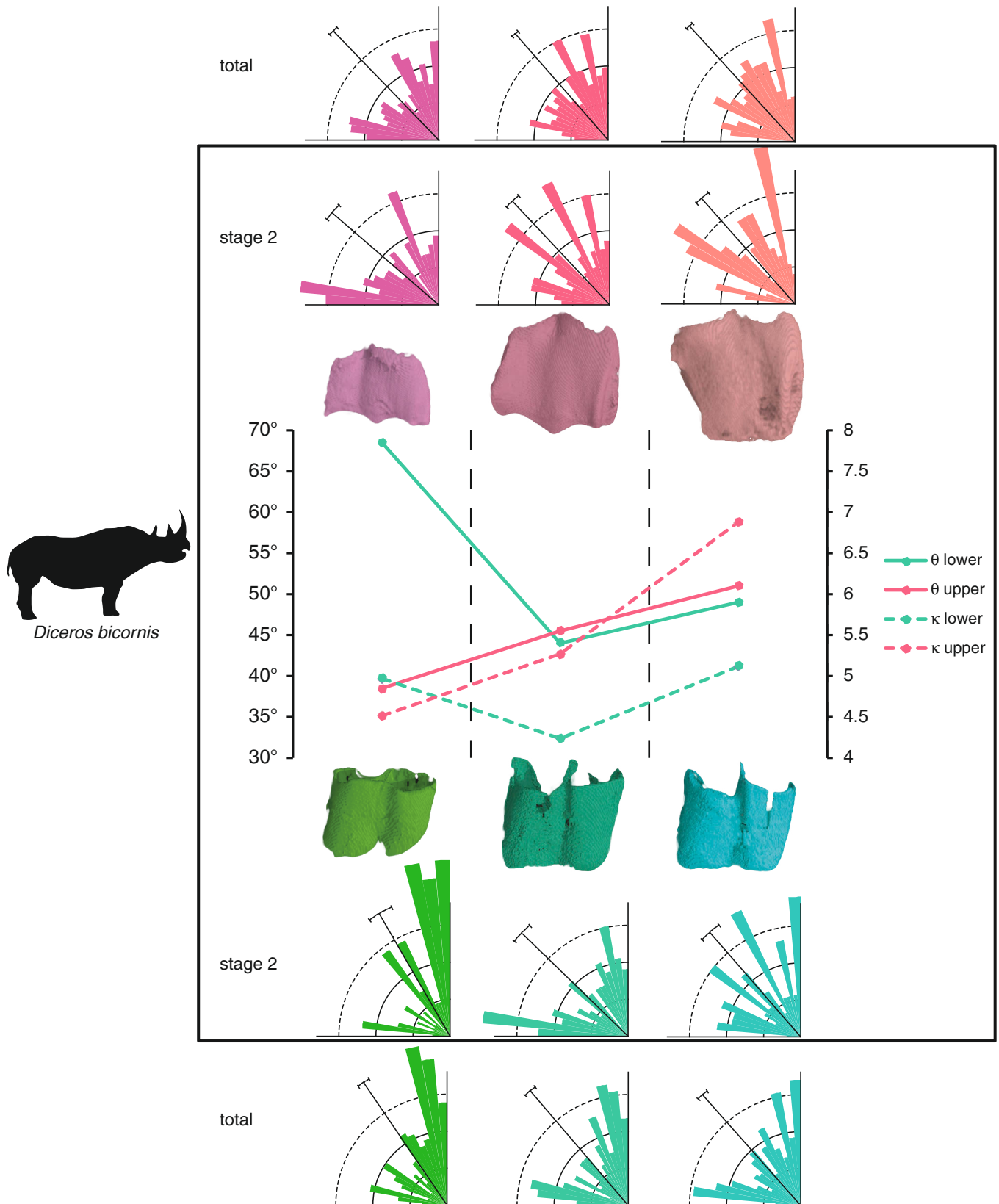


**Fig. 8.A11.** Summary of the most important statistical parameters for *Diceros bicornis*. ERAs are displayed as rose diagrams per tooth position for wear stage 2 and in total. The upper row shows upper M1–M3 (from left to right); the antagonistic lower teeth are in the lower row. The graphs show circular median ( $\theta$ ) and concentration ( $\kappa$ ) values per tooth position for stage 2.

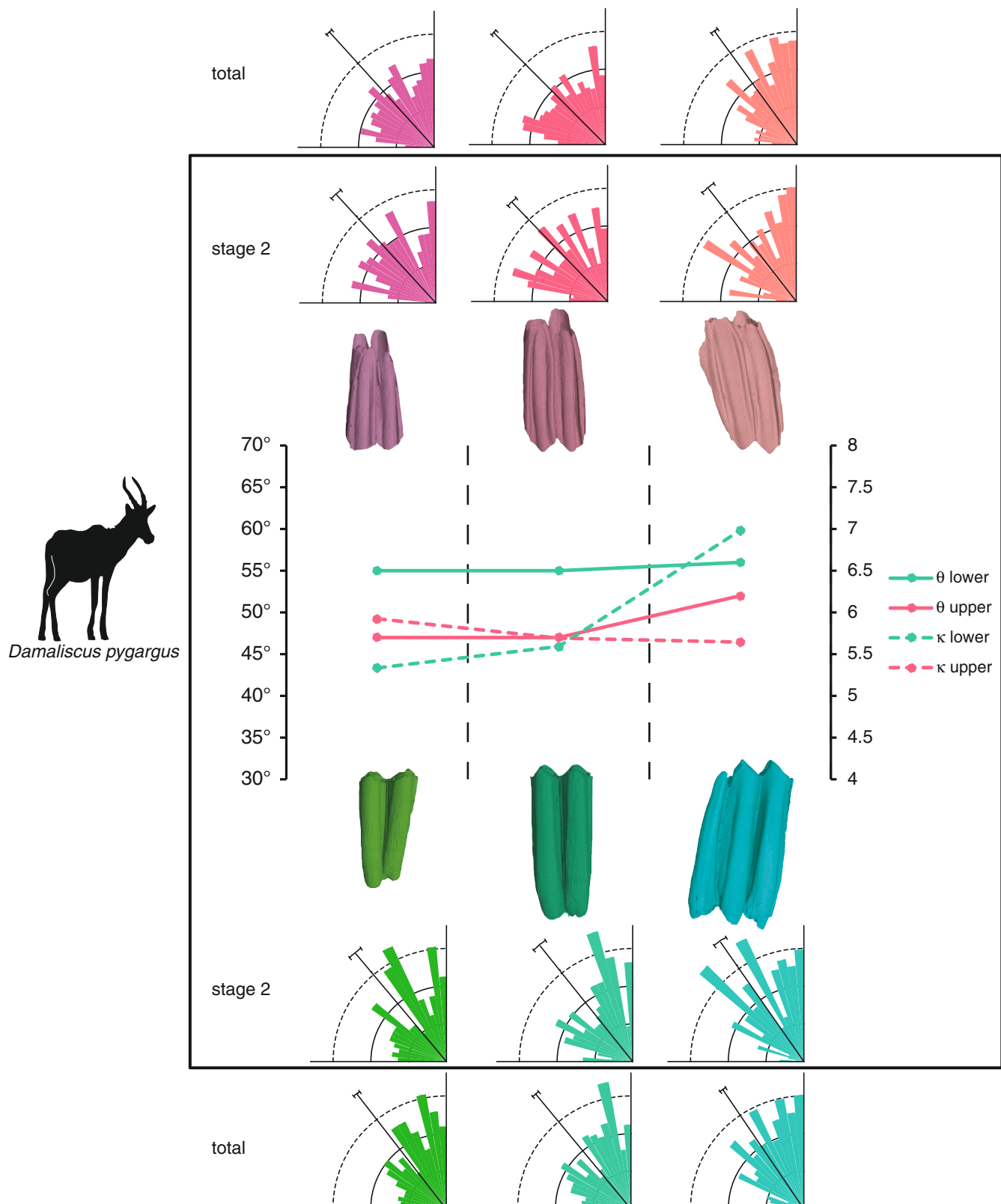


**Fig. 8.A12.** Summary of the most important statistical parameters for *Damaliscus pygargus*. ERAs are displayed as rose diagrams per tooth position for wear stage 2 and in total. The upper row shows upper M1–M3 (from left to right); the antagonistic lower teeth are in the lower row. The graphs show circular median ( $\theta$ ) and concentration ( $\kappa$ ) values per tooth position for stage 2.

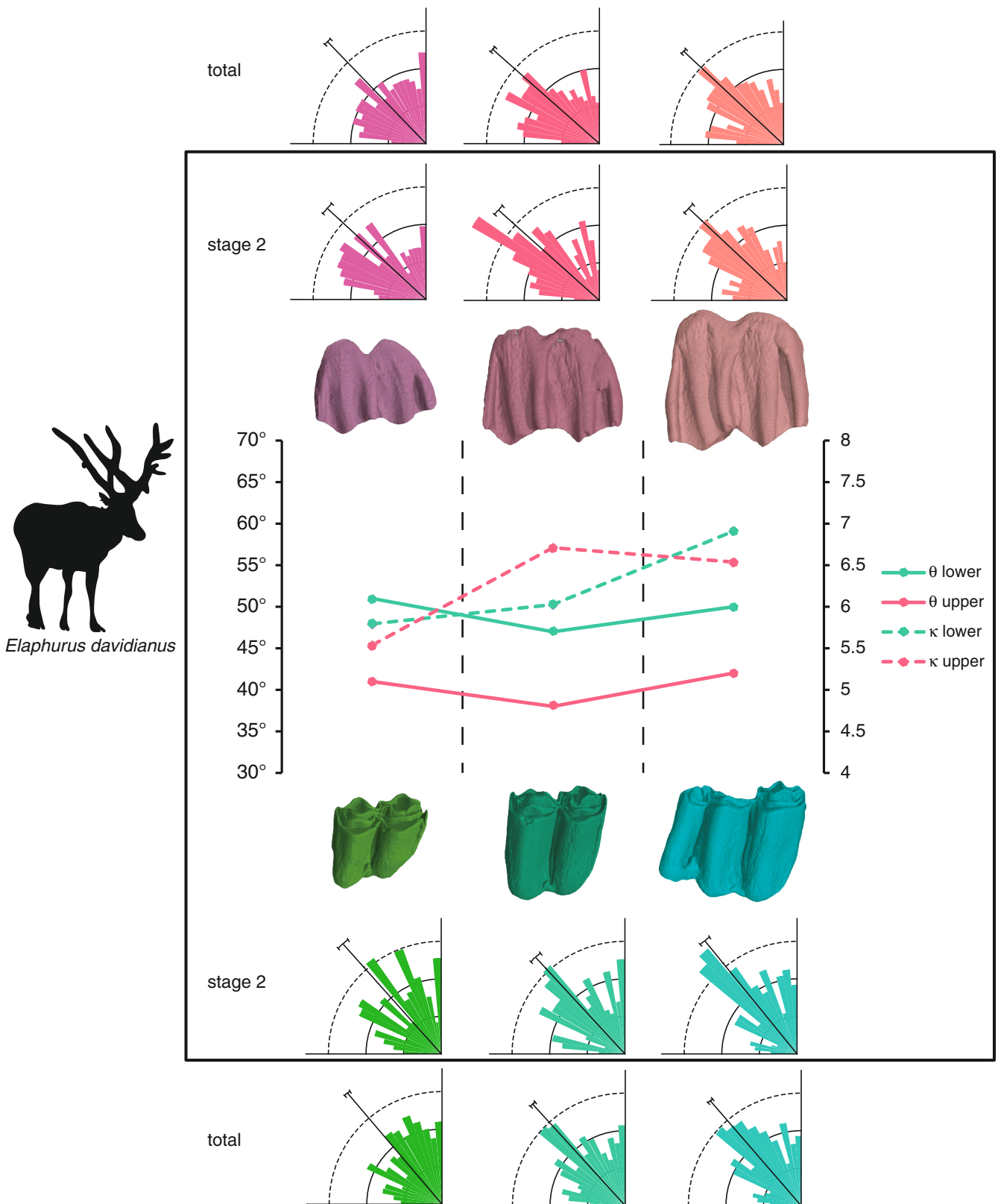


**Fig. 8.A13.** Summary of the most important statistical parameters for *Elaphurus davidianus*. ERAs are displayed as rose diagrams per tooth position for wear stage 2 and in total. The upper row shows upper M1–M3 (from left to right); the antagonistic lower teeth are in the lower row. The graphs show circular median ( $\theta$ ) and concentration ( $\kappa$ ) values per tooth position for stage 2.

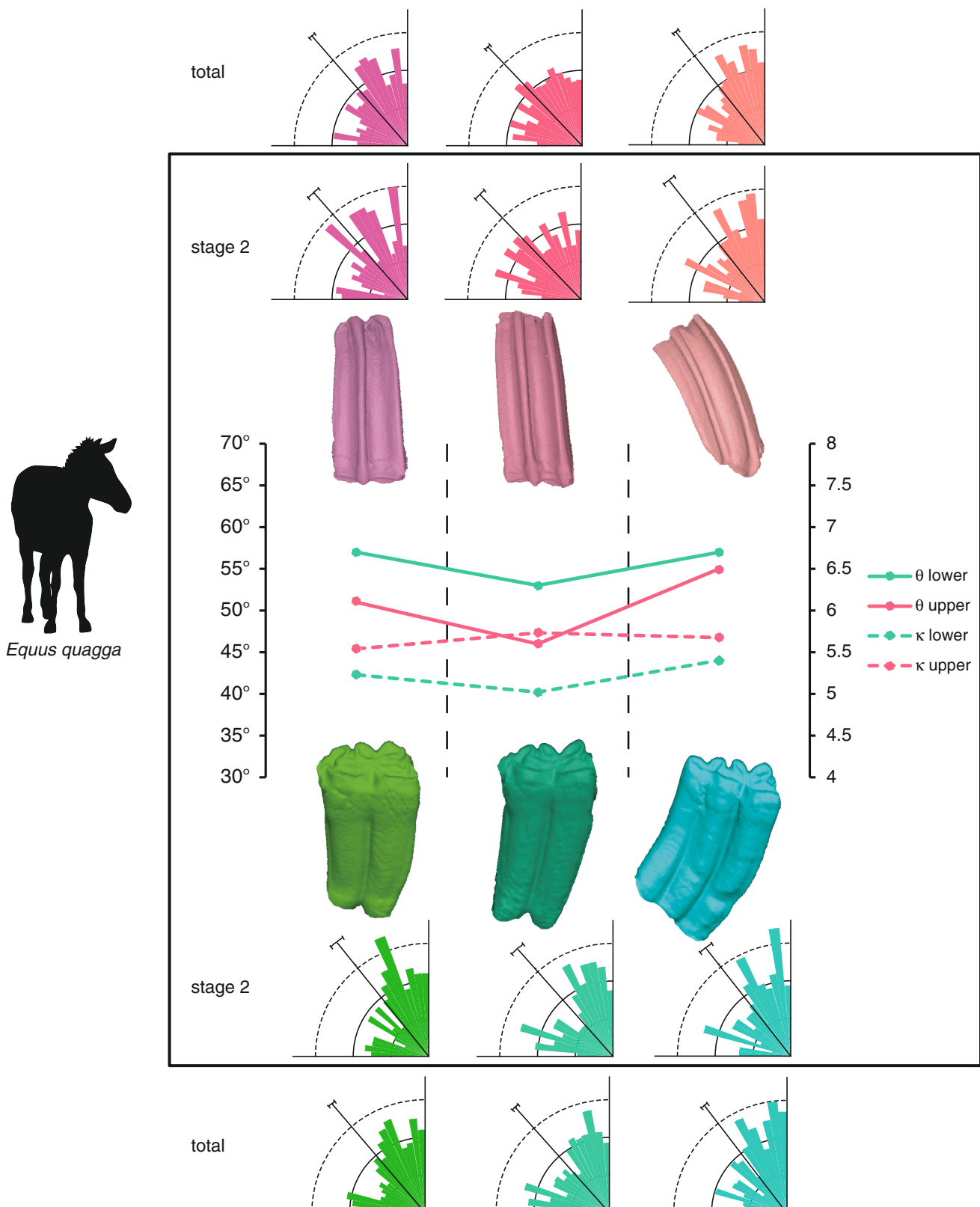


**Fig. 8.A14.** Summary of the most important statistical parameters for *Equus quagga*. ERAs are displayed as rose diagrams per tooth position for wear stage 2 and in total. The upper row shows upper M1–M3 (from left to right); the antagonistic lower teeth are in the lower row. The graphs show circular median ( $\theta$ ) and concentration ( $\kappa$ ) values per tooth position for stage 2.

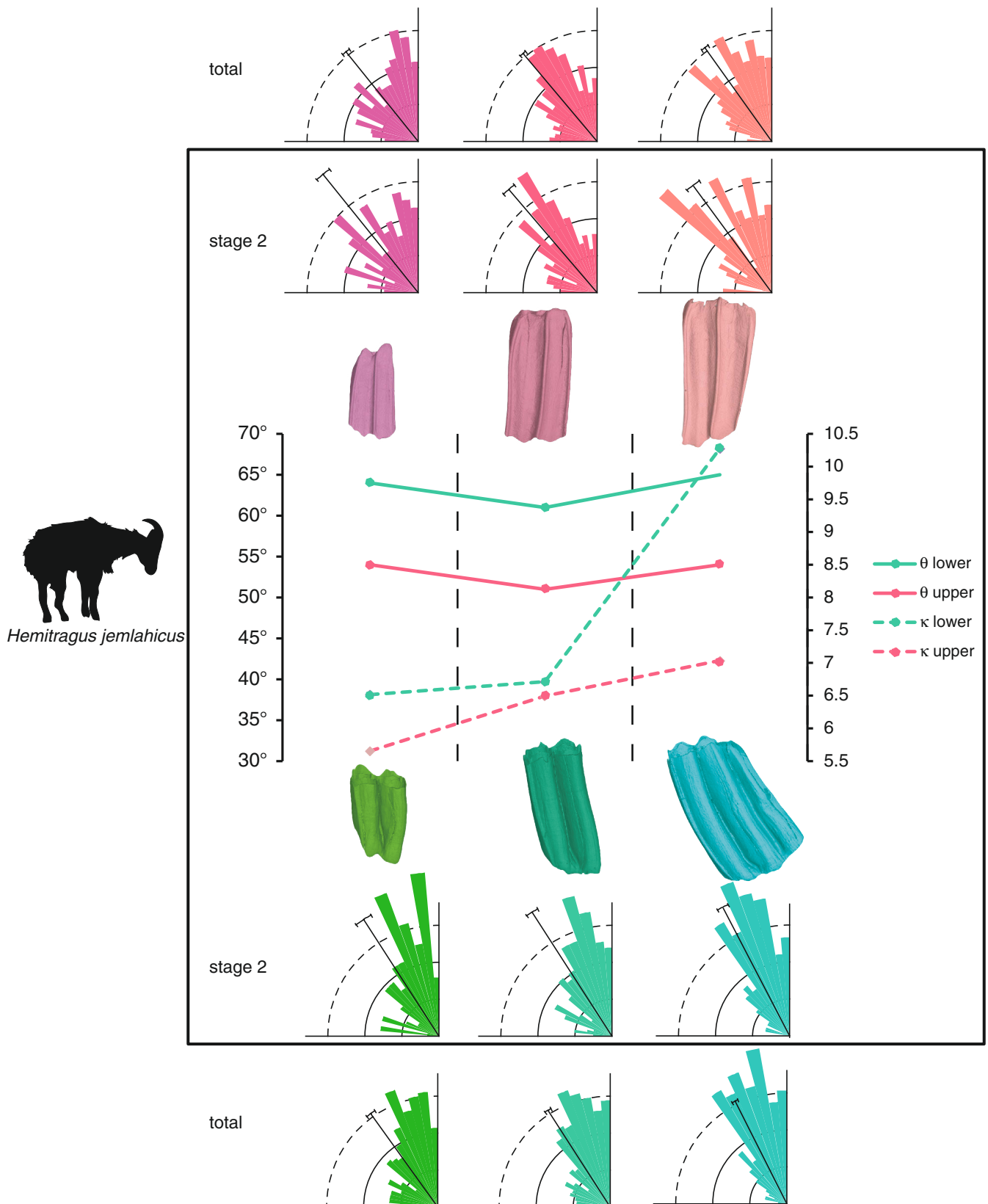


**Fig. 8.A15.** Summary of the most important statistical parameters for *Hemitragus jemlahicus*. ERAs are displayed as rose diagrams per tooth position for wear stage 2 and in total. The upper row shows upper M1–M3 (from left to right); the antagonistic lower teeth are in the lower row. The graphs show circular median ( $\theta$ ) and concentration ( $\kappa$ ) values per tooth position for stage 2.

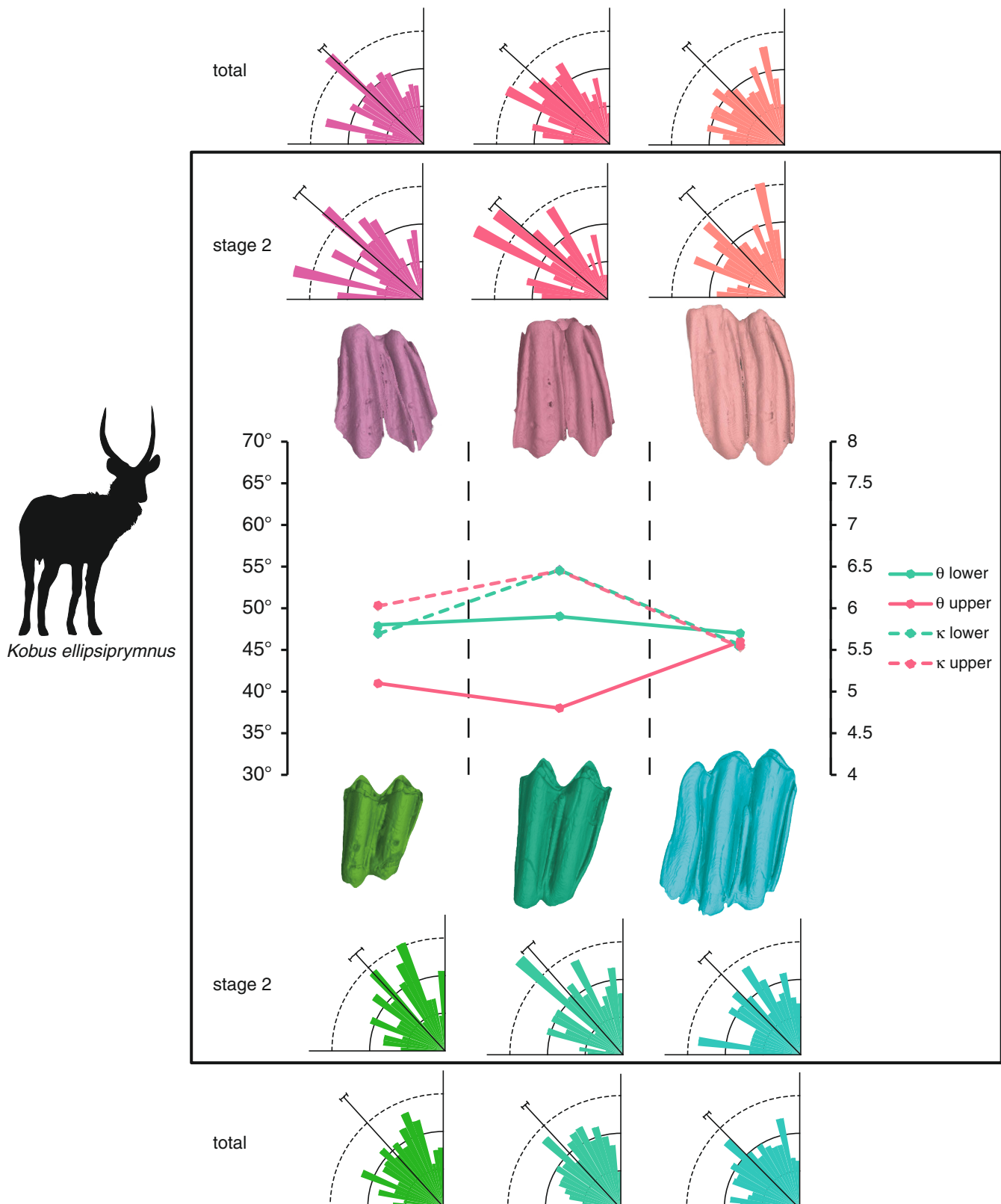


**Fig. 8.A16.** Summary of the most important statistical parameters for *Kobus ellipsiprymnus*. ERAs are displayed as rose diagrams per tooth position for wear stage 2 and in total. The upper row shows upper M1–M3 (from left to right); the antagonistic lower teeth are in the lower row. The graphs show circular median ( $\theta$ ) and concentration ( $\kappa$ ) values per tooth position for stage 2.

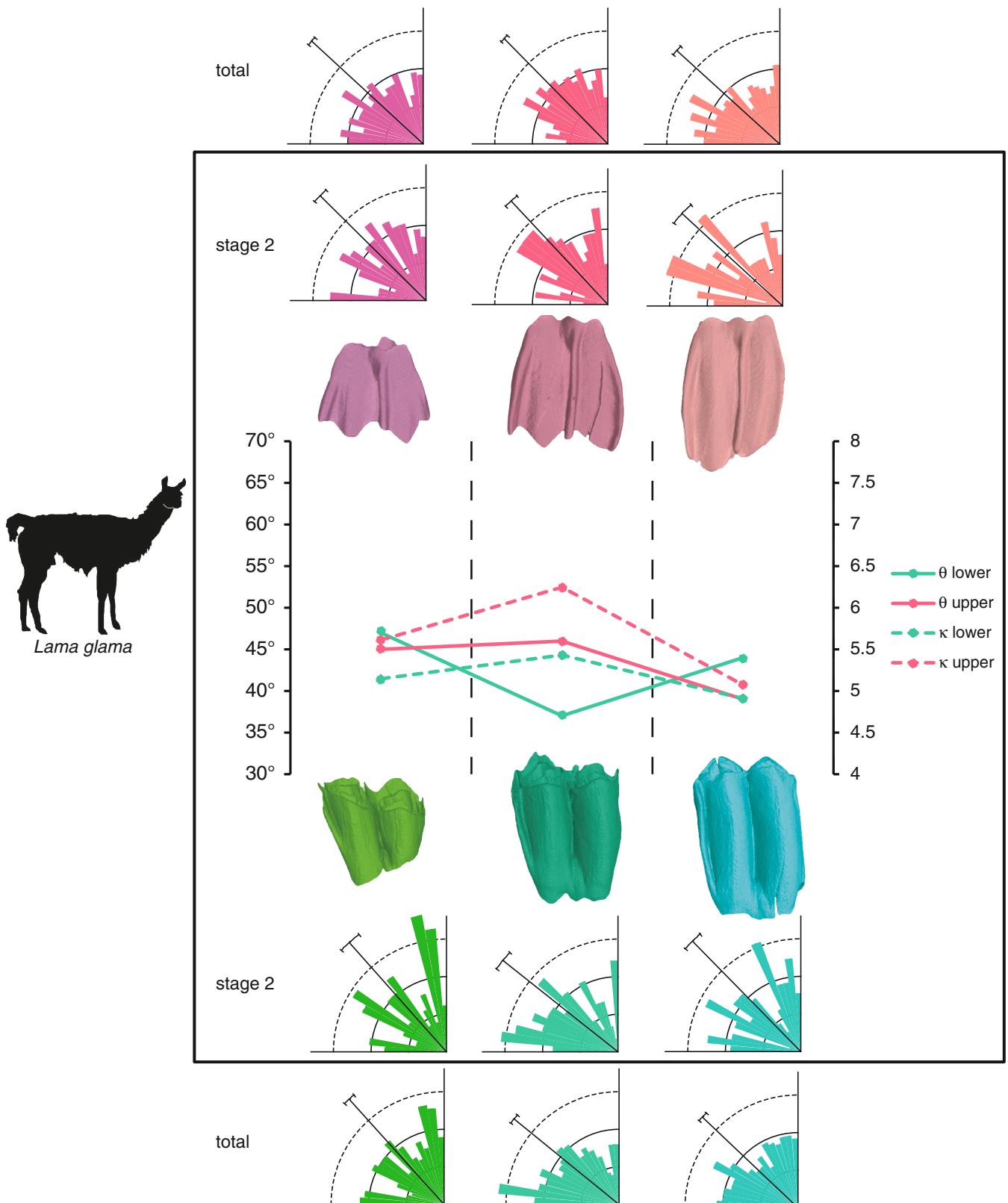


**Fig. 8.A17.** Summary of the most important statistical parameters for *Lama glama*. ERAs are displayed as rose diagrams per tooth position for wear stage 2 and in total. The upper row shows upper M1–M3 (from left to right); the antagonistic lower teeth are in the lower row. The graphs show circular median ( $\theta$ ) and concentration ( $\kappa$ ) values per tooth position for stage 2.

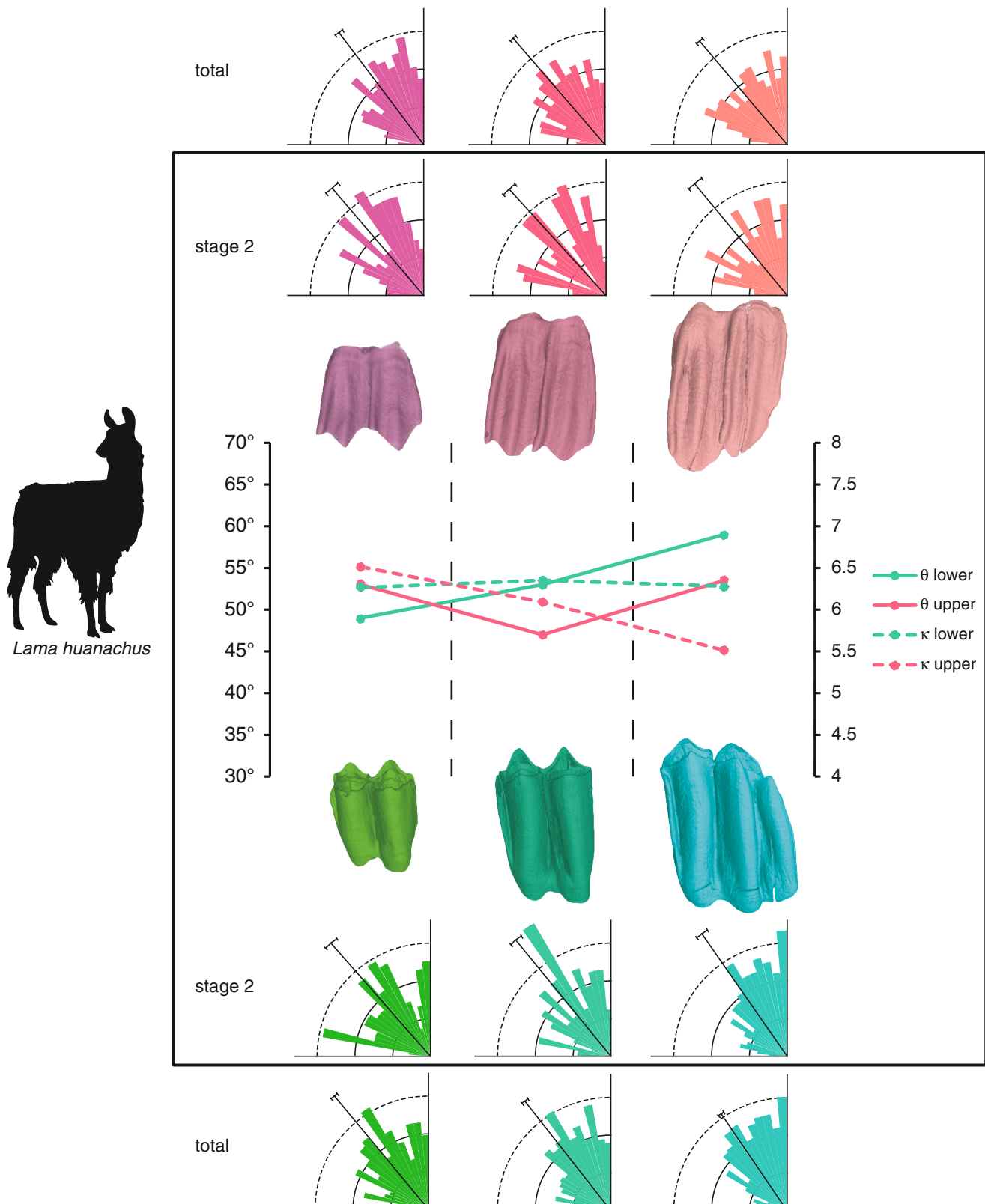


**Fig. 8.A18.** Summary of the most important statistical parameters for *Lama huanachus*. ERAs are displayed as rose diagrams per tooth position for wear stage 2 and in total. The upper row shows upper M1–M3 (from left to right); the antagonistic lower teeth are in the lower row. The graphs show circular median ( $\theta$ ) and concentration ( $\kappa$ ) values per tooth position for stage 2.

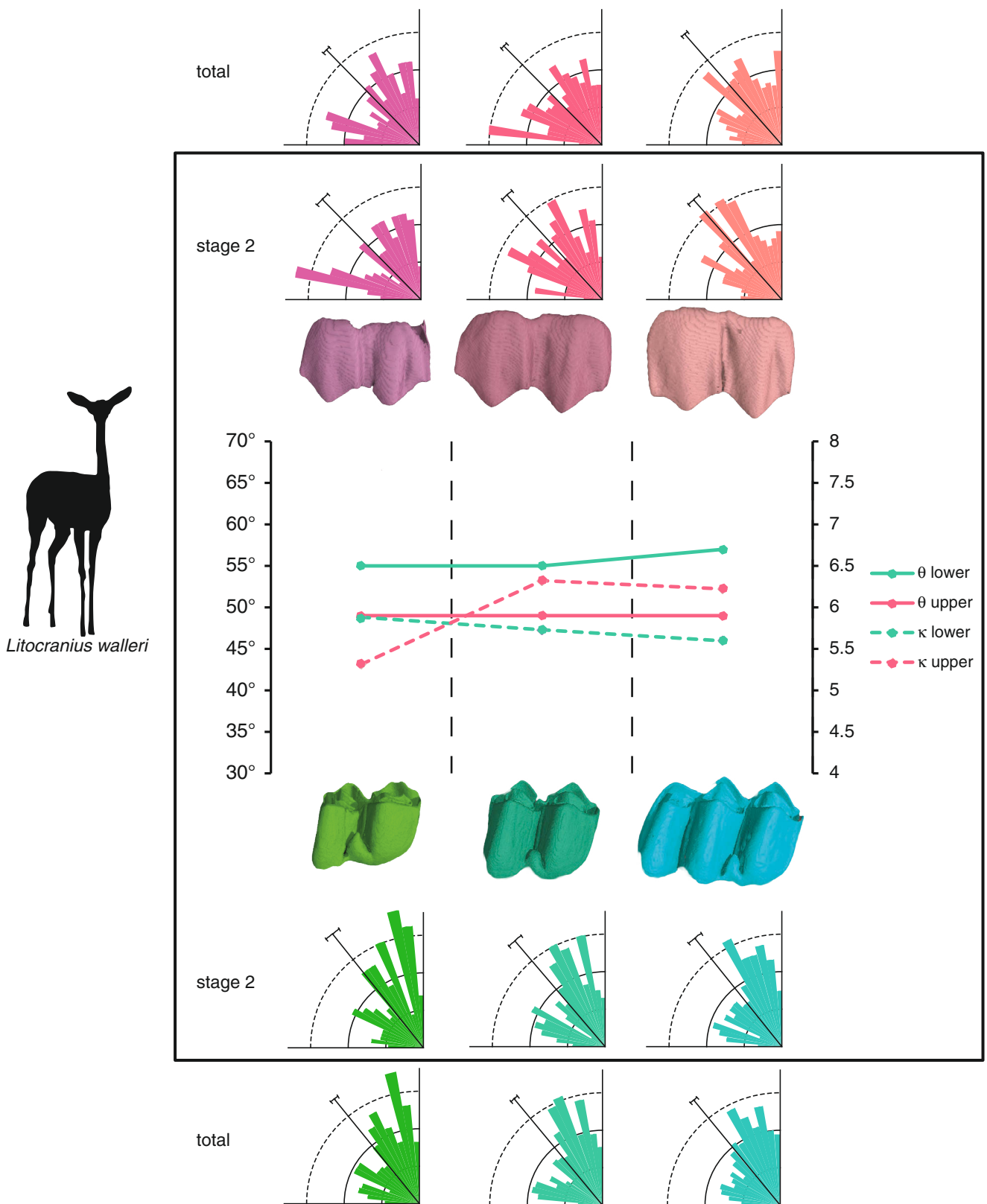


**Fig. 8.A19.** Summary of the most important statistical parameters for *Litocranius walleri*. ERAs are displayed as rose diagrams per tooth position for wear stage 2 and in total. The upper row shows upper M1–M3 (from left to right); the antagonistic lower teeth are in the lower row. The graphs show circular median ( $\theta$ ) and concentration ( $\kappa$ ) values per tooth position for stage 2.

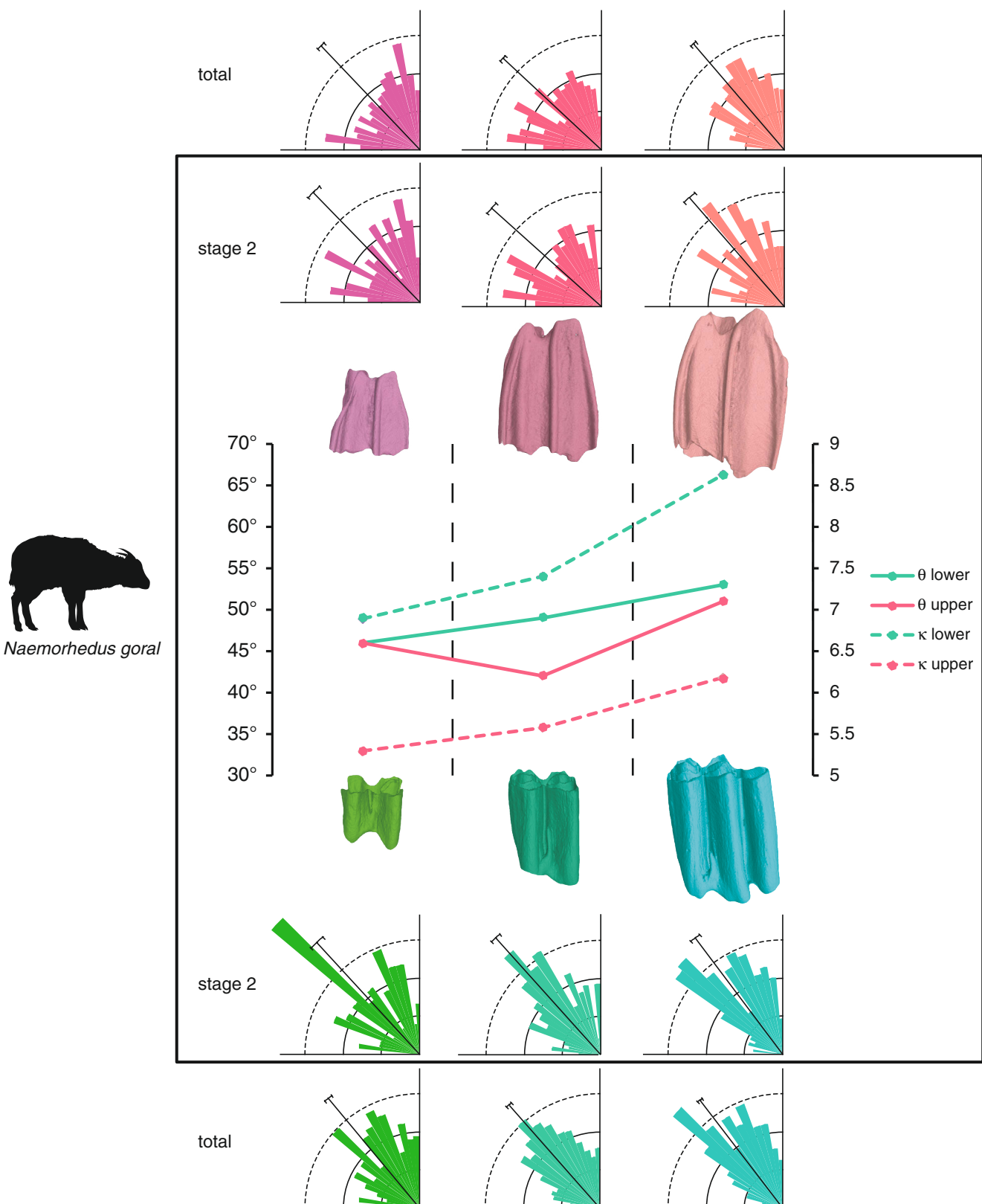


**Fig. 8.A20.** Summary of the most important statistical parameters for *Naemorhedus goral*. ERAs are displayed as rose diagrams per tooth position for wear stage 2 and in total. The upper row shows upper M1–M3 (from left to right); the antagonistic lower teeth are in the lower row. The graphs show circular median ( $\theta$ ) and concentration ( $\kappa$ ) values per tooth position for stage 2.

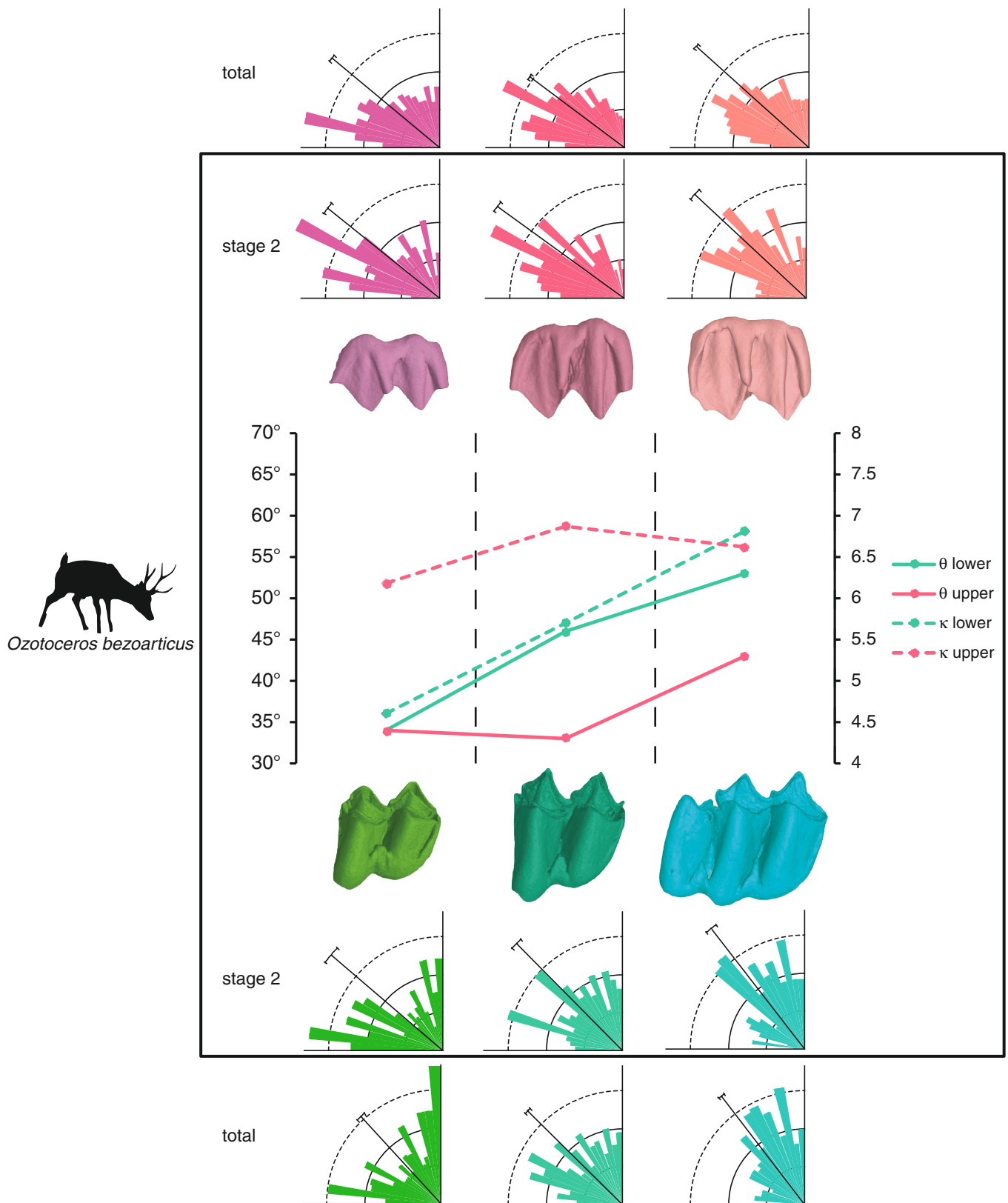


**Fig. 8.A21.** Summary of the most important statistical parameters for *Ozotoceros bezoarticus*. ERAs are displayed as rose diagrams per tooth position for wear stage 2 and in total. The upper row shows upper M1–M3 (from left to right); the antagonistic lower teeth are in the lower row. The graphs show circular median ( $\theta$ ) and concentration ( $\kappa$ ) values per tooth position for stage 2.

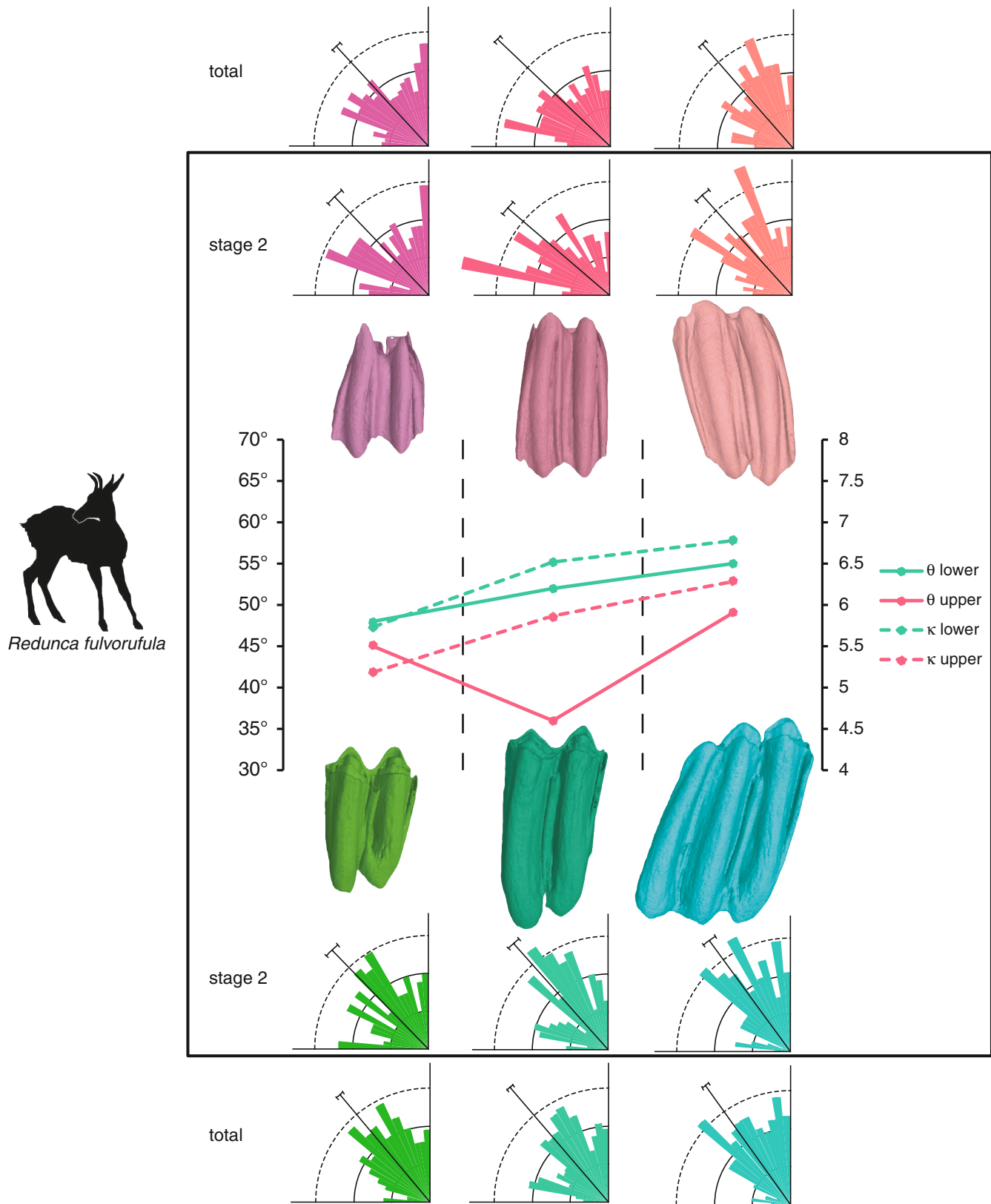


**Fig. 8.A22.** Summary of the most important statistical parameters for *Redunca fulvorufa*. ERAs are displayed as rose diagrams per tooth position for wear stage 2 and in total. The upper row shows upper M1–M3 (from left to right); the antagonistic lower teeth are in the lower row. The graphs show circular median ( $\theta$ ) and concentration ( $\kappa$ ) values per tooth position for stage 2.

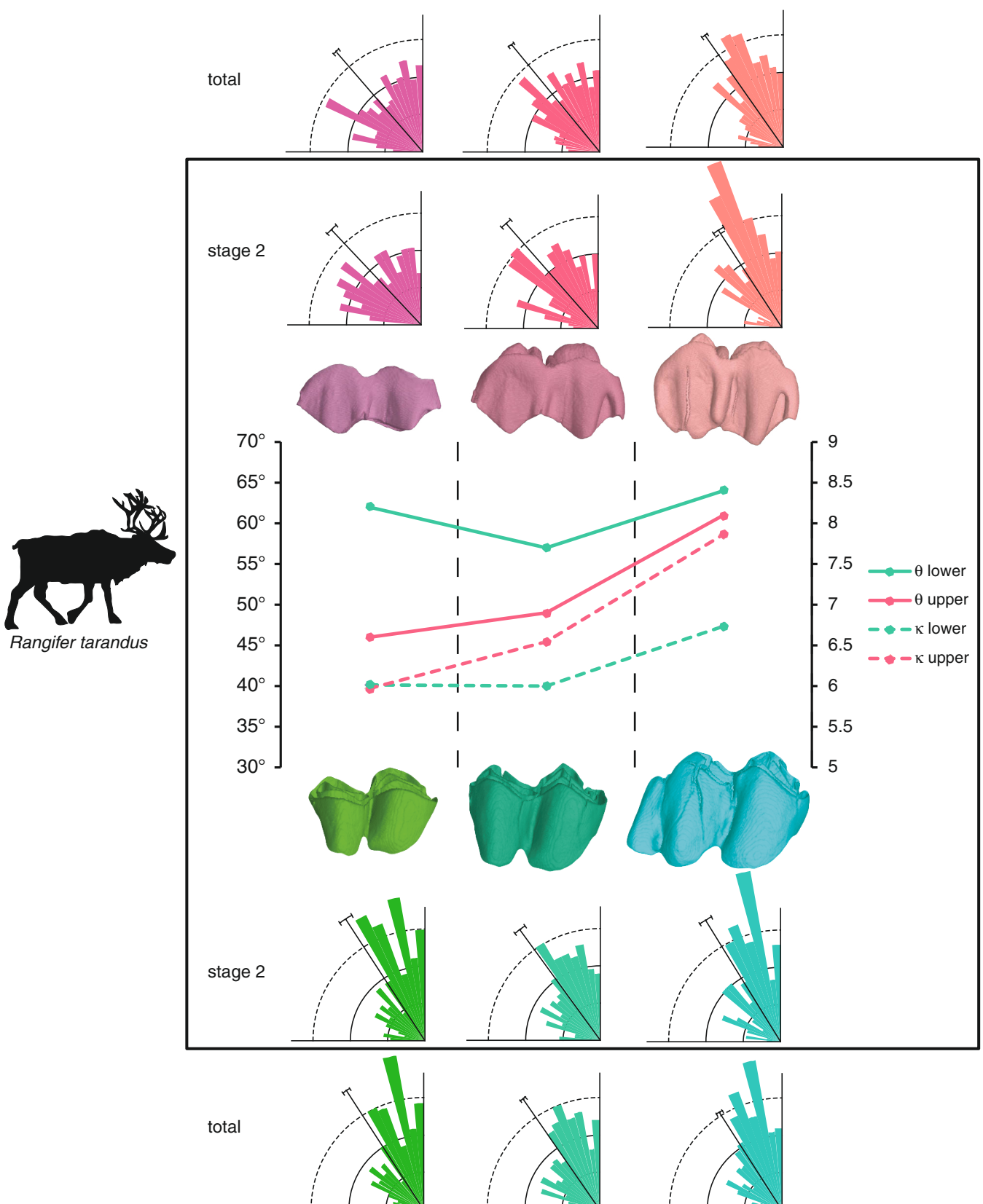


**Fig. 8.A23.** Summary of the most important statistical parameters for *Rangifer tarandus*. ERAs are displayed as rose diagrams per tooth position for wear stage 2 and in total. The upper row shows upper M1–M3 (from left to right); the antagonistic lower teeth are in the lower row. The graphs show circular median ( $\theta$ ) and concentration ( $\kappa$ ) values per tooth position for stage 2.